Universidade Federal do Rio Grande do Sul

Instituto de Geociências

Programa de Pós-Graduação em Geociências

GEOLOGIA ISOTÓPICA E GEOCRONOLOGIA DO COMPLEXO METAMÓRFICO PORONGOS E SUÍTE METAMÓRFICA VÁRZEA DO CAPIVARITA, CINTURÃO DOM FELICIANO, SUL DO BRASIL: IMPLICAÇÕES PARA A EVOLUÇÃO DO GONDWANA EM SUA MARGEM OCIDENTAL

Leonardo Gruber

Orientadora: Profa. Dra. Carla Cristine Porcher

Porto Alegre – 2016

Universidade Federal do Rio Grande do Sul

Instituto de Geociências

Programa de Pós-Graduação em Geociências

GEOLOGIA ISOTÓPICA E GEOCRONOLOGIA DO COMPLEXO METAMÓRFICO PORONGOS E SUÍTE METAMÓRFICA VÁRZEA DO CAPIVARITA, CINTURÃO DOM FELICIANO, SUL DO BRASIL: IMPLICAÇÕES PARA A EVOLUÇÃO DO GONDWANA EM SUA MARGEM OCIDENTAL

Leonardo Gruber

Orientadora: Profa. Dra. Carla Cristine Porcher

BANCA EXAMINADORA

Prof. Dr. Enrique Carlos Masquelin, Universidad de La República, Uruguay
Dra. Andréia Oliveira Monteiro da Silva Gross, Companhia de Pesquisa de Recursos Minerais – CPRM – Serviço Geológico do Brasil
Profa. Dra. Márcia Elisa Boscato Gomes, Universidade Federal do Rio Grande do Sul, RS, Brasil

Tese de Doutorado apresentada como requisito parcial para a obtenção do Título de Doutor em Ciências.

Porto Alegre, Março de 2016

UNIVERSIDADE FEDERAL DO RIO GRANDE DO SUL
Reitor: Carlos Alexandre Netto
Vice-Reitor: Rui Vicente Oppermann
INSTITUTO DE GEOCIÊNCIAS
Diretor: André Sampaio Mexias
Vice-Diretor: Nelson Luiz Sambaqui Gruber

Gruber, Leonardo
Geologia isotópica e geocronologia do Complexo Metamórfico Porongos e Suíte Metamórfica Várzea do Capivarita, Cinturão Dom Feliciano, sul do Brasil implicações para a evolução do gondwana em sua margem ocidental. / Leonardo Gruber. - Porto Alegre: IGEO/UFRGS, 2016.
[114 f.] il.

Tese (Doutorado).- Universidade Federal do Rio Grande do Sul. Programa de Pós-Graduação em Geocências. Instituto de Geociências. Porto Alegre, RS - BR, 2016.

Orientador(es):Carla Cristine Porcher

1. Proveniência 2. Geocronologia 3. Geoquímica isotópica 4. Gondwana I. Título.

CDU 55

Catalogação na Publicação
Biblioteca Instituto de Geociências - UFRGS
Sibila Francine T. Binotto CRB 10/1743

Universidade Federal do Rio Grande do Sul - Campus do Vale Av. Bento Gonçalves, 9500
Porto Alegre - RS - Brasil
CEP: 91501-970 / Caixa Postal: 15001.
Fone: +55 51 3308-6329 Fax: +55 51 3308-6337
E-mail: bibgeo@ufrgs.br

Resumo

Proveniência por métodos isotópicos em duas unidades litodêmicas – o Complexo Metamórfico Porongos (CMP) no domínio central-oriental do Cinturão Dom Feliciano (CDF) e a Suíte Metamórfica Várzea do Capivarita (SMVC), localizada no domínio leste do CDF - apresentou áreas-fonte similares nos dois casos: Os metassedimentos do CMP, na região das Antiformes de Santana da Boa Vista e Serra dos Pedrosas, foram depositados entre 785 e 595 Ma (U-Pb em zircão detrítico por LA-ICP-MS). Apresentam registros de áreas-fonte com predominância de idades de ca. 2.2 – 2.0 Ga, mesmas idades do embasamento da região, o Complexo Encantadas. As assinaturas isotópicas de $^{207}Pb/^{204}Pb$ X $^{206}Pb/^{204}Pb$ mostraram pouca relação dos metassedimentos do CMP com áreas-fonte do cráton Rio de La Plata, e εNd variando entre -13 a -6.5, com valores menos negativos para amostras onde foram obtidos zircões com mesma idade do vulcanismo félsico do CMP. Outros registros incluem idades de 1.5-1.4 Ga, cujas assinaturas εHf indicam fontes juvenis, possivelmente relacionadas a um sistema de rifteamento registrado nos Anortositos Capivarita. Na Antiforme Capané, zircões datados em SHRIMP e LA-ICP-MS de rochas metavulcânicas intermediárias a félsicas indicaram idades de 663 ± 2.7 Ma, representando um vulcanismo mais jovem do que aquele encontrado anteriormente no CMP, vinculado à fusão parcial crustal. Novos dados U-Pb em zircão confirmam registro do metavulcanismo de 783.4 ± 3.9 Ma nos metassedimentos, comparáveis a idades obtidas nos Gnaisses Cerro Bori, interpretados como um arco continental de ca. 800 Ma. Zircões detríticos de rochas metassedimentares da SMVC apresentaram registros de ca. 2.2 – 2.0 Ga, além de idades de ca. 1.4 Ga e idade máxima de deposição de 714.3 ± 3.9 Ma, com pico metamórfico registrado em borda metamórfica de zircões com 618 ± 7.3 Ma εHf predominantemente negativas. Mármores apresentaram razões $^{87}Sr/^{86}Sr$ de 0.70609, o que permite deduzir uma idade de deposição mais antiga que 715 Ma, próximo dos valores encontrados em mármores na região de Arroio Grande. A comparação dos isótopos de Hf com rochas do Cinturão Damara nos crátons Kalahari e Congo, cuja amalgamento junto ao Rio de La Plata deu origem ao Gondwana Ocidental, mostram que existe pouca ou nenhuma relação com áreas-fonte dos metassedimentos do CMP e SMVC no Neoproterozóico. Estes dados levam a dedução de que acresção de terrenos ou microcontinentes com características de embasamento, nesse caso denominado aqui como Embasamento Encantadas, cuja evolução se dá com acresção de um arco continental de idades entre 780 e 660 Ma, é a origem de parte das áreas-fonte do CMP, e possivelmente foi um dos eventos tectônicos que controlaram evolução do terreno ao longo do CMP e SMVC.

Palavras-chave: Proveniência; Geocronologia; Geoquímica Isotópica; Gondwana

Abstract

Isotopic provenance realized in two lithodemic units – Porongos Metamorphic Complex (PMC), in the central-eastern domain of the Dom Feliciano Belt (DFB) and the Várzea do Capivarita Metamoprhic Suite (VCMS), in the eastern domain of the same belt – presented similar source-areas in both cases: The PMC metasediments, in Santana da Boa Vista and Serra dos Pedrosas Antiforms were deposited between 785 and 595 Ma (LA-ICP-MS detrital zircon U-Pb). Both PMC and VCMS displayed source-areas with ages varying from ca. 2.2 – 2.0 Ga, which is the same age presented in the regional basement, the Encantadas Complex. $^{207}Pb/^{204}Pb$ X $^{206}Pb/^{204}Pb$ isotopic signatures displayed little resemblance between CMP metasediments and possible source-areas in the Rio de La Plata Craton, and εNd varied between -13 to -6.5, with less negative values in samples were where obtained zircons with the same age of felsic volcanism in the PMC. Others records included ages from 1.5 to 1.4 Ga, with εHf signatures indicating juvenile sources, possibly related to a rifting system recorde in the Capivarita Anorthosite. In the Capané Antiform, SHRIMP and LA-ICP-MS U-Pb zircon ages from felsic to intermediary metavolcanic rocks displayed 663 ± 2.7 Ma, which is a younger record than the previously obtained in the PMC, and can be related to partial crustal fusion. Also new U-Pb detrital zircon ages confirm the record of the metavolcanics of 783.4 ± 3.9 Ma in the metasediments, comparable to the ages obtained in the Cerro Bori orthogneisses, interpreted as a continental arc of ca. 800 Ma. Metasedimentary rocks of VCMS displayed zircons with ca. 2.2-2.0 Ga, besides ages of ca. 1.4 Ga and maximum depositional age of 714.3 ± 3.9 Ma, with metamorpich peak recorded in metamorphic rims of 618 ± 7.3 Ma and negative εHf signatures. Marbles presented $^{87}Sr/^{86}Sr$ ratios of 0.70609, which can be deducted as an older than 715 Ma depositional age, near values obtained to Arroio Grande marbles. Comparison of Hf signatures with rocks from Damara Belt of Kalahari and Congo Cratons, whose assembly with Rio de La Plata to form West Gondwana in Neoproterozoic, displayed little to no relationship with the source-areas of PMC and VCMS metasediments I in the Neoproterozoic. This indicates that terrain or a microcontinent accretion with basement features, in this case the Encantadas Basement, whose evolution underwent accretion in a continental arc between 780 to 660 Ma, it's the source to part of the PMC , and possible was one of the tectonic events that controlled terrain evolution in the PMC and VCMS.

Keywords: Provenance; Geochronology; Isotope Geochemistry; Gondwana

Sumário

Sobre a Estrutura da Tese

Esta tese de doutorado foi estruturada com base em artigos científicos, submetidos de acordo com as normas vigentes do Programa de Pós-Graduação em Geociências em revistas científicas com conceito QUALIS B ou maior.

Sua organização prevê uma Introdução, com o intuito de embasar as questões científicas que permearam o desenvolvimento da tese. O capítulo de Introdução faz um resumo do problema e um resumo das metodologias utilizadas na resolução do mesmo, seguido de uma análise integradora dos artigos submetidos à revisão.

Por fim, um capítulo de Conclusão, que resume os principais pontos discutidos nos artigos e levanta conclusões que não foram discutidas nos artigos por estarem além do escopo dos mesmos.

1 – Introdução

1.1 – Contextualização do Problema Científico

A paleogeologia é o ramo das geociências que estuda características geológicas expostas tempos atrás em superfície, mas subsequentemente soterrados por rochas formadas em tempos posteriores; também é entendida como o estudo geológico de dada região durante o tempo geológico, utilizando de métodos que permitam inferir sobre características paleocontinentais, litológicas, topográficas e estruturais (e.g. Levorson, 1933; Bluth e Kump, 1991); estas características controlam o desenvolvimento de drenagens, circunstâncias de eventos deformacionais, extensão de paleoceanos e lagos, bem como formação de antigas cadeias de montanhas. O resultado final de um estudo paleogeológico é um mapa geológico de uma superfície antiga. No caso do estudo da reconstrução e evolução da crosta continental ao longo dos éons, principalmente no estudo de rochas anteriores ao Fanerozóico, se torna uma ciência dependente da comparação de ambientes antigos aos atuais, já que o registro petrológico pode vir a representar uma pequena porção preservada de uma sucessão de sistemas tectônicos. Estes sistemas, por sua vez, englobam relações complexas entre bacias sedimentares, consumo de placas oceânicas e geração de fusões magmáticas em diversos ambientes, com variações tanto temporais (verticais) quanto laterais (ambientais). Comumente, utilizamos o conceito de tempo geológico como o proposto por James Hutton em 1788 (*no vestige of a beginning, no prospect of an end*), mas estudos recentes indicam que usar o ambiente atual como base de comparação no desenvolvimento de modelos de evolução crustal antigos acaba por desconsiderar o quão restrito e localizado é o registro (aquele que obtemos em campo) em relação ao ambiente que o gerou (a crosta paleogeológica). Por exemplo, o volume de terra que se encontra em bacias sedimentares na crosta continental representa em torno de 16% do total de área subaérea do globo, enquanto que o restante da superfície encontra-se acima da linha de erosão, potencialmente desaparecendo do registro geológico com o tempo (Nyberg e Howell, 2015).

Sendo o registro geológico antigo algo tão pontual e, em alguns casos, pouco representativo do todo, torna-se necessário o estudo químico e isotópico da geologia aflorante segundo rochas e minerais que permitam avaliar as características pré-deformacionais da paleogeografia, objetivando uma quantificação dos diferentes processos formadores destas rochas e sua evolução durante o tempo geológico.

Abordagens multidisciplinares envolvendo datação, geologia isotópica, geofísica e paleontologia, além de modelamento matemático do comportamento das placas antigas para reconstrução crustal são atualmente alternativas para o desenvolvimento de estudos paleogeológicos. Um bom exemplo é o trabalho de Li *et al* (2008) para reconstruir o modelo geodinâmico de formação e quebra do supercontinente Rodínia. O esforço destes autores abriu uma nova onda de interesses em paleogeologia, bem como a possibilidade de aplicar tais metodologias para o desenvolvimento de modelos paleogeográficos mais antigas ainda.

No estado do Rio Grande do Sul, todo o registro geológico Neoproterozóico se encontra no Cinturão Dom Feliciano (CDF), que é entendido como resultante da orogenia gerada da colisão entre os crátons Rio de La Plata, Congo e Kalahari, além de terrenos e arcos intermitentes. Embora existam hipóteses divergentes a respeito da origem, quantidade ou mesmo existência de arcos e terrenos aglutinados na colisão entre duas prováveis placas continentais (e.g., Fernandes *et al*., 1995 a e b; Chemale 2000, 2012; Saalmann *et al*., 2010; Frimmel *et al*., 2011), é certo que a evolução do orógeno se deu através da acresção de um arco de ilhas a uma margem acrescionária contígua ao cráton Rio de La Plata – arco Passinho - (Saalmann *et al*., 2006; Lena *et al*., 2014), quase concomitantemente a aglutinação de um terreno (Frimmel *et al*., 2011) ou arco continental (Lenz *et al*., 2012), interpretado como um microcontinente (Chemale *et al*., 2012), cuja colisão com a margem acrescionária do La Plata se deu durante a aglutinação do Gondwana Ocidental. Essa convergência talvez possa ser entendida como a mesma que gerou o Arco Continental Cerro Bori, no Uruguai (Lenz *et al*., 2012), com idades compatíveis com os metassedimentos da formação Punta Mogotes, também no Uruguai (Rapela *et al*., 2011), e possivelmente está vinculada ao vulcanismo ácido contido no Complexo Metamórfico Porongos (CMP) (idade de cristalização de zircões de origem magmática caracterizada por Porcher *et al*., 1999). É válido observar que os mesmos padrões de idades são reconhecidos para o contexto geral de aglutinação do Gondwana em outras áreas na América do Sul e África, com um componente mais antigo, de ca. 950 – 650 Ma, com vulcanismo associado à subducção e geração e bacias geradas em cinturões relacionados a acresção crustal; e um componente mais jovem, de ca. 700 – 520 Ma, formado pela colagem de cinturões orogênicos ao longo das margens cratônicas (Cordani *et al*., 2013).

Dentre as várias reconstruções paleocontinentais existentes (e.g. Hoffman 1991; Dalla Sala *et al*., 1992; Rogers, 1996; Dalziel, 1997; Meert e Torsvik, 2003; Li *et al*., 2008), a gênese e posição original da crosta onde atualmente afloram rochas pertencentes ao CDF ainda é pouco discutida, uma vez que não existem estudos paleomagnéticos de rochas ígneas locais da época, então a reconstrução paleogeológica precisa ser referenciado a partir de cratons adjacentes.

Tanto o CMP quanto a Suíte Metamórfica Várzea do Capivarita (SMVC) consistem de litodemas gerados durante o amalgamento do Gondwana. O CMP está localizado na porção centro-oriental do domínio leste do CDF, e é entendido como seqüências sedimentares e vulcânicas, metamorfizadas em fácies xistos verdes e localmente fácies anfibolito (Jost & Bitencourt, 1980). Estas seqüências foram depositadas sobre um embasamento siálico paleoproterozóico - Complexo Encantadas – e se encontram intercaladas tectonicamente quartzo-milonitos, filonitos e metacherts. Diversos ambientes tectônicos e idades máximas e mínimas de deposição já foram sugeridas para os metassedimentos do CMP, as mais atuais interpretando as idades mais antigas dos quartzitos da antiforme de Santana da Boa Vista como depositados em um ambiente de margem passivo (Gruber *et al*., 2011; Pertille *et al*., 2015a) mais jovens obtidas em xistos como início da fase forearc da bacia do Camaquã (Pertille *et al*., 2015b). Já a SMVC está localizada no domínio leste, e é entendida como tetos pendentes em ortognaisses, incluindo nas porções paraderivadas metassedimentos típicos de sedimentação em margem passiva marinha, incluindo metapelitos e mármores, metamorfizados em fácies anfibolito superior a granulito (Fragoso-César, 1991).

1.2 – Objetivos e Métodos Propostos na Resolução dos Problemas Científicos

Com o objetivo de entender a relação entre distância de área-fonte e posição da(s) paleobacia(s) estudada(s) durante a evolução do Gondwana, e a evolução geocronológica e geodinâmica da porção do CDF no qual os litodemas em estudo estão localizados, utilizou-se neste trabalho os métodos U-Pb e Lu-Hf, tanto em zircão de rochas metassedimentares quanto metavulcânicas, Sr-Sr em calcários além de Sm-Nd e Pb-Pb em rocha-total.

Os métodos em rocha-total se baseiam, no caso de rochas metassedimentares em dois princípios: 1 – a composição isotópica representa uma média ponderada entre os diferentes minerais que formam a rocha, por consequência, suas áreas-fonte estão representadas na média; e 2 – os processos posteriores à diagênese não alteraram a composição isotópica dos mesmos.

No caso do sistema Sm-Nd, a imobilidade desses elementos na maioria dos processos crustais acaba tornando-os excelentes para análises geoquímicas e isotópicas que objetivem informações sobre os protólitos amostrados. A partir dos dados de fator de evolução do Nd em relação a uma crosta condrítica uniforme, e sua idade de depleção mantélica, é possível caracterizar o ambiente de formação dos protólitos, bem como a idade de extração do material fundido do manto que mais tarde daria origem aos metassedimentos estudados (e.g., DePaolo e Wasserburg, 1976; DePaolo, 1981; Taylor e McLennan, 1985).

Para as análises de Pb, compara-se a razão de Pb Uranogênico ($^{207}Pb/^{206}Pb$) e Thorogênico ($^{208}Pb/^{206}Pb$) com as razões encontradas em rochas crustais típicas dos crátons adjacentes à área em estudo, permitindo então uma comparação entre a composição da área-fonte e a composição dos sedimentos depositados, bem como sua relação com a curva de evolução Thoro-Uranogênica de Stacey e Kramer, indicando fontes únicas ou variantes de acordo com a integridade dos dados para os quatro conjuntos de isótopos ($^{208}Pb/^{206}Pb$ X $^{206}Pb/^{204}Pb$ e $^{207}Pb/^{204}Pb$ X $^{206}Pb/^{204}Pb$ (e.g. Stacey and Kramer, 1975; Tosdal, 1996; Schwartz e Gromet, 2004; Loewy *et al*., 2011).

No método $^{87}Sr/^{86}Sr$, as razões de Sr obtidas são comparadas às curvas de variação isotópica de Sr ao longo da história geológica, dando uma ideia da composição do oceano que gerou os carbonatos antes de sua deposição, além de poder ser utilizada como aproximação da idade de deposição dos mesmos (e.g Jacobsen e Kaufman, 1999).

Tanto U-Pb quanto Lu-Hf foram efetuados no zircão, que é um ortossilicato de zircônio (dodecaedros de ZrO_8 dividindo pontas e cantos com tetraedros de SiO_4) que tende a incorporar elementos terras-rara, sendo também resistente a processos posteriores à sua cristalização magmática (em torno de 900°C) (Finch e Hanchar., 2003). No caso do U-Pb, que é usado principalmente para datação no zircão, o decaimento do sistema U para Pb, onde o Pb não é incorporado na cristalização do mineral, possibilita a geração de idades concordantes entre as diferentes razões (concórdia) e discordantes (discórdia). Alguns processos, tais como metamictização, refusão, e em alguns casos específicos, remobilização de U em líquidos hidrotermais ou perda de Pb em fraturas, podem acarretar discordância na idade obtida, gerando uma idade de protólito (ou fusão inicial) de intercepto superior no diagrama concórdia, e uma idade secundária, de intercepto inferior, geralmente relacionada aos processos citados anteriormente.

O sistema Lu-Hf comporta-se geoquimicamente de maneira semelhante ao Sm-Nd e foi utilizado neste estudo para caracterizar a idade de extração mantélica da fusão que deu origem ao cristal. A quantidade de ^{176}Hf radiogênico (produto do decaimento do ^{176}Lu) em relação ao ^{177}Hf incorporado pelo zircão durante a cristalização pode ser usado da mesma maneira que Sm-Nd para cálculo de um εHf, onde fusões mantélicas possuem pouco ou nenhum fracionamento, e fusões crustais são muito fracionadas (e.g. Patchett *et al.*, 1981; Kinny e Maas, 2003).

2 – Análise Integradora

2.1 – Primeiro Artigo

Isotope geochemistry (Sm-Nd and Pb-Pb) and U-Pb geochronology on provenience and syn-depositional volcanism in Porongos Metamorphic Complex metasediments (Santana da Boa Vista Antiform), Dom Feliciano Belt, Brazil

Leonardo Gruber, Carla Cristine Porcher, Edinei Koester, Anelise L. Bertotti, Cristine Lenz, Luís Alberto D'Ávilla Fernandes, Marcus Vinícius Dorneles Remus

- Submetido ao *Journal of South American Earth Sciences (Elsevier)*

A motivação científica central neste artigo foi entender a relação de idade entre as rochas metassedimentares (metapelitos, quartzitos, quartzo-milonitos) e as rochas metavulcânicas ácidas datadas em outros trabalhos para o CMP, principalmente na região de Santana da Boa Vista e Serra dos Pedrosas. Secundariamente foram realizados estudos em rocha-total, esperando-se caracterizar as amostras analisadas e comparar estas características com dados de outros autores sobre embasamento e crátons adjacentes no que se espera que tenha sido a configuração do Gondwana à época de deposição. Foram encontrados zircões de rochas metapelíticas com idades extremamente compatíveis com rochas metavulcânicas locais, permitindo então entender a deposição sedimentar de parte do CMP como síncrona ao vulcanismo que afetou a paleobacia no Toniano (ca. 780 Ma).

Os dados de rocha-total serviram para indicar que existe uma área-fonte com εNd mais jovem (T_{DM} de 1.2 Ga) e menos negativa (εNd -6.5) que a totalidade das outras análises obtidas, sendo estas outras todas comparáveis a análises realizadas em rochas do embasamento do CDF, com εNd em torno de -10.1 a -24.5 e T_{DM} variando de 1.64 a 2.2 Ga, mostrando fusão de material crustal na origem dos protólitos. Essa análise possivelmente é indicadora de metassedimentos oriundos de vulcanismo vicinal à bacia. Já as análises de Pb permitiram aos autores distinguir que, entre as possíveis áreas-fonte para os metassedimentos, não havia indícios de rochas com composições típicas do cráton La Plata. Possivelmente estas áreas-fonte sejam oriundas do conjunto de crátons e terrenos Africanos do Kalahari e Congo.

Foi possível estipular uma mínima idade de deposição para os metassedimentos, tornando possível admitir que a deposição do PMC na região de Santana da Boa Vista e na Serra dos Pedrosas foi depositado entre 815 (idade máxima admitindo a incerteza para os zircões de origem vulcânica) e 595 Ma (idade mínima admitindo a incerteza). Uma idade igualmente jovem, obtida em quartzo-milonitos ao sudoeste da antiforme de Santana da Boa Vista por Gruber *et al*. (2011) pode ser então entendida como uma deposição tardia dentro desse sistema de colisão da margem acrescionária do La Plata e Congo/Kalahari.

2.2 – Segundo Artigo

Geochronology (U-Pb) and isotope geochemistry (Sr/Sr) applied to the Varzea do Capivarita Metamorphic Suit, Dom Feliciano Belt, Southern Brazil: Insights and paleogeographical implications to Western Gondwana evolution

Leonardo Gruber, Carla Cristine Porcher, Humberto Geller, Luís Alberto D'Ávilla Fernandes, Edinei Koester

- Submetido à *Geochemica Brasiliensis (Sociedade Brasileira de Geoquímica)*

Para este artigo, foram coletadas amostras metassedimentares de teto pendente na Suíte Metamórfica Várzea do Capivarita (SMVC), com o objetivo de identificar a proveniência U-Pb, e sua relação com os dados de proveniência da paleobacia Porongos. Adicionalmente foram realizadas análises de $^{87}Sr/^{86}Sr$ e $^{207}Pb/^{204}Pb$ X $^{206}Pb/^{204}Pb$ em mármores do mesmo teto pendente, na tentativa de relacionar a idade e o ambiente de deposição destes com outros ambientes marinhos da época. As análises isotópicas dos mármores indicam possível relação dos mesmos com dolomitos estromatólitos do cinturão Gariep, assim como uma possível área-fonte cuja razão de Pb é a mesma que originou o arco continental Cerro Bori (ca. 800 Ma) (Lenz *et al*., 2012).

Os resultados permitiram concluir que os metassedimentos da SMVC compartilham boa parte das mesmas fontes que os metassedimentos do CMP, mas possuem idades máximas de deposição diferentes do que foi encontrado para o CMP nas antiformes de Santana da Boa Vista e Serra dos Pedrosas. O anortosito Capivarita, interpretado como resultado de um evento de rifteamento de ca. 1.5 Ga (Chemale *et al*., 2012) é uma das fontes principais para os metassedimentos da SMVC. Com a mesma idade, existem dados interpretados como um rift junto a margem Sudoeste do Laurentia e Antártica Leste (Mulder *et al*., 2015), que podem muito bem ser relacionados aos eventos da nossa crosta.

O resultado de Sr permitiu inferir uma idade de deposição mínima de ca. 715 Ma para os mármores, baseada em zircões detríticos de bandas metapelíticas com a mesma S0 dos mármores. A razão de Sr de 0.70609 possivelmente é indicativa da deposição original dos mármores, podendo ser correlacionada à glaciação Esturtiana (717-660 Ma) (Rooney *et al*., 2015), ou depositada no mesmo ambiente marinho raso que carbonatos da formação Kaigas (Cráton Kalahari) (Frimmel *et al*., 2011).

2.3 – Terceiro Artigo

Comparison between U-Pb zircon ages and Hf isotopic signatures of Porongos Metamorphic Complex and Várzea do Capivarita Metamorphic Suit in Dom Feliciano Belt, South America: Implications to West Gondwana evolution

Leonardo Gruber, Carla C. Porcher, Edinei Koester, Anelise L. Bertotti, Luís Alberto D'ávilla Fernandes

- Submetido à *Brazilian Journal of Geology (Sociedade Brasileira de Geologia)*

Neste artigo foi utilizado o método de Lu-Hf em zircões detríticos e vulcânicos, datados tanto neste trabalho quanto outros previamente publicados (Gruber *et al*., 2011 e o segundo artigo que compõe o corpo da presente tese), com o intuito de identificar os tipos de áreas-fonte que contribuíram com os metassedimentos do CMP e sua relação com a evolução entre os supercontinentes Rodínia-Gondwana.

Datações U-Pb em zircões de rochas metavulcânicas corroboram registro de vulcanismo em ca. 780 Ma no CMP, e a datação de um novo conjunto de metavulcânicas, mais jovens, de ca. 660 Ma, indica a existência de outro evento vulcânico, cujas assinaturas εHf são essencialmente as mesmas das datações anteriores. Estes dados levam a interpretação de que os litodemas metavulcanossedimentares do CMP são compostos por formações depositadas em tempos diferentes em um mesmo contexto de convergência entre placas tectônicas. A comparação dos dados de εHf com unidades nos crátons Congo e Kalahari (Foster *et al*., 2015), mostra que tanto o CMP quanto a SMVC apresentam um registro diferente de assinaturas no Neoproterozóico, indicando áreas-fonte diferentes do esperado se houvesse influência da crosta Africana junto á margem do cráton Rio de La Plata nesse período. Juntando estas observações às sugestões de outros autores sobre terrenos/microcontinentes sendo aglutinados durante o fechamento do oceano Adamastor durante o final do Neoproterozóico, é possível admitir com certeza que existe um vulcanismo ácido, possivelmente relacionado à acresção de um arco continental ao que deveria ser uma das margens do Rio de La Plata durante o Criogeniano, e o desenvolvimento desta margem continental ativa possui uma fase final em torno de 660 Ma, registrado também no CMP em zircões de rocha metavulcânica intermediária a félsica.

3 – Conclusões

Dentre os dados apresentados na presente Tese, a similaridade de idades entre os metassedimentos do CMP e SMVC indica que ambas tiveram as mesmas áreas-fonte disponíveis próximas, entre elas: *i* - o Complexo Encantadas (2.2 – 2.0 Ga), com um ambiente de arco, possivelmente um arco de ilhas; *ii* - um possível sistema de rifteamento entre 1.5 e 1.3 Ga (Anortosito Capivarita), e *iii* fontes de idade Mesoproterozóica de menor importância (1.2 – 1.1 Ga), possivelmente indicando áreas-fonte distais, de pequena extensão ou altos topográficos ou outra feição de paleogeografia que impediu a deposição destes sedimentos. O mesmo ambiente de margem continental passiva das sequências de quartzitos do CMP pode ser extendido para os metapelitos e mármores da SMVC. Porém, a deposição final dos sedimentos do CMP é mais jovem (ca. 590 Ma), indicando que a evolução da margem retrabalhada do Rio de La Plata é controlada pela acresção e retrabalhamento de arcos e terrenos com mesmas áreas-fonte.

Dentre as idades Neoproterozóicas, a datação de um conjuto de zircões provenientes de rochas vulcânicas intermediárias a ácidas idade de ca. 800-780 Ma indicam a continuidade de um sistema de arco continental que possivelmente se extendeu pela margem retrabalhada do cráton Rio de La Plata, onde posteriormente haveria a aglutinação com os crátons Kalahari e Congo. A deposição dos sedimentos durante o período entre 780 e 660 Ma parece ter sido amplamente controlada pela geração de arcos vulcânicos na margem retrabalhada do cráton Rio de La Plata; no caso em estudo, um arco continental de ca. 800 Ma, cujos registros no CMP são tanto rochas metavulcânicas ácidas a intermediárias, quanto metassedimentares, possivelmente depositadas em um ambiente de backarc intermitente. Este mesmo arco pode ser entendido como primeira fase de acresção de um microcontinente ou terreno (sugerido aqui como Embasamento Encantadas para evitar interpretações tectônicas dos termos terreno e microcontinente) ao complexo acrescionário Passinho na margem do cráton Rio de La Plata. Esta aglutinação teria uma fase final em torno de 660 Ma, gerando fusão parcal registrada no metavulcanismo intermediário a félsico do CMP. Ocorre então o amalgamento final do Gondwana, e a geração do batólito Pelotas, com sedimentação oriunda de áreas-fonte predominantemente mais jovens (<640 Ma), relativa à fase de foreland da bacia do Camaquã.

4 – Referências Bibliográficas

Bluth, G. J. S, and Kump, L. R. 1991. Phanerozoic paleogeology. *American Journal of Science*, Vol. 291, pp.284-308.

Chemale, F. 2000. Evolução Geológica do Escudo Sul-rio-grandense. In: Holz, M.; De Ros, L. F. (eds.). **Geologia do Rio Grande do Sul**. Porto Alegre, CIGO/UFRGS, p. 13-52.

Chemale, F., Mallmann, G., Bitencourt, M.F., Kawashita, K. 2012. Time constraints on magmatism along the Major Gercino Shear Zone, southern Brazil: Implications for West Gondwana reconstruction. *Gondwana Research* 22, 184-199.

Cordani, U. G., Pimentel, M.M., Araújo, C.E.G., Fuck, R.A. 2013. The significance of the Transbrasiliano-Kandi tectonic corridor for the amalgamation of West Gondwana. *Brazilian Journal of Geology*, 43 (3): 583-597.

Dalla Salda, L. H., Cingolani, C. A., and Varela, R., 1992a, The Early Paleozoic orogenic belt of the Andes in southwestern South America: Result of Laurentia-Gondwana collision? *Geology*, v. 20, p. 617–620.

Dalziel, I.W.D. 1997. Neoproterozoic-Paleozoic geography and tectonics: Review, hypothesis, environmental speculation. *GSA Bulletin*; v. 109; no. 1; p. 16–42.

DePaolo, D.J. and Wasserburg, G.J. 1976. Nd isotopic varations and petrogenetic models. *Geophysic Research Letters*, 3, 249-252.

DePaolo, D.J. 1981. A neodymium and strontium isotopic study of the Mesozoic calc-alkaline granitic batholiths of the Sierra Nevada and Peninsular Ranges. *California Journal of Geophysical Research* 86, 10470–10488.

Fernandes, L.A.D., Menegat, R., Costa, A.F.U., Koester, E., Kramer, G., Tommasi, A., Porcher, C.C., Ramgrab, G.E., Camozzato, E. 1995a. Evolução tectônica do Cinturão Dom Feliciano no Escudo Sul-rio-grandense: Parte I - uma contribuição a partir do registro geológico. *Revista Brasileira de Geociências*, 25: 351-374

Fernandes, L.A.D., Menegat, R., Costa, A.F.U., Porcher, C.C., Tommasi, A., Kraemer, G., Rambgrab, G.E., Camozzato, E. 1995b. Evolução tectônica do Cinturão Dom Feliciano no Escudo Sul-riograndense: uma contribuição a partir das assinaturas geofísicas. *Revista Brasileira de Geociências*, 25, 375–384.

Finch, R.J. & Hanchar, J.M. 2003. Structure and Chemistry of Zircon and Zircon-Group Minerals *in Reviews in Mineralogy & Geochemistry Vol. 53*: Zircon, John M. Hanchar & Paul W.O. Hoskin, editors.

Fragoso-César, A. R. S. 1991. **Tectônica de Placas no Ciclo Brasiliano: As Orogenias dos Cinturões Dom Feliciano e Ribeira no Rio Grande do Sul.** Tese de Doutorado, USP, São Paulo. 367 p.

Frimmel, H.E., Basei, M.S., Gaucher, C. 2011. Neoproterozoic geodynamic evolution of SW Gondwana: a southern African perspective. *Int J Earth Sci (Geol Rundsch)*, 100:323–354

Foster, D.A., Goscombe, B.D., Newstead, B., Mapani, B., Mueller, P.A., Gregory, L.C., Muvangua, Foster, D.A., Goscombe, B.D., Newstead, B., Mapani, B., Mueller, P.A., Gregory, L.C., Muvangua, E. 2015. U–Pb age and Lu–Hf isotopic data of detrital zircons from the Neoproterozoic Damara Sequence: Implications for Congo and Kalahari before Gondwana. *Gondwana Research*, 28 (1), pp. 179-190. doi:10.1016/j.gr.2014.04.011E.

Frimmel, H.E., Basei, M.S., Gaucher, C. 2011. Neoproterozoic geodynamic evolution of SW Gondwana: a southern African perspective. *Int J Earth Sci (Geol Rundsch)*, 100:323–354

Gruber, L., Porcher, C. C., Lenz, C., Fernandes, L.A.D. 2011. Proveniência de metassedimentos das sequências Arroio Areião, Cerro Cambará e Quartzo Milonitos no Complexo Metamórfico Porongos, Santana da Boa Vista, RS. *Pesquisas em Geociências*, Vol 38, n.1: 205-224.

Hoffman, P. F., 1991, Did the breakout of Laurentia turn Gondwana inside out?: *Science*, v. 252, p. 1409–1412.

Jacobsen, S.B and Kaufman, A.J. 1999. The Sr, C and O isotopic evolution of Neoproterozoic seawater. *Chemical Geology*, 161: 37–57.

Jost, H. & Bitencourt, M.F. 1980. Estratigrafia e tectônica de uma fração da faixa de Dobramentos de Tijucas no Rio Grande do Sul. *Acta Geologica Leopoldensia*, 4(7): 27-60.

Kinny, P.D., Maas, R. 2003. Lu-Hf and Sm-Nd isotope systems in zircon. *Reviews in Mineralogy and Geochemistry* 53, 327-341.

Lena, L., Pimentel, M.M., Phillip, R.P., Armstrong, R., Sato, K. The evolution of the Neoproterozoic São Gabriel juvenile terrane, southern Brazil based on high spatial resolution U-Pb ages and δ18O data from detrital zircons. *Precambrian Research*, 247, 126-138.

Lenz, C.C., Porcher, C.C., Fernandes, L.A.D., Masquelin, H., Koester, E., Conceição, R.V. 2012 Geochemistry of the Neoproterozoic (800–767 Ma) Cerro Bori orthogneisses, Dom Feliciano Belt in Uruguay: tectonic evolution of an ancient continental arc. *Mineralogy and Petrology*, 107(5):785-806.

Levorson, A.I. 1933. Studies in Paleogeology. *Bulletin of the American Association of Petroleum* Geology, Vol. 17, pp. 1107-1132.

Li, Z.X., Bogdanova, S.V., Collins, A.S., Davidson, A., de Waele, B., Ernst, R.E., Fitzsimons, I.C.W., Fuck, R.A., Gladkochub, D.P., Jacobs, J., Karlstrom, K.E., Lu, S., Natapov, L.M., Pease, V., Pisarevsky, S.A., Thrane, K., Vernikovsky, V. 2008. Assembly, configuration, and break-up history of Rodinia: A synthesis, *Precambrian Research*. v. 160, 1-2: 179-210.

Loewy, S. L., Dalziel, I.W.D., Pisarevsky, S., Connely, J.N., Tait, J., Hanson, R.E., Bullen, D. Coasts Land crustal block, East Antarctica: A tectonic tracer for Laurentia? *Geology*, v.39, p.859-862. doi:10.1130/G32029.1;

Meert, J.G., Torsvik, T.H., 2003. The making and unmaking of a supercontinent: Rodinia revisited. *Tectonophysics* 375, 261–288.

Mulder, J.A., Halpin, J.A., Daczko, N.R. 2015. Mesoproterozoic Tasmania: Witness to the East Antartica-Laurentia connection with Nuna. *Geology*, published online on 28 July 2015 as doi:10.1130/G36850.1

Nyberg, B., and Howell, J.A. 2015. Is the present the key to the past? A global characterization of modern sedimentary basins. *Geology*, v. 43, p. 643-646.

Patchett, P.J., Kouvo, O., Hedge, C.E. and Tatsumoto, M. 1981. Evolution of continental crust and mantle heterogeneity: evidence from Hf isotopes. *Contribs. Mineral. Petrol*. 78, 279-297.

Pertille, J., Hartman, L.A., Phillip, R.P. 2015a. Zircon U-Pb age constraints on the Paleoproterozoic sedimentary basement of the Ediacaran Porongos Group, Sul-Riograndense Shield, southern Brazil. *Journal of South American Earh Sciences*, 63, pp.334-345. DOI: 10.1016/j.jsames.2015.08.005

Pertille, J., Hartmann, L.A., Phillip, R.P., Petry, T.S., Lana, C.C. 2015b. Origin of the Ediacaran Porongos Group, Dom Feliciano Belt, southern Brazilian Shield, with emphasis on whole rock and detrital zircon geochemistry and U-Pb, Lu-Hf isotopes. *Journal of South American Earth Sciences*, 64, pp. 69-93. DOI: 10.1016/j.jsames.2015.09.001

Porcher, C. C., Macnaughton, N. J., Leite, J. A. D., Hartmann, L. A., Fernandes, L.A.D. 1999. Idade SHRIMP do vulcanismo ácido do Complexo Metamórfico Porongos, RS.. In: **1º SIMPÓSIO SOBRE VULCANISMOS E AMBIENTES ASSOCIADOS**, 1999, Gramado. Resumos... 1999. Sociedade Brasileira de Geologia.

Rapela, C.W., Fanning, C.M., Casquet, C., Pankhurst, R.J., Poiré, L.S.D. Baldo, E.G. 2011. The Rio de la Plata craton and the adjoining Pan-African/brasiliano terranes: Their origins and incorporation into south-west Gondwana, *Gondwana Research*, (20):4, p. 673-690.

Rogers, J.J.W., 1996. A history of continents in the past three billion years. *Journal of Geology* 104, 91–107.

Rooney, A.D., Strauss, J.V., Brandon, A.D., Macdonald, F.A. 2015. A Cryogenian chronology: Two long-lasting synchronous Neoproterozoic glaciations. *Geology*, 43, 459-462. doi:10.1130/G36511.1.

Saalmann, K., Remus, M. V. D., Hartmann, L.A, Koester, E., Conceição, R.V. 2006. Sm–Nd isotope geochemistry of metamorphic volcano-sedimentary successions in the São Gabriel Block, southernmost Brazil: evidence for the existence of juvenile Neoproterozoic oceanic crust to the east of the Rio de la Plata craton. *Precambrian Research* 136 , 159–175.

Saalmann, K., Gerdes, A., Lahaye, Y., Hartmann, L.A., Remus, M.V.D., Läufer, A. 2010. Multiple accretion at the eastern margin of the Rio de la Plata craton: the prolonged Brasiliano orogeny in southernmost Brazil. *International Journal of Earth Sciences*, (100) 355-378.

Schwartz, J. J., Gromet, L. P. 2004. Provenance of a late Proterozoic early Cambrian basin, Sierras de Córdoba, Argentina. *Precambrian Research* 129:1–21.

Stacey, J.S., and Kramers, J.D. 1975. Approximation of terrestrial lead isotope evolution by a two-stage model. *Earth and Planetary Science Letters*, v. 26, p. 207–221, doi:10.1016/0012-821X(75)90088-6.

Taylor, S.R., and McLennan, S.M. 1985. **The continental crust: its composition and evolution**. Blackwell, Oxford.

Tosdal, R.M. 1996. The Amazon–Laurentia connection as viewed from the Middle Proterozoic rocks in the central Andes, western Bolivia and northern Chile: *Tectonics*, v. 15, p. 827–842, doi:10.1029/95TC03248.

Research Paper

Dear Leonardo,

We have received your article "Isotope geochemistry and geochronology on record of syn-depositional volcanism in Porongos Metamorphic Complex, Santana da Boa Vista Antiform, Dom Feliciano Belt, Brazil: Onset of an 800 Ma continental arc" for consideration for publication in Journal of South American Earth Sciences.

Your manuscript will be given a reference number once an editor has been assigned.

To track the status of your paper, please do the following:

1. Go to this URL: http://ees.elsevier.com/sames/

2. Enter these login details:
Your username is: leonardogruber@gmail.com
If you need to retrieve password details, please go to:
http://ees.elsevier.com/sames/automail_query.asp

3. Click [Author Login]
This takes you to the Author Main Menu.

4. Click [Submissions Being Processed]

Thank you for submitting your work to this journal.

Kind regards,

Elsevier Editorial System
Journal of South American Earth Sciences

Isotope geochemistry and geochronology on record of syn-depositional volcanism in Porongos Metamorphic Complex, Santana da Boa Vista Antiform, Dom Feliciano Belt, Brazil: Onset of an 800 Ma continental arc

Leonardo Gruber[1], Carla Cristine Porcher[2], Edinei Koester[2], Anelise L. Bertotti[3], Cristine Lenz[3], Luís Alberto D'Ávilla Fernandes[2], Marcus Vinícius Dorneles Remus[2]

1 - Programa de Pós-graduação em Geologia da Universidade Federal do Rio Grande do Sul - Instituto de Geociências, Av. Bento Gonçalves, 9500. Porto Alegre, RS, Brasil - CEP 91501-970. leonardogruber@gmail.com*
2 - Departamento de Geologia, UFRGS. Av. Bento Gonçalves, 9500. Porto Alegre, RS, Brasil - CEP 91501-970. Carla.porcher@ufrgs.br; koester@ufrgs.br; marcos.remus@ufrgs.br; ladfernandes@gmail.com
3 – Núcleo de Geologia, UFS - Cidade Universitária Prof. José Aloísio de Campos, Av. Marechal Rondon, s/n Jardim Rosa Elze - CEP 49100-000 - São Cristóvão, SE, Brasil. crislenz@yahoo.com.br; aneber79@gmail.com.

*Corresponding author.

ABSTRACT

The Porongos Metamorphic Complex (PMC) is composed of supracrustal rocks, predominantly pelitic micaschist, quartzite and felsic metavolcanic rocks. It represents remains of a Neoproterozoic sedimentary basin developed in the western Gondwana, now located in the central section of Dom Feliciano Belt in southern Brazil. Detrital zircon age spectra and isotope signature comparison shows that there are at least three main source-areas for the Porongos sediments: (i) one that can be related to Paleoproterozoic terrains; (ii) a younger component with Mesoproterozoic (1.5 - 1.2 Ga) ages; and (iii), a Neoproterozoic source with magmatic zircons (0.8 Ga), with relative age distribution mostly between 1.7 and 1.0 Ga, T_{DM} ages between 2.58 and 1.71 Ga, and younger ages of ca. 1.21 Ga, which can be related to 1.4 - 1.0 African signature sources. Twenty zircon grains from a metasandstone rock yield $^{206}Pb/^{238}U$ age of 804 ± 12 Ma, which is related to metavolcanic samples from PMC and correlates with the Neoproterozoic Cerro Bori Continental Arc, indicating a syn-depositional volcanism in the sedimentary record. The depositional setting for these sequences can be understood as an evolution between a passive margin developed after 1.6 Ga and a terrain-collisional setting (ca. 570 Ma).

Keywords: Porongos Metamorphic Complex; Provenance; U-Pb zircon ages; Sm-Nd; Pb-Pb; Isotope Geochemistry; Geochronology

1. INTRODUCTION

Understanding the tectonic evolution of Neoproterozoic mobile belts in South America depends heavily on accurate and robust geochronological and isotopic constraints, since much of the geological record is not preserved. The Neoproterozoic Dom Feliciano Belt (DFB) was formed by the interactions between the cratons Rio de la Plata, in the west (Fig. 1a), Kalahari and Congo to the east (e.g. Fernandes et al., 1995a; Frantz et al., 1999; Chemale., 2000). The tectonic interactions between these three cratonic blocks have been intensively investigated (e.g. Basei et al., 2008; Saalmann et al., 2010; Rapella et al., 2011), and despite the controversies upon age of sedimentation, provenance and tectonic evolution raised by the different authors, it is clear that DFB represents one of the key areas to understand the assembly and evolution of west Gondwana during mid to late Neoproterozoic.

Studies have addressed several different aspects of the evolution of DFB, including: structural and geophysical-based divisions on three domains (Fig.1b), the age of deposition of the post-collisional sedimentary sequences, age of metamorphism and emplacement of granite intrusions and evolution of its calc alkaline arc magmatism of Pelotas Batolith (Fig.1c) (e.g. Fernandes et al., 1995a; Phillip and Machado, 2005; Borba et al., 2006; Basei et al., 2008; Saalmann et al., 2010; Rapela et al., 2011; Chemale et al., 2012). The metasedimentary rocks exposed in the three domains had also been investigated in various works (e.g. Basei et al., 2008; Gruber et al., 2011; Lena et al., 2015; Lopes et al., 2015; Pertille et al., 2015a and b).

The lithodemic units of the Porongos Metamorphic Complex (PMC) (Fig. 2a) are exposed along the central portion of the Dom Feliciano Belt. These comprise mainly phyllite, meta-psamites, meta-conglomerates, mica schist and quartz mylonite (mylonitic quartzites) with interbedded metaultramafic and metavolcanic rocks, marbles and minor amphibolites intruded by granitoids sheets, all deformed and metamorphosed under greenschist to amphibolite facies conditions (Jost and Bitencourt, 1980; Jost, 1982; Porcher and Fernandes, 1990; Remus et al., 1987; 1990; 1991). The sequences of quarzites were designed as Santana Formation, with maximum depositional ages of ca. 1.7 Ga (Pertille et al., 2015b), coinciding with stabilization of Columbia's supercontinent formation. The metapelitic sequences (Arroio Areião, Cerro Cambará lithodemic units) displays a more incongruent maximum depositional age, thus being studied here in more detail.

The depositional age of schists are constrained between age a minimum depositional age obtained from metavolcanic rocks of ca. 780 Ma (Porcher et al., 1999), and age components with maximum depositional age indicated by Gaussian peaks of ca. 570 - 620 Ma (Basei et al., 2008; Pertille et al., 2015b). Previous works considered the deposition age as ca. 880 Ma, as suggested by maximum depositional ages from Santana fm. with U-Pb detrital zircon ages (Hartmann et al., 2004; Saalmann et al., 2006; Pertille et al., 2015a), which could still hold significance, taking in account that different lithodemic units could have been deposited at different times.

Uncertainties in these depositional ages have resulted in different interpretations about evolution of PMC and, therefore, these same uncertainties remains to the central part of the DFB, including diachronism of volcanic events and sedimentary deposition on the passive/rifting margins of Congo/Kalahari and La Plata cratons.

We present data on whole-rock (Sm-Nd, Pb-Pb) and zircon U-Pb detrital zircon ages which may help to recognize source-areas, besides the possibility of a syn-depositional volcanism in the vicinity of the paleobasin. Also, we aim to constraint the relative situation and tectonic significance of the PMC in the geodynamic model of pre-Gondwana assemblage.

INSERT FIGURE 1

INSERT FIGURE 2

2 – GEOLOGIC SETTING

The PMC crops out in the Central Domain (Fernandes et al. 1995a) (Fig.2a) of the DFB in Rio Grande do Sul state. The DFB is the southern Brazil part of a long and discontinuous Neoproterozoic orogenic belt (Fig. 1-b and c). It can be resumed as follows: from west (proximal to La

Plata craton) to east (Atlantic margin) are the São Gabriel Block, composed of juvenile calk-alcaline granitoids and metasedimentary sequences deposited in a backarc system (Hasui et al., 1975; Almeida, 1981; Hartmann et al., 2000; Saalmann et al., 2005); east of São Gabriel Block stands the Camaquã Basin, a late-to-post orogenic fault-bonded basin with development in the late Neoproterozoic (Borba et al., 2006). The most prominent tectonic domain of DFB is the Pelotas Batholith, composed of six granite suites and small exposures of granitic-gneissic complexes and Paleoproterozoic basement (Phillip & Machado, 2005).

In the Rio Grande do Sul district, the DFB can be divided in three major tectonic domains (Fernandes et al., 1995a and b) (Fig.1b): (*i*) the western domain, separated from the central domain by the Caçapava Suture, is interpreted as a magmatic arc with juvenile crust and tectonically interleaved with remnants of ophiolites and supracrustal rocks. It is separated from the Rio de La Plata craton by the São Gabriel Suture (Fernandes et al., 1995b); (*ii*) the central domain is composed by palaeoproterozoic rocks interpreted as a tectonically reworked segment of the Rio de La Plata Craton. It was separated from the mainland during the opening of a marginal basin which widening evolved into the Charrua Sea (Fragoso-César, 1991); and (*iii*) the eastern domain is composed of calc-alkaline orogenic granitoids interpreted as part of a Neoproterozoic continental-margin magmatic arc and is separated from the central domain by the Porto Alegre Suture, a major gravimetric and magnetometric anomaly.

In the southern continuation (Uruguay), the DFB is represented by its eastern domain. Following recent works, the DFB were considerate as separated from La Plata craton by the Sierra Balena Shear Zone (SBSZ) to the west, which overprint the Porto Alegre Suture in Brazil. The age of low temperature of latest stage of deformation in the SBSZ was dated by ^{40}Ar-^{39}Ar at 580-550 Ma (Oyhantçabal et al., 2010). The eastern domain oldest lithodemic units are represented in the Cerro Olivo Complex (Gross et al., 2009), intruded by the ca. 800 Ma Cerro Bori orthogneisses, interpreted as a Neoproterozoic continental volcanic arc (Lenz et al., 2011).

The PMC outcrops in a NE-SW trending terrain 150 km long and 10 to 15 km wide, with minor segments of its basement, the Encantadas Complex, tectonically interleaved in the west portion. The PMC is composed mainly of metasedimentary and metavolcanic sequences intruded by granitoid sheets. However the original stratigraphy is poorly preserved due to superimposed deformation and metamorphism including high strain zones (Jost & Bitencourt, 1980; Fernandes et al., 1992; 1993).

The lithodemic units comprising DFB are affected by syn-to-post accretionary strain of what is interpreted as successive subductions and collisions (Fernandes et al., 1995a; Frantz et al., 1999) or the collision of a microplate or terrain on the reworked margin (Tandilla belt) of La Plata craton; (Chemale., 2000; Rapela et al., 2011; Chemale et al., 2012). This same strain is responsible, at least in part, for the obliteration of the original framework of the PMC metasedimentary sequences and intrusive rocks. Lack of primary contacts, bedding and way-up criteria also cause stratigraphic relationship to be a problematic issue. The best constraining regarding the PMC paleobasin fill is suggested by lack of Neoproterozoic zircon detrital grains in the quartzites of Santana Formation, with a maximum depositional age for these quartzites of ca. 1.7 Ga (Pertille et al., 2015a).

The outcropping pattern of the PMC is controlled by regional NE-SW antiforms, that folded the main ductile fabric, and by late NE-SW strike slip and normal faults. In the PMC central-west portion, the metasedimentary lithodemic units outcropping are exposed along the limbs of the Santana da Boa Vista Antiform, in the central region of the PMC (Fig. 2a), classified accordingly to having an autochthone and para-autochthone origin and named as Arroio Areião schists and the Cerro Cambará schists, respectively (Jost & Bitencourt, 1980). These units are interlayered by mylonitic granitoids and quartz mylonite lenses. This antiform structure continues to the south, with the same conditions of tectonic imbrication (Porcher, 1990) in the Serra do Godinho Antiform, where metandesitic rocks are observed in the sequence (Chemale, 2000). Basement rocks (mainly high-grade gneisses and amphibolites of the Encantadas Complex) exposed in these antiforms cores are in tectonic contact with PMC rocks by folded shear zones with top to NE-SW stretching lineation and top to NE cinematic indicators (Porcher and Fernandes, 1990). To the central-north of this structure is the Serra dos Pedrosas Antiform, whose rocks comprise metapelites and metavolcanics from the Cerro Cambará, Rincão do Maranhão and Cerro do Facão schists. These display a higher degree of metamorphism with P-T conditions up to amphibolite facies. The timing of peak of progressive metamorphism was estimated with the mylonitic fabric that reworked the progressive metamorphic assemblage was dated on 507 ± 38 to 524 ± 17 in mylonitic schists in the western area of PMC (Lenz 2006).

Schists from both Arroio Areião and Cerro Cambará schists have almost the same mineralogy and textures, with S2 foliation and main mineralogy of chlorite ± muscovite ± biotite and quartz. In the northwest of PMC, serpentinites interpreted as being of ophiolite signature occur in the Capané Antiform, associated with basic to acidic metavolcanic rocks, alkaline orthogneiss and metasedimentary rocks ranging from metaconglomerates to pelitic schists (Marques et al., 2003; Gollmann et al., 2008). The meta-ultramafic lithodemic unit is interpreted as a mélange tectonically emplaced in the volcanic and sedimentary rocks, which is interpreted as a subduction of oceanic crust (Marques et al., 1998a, 1998b). Ar-Ar ages obtained from micas in the Capané schists displayed ages of ca. 600 Ma, thus indicating a possible minimum age deposition to these schists sequences (Porcher et al., 2010).

INSERT FIGURE 3

4 - SAMPLES

Fourteen samples were collected in the western, eastern and southeastern limbs of the Santana da Boa Vista and Cerro do Godinho Antiforms. Sample location is shown in Figure 2a. Samples consist of metapelites, mainly chlorite-muscovite schists (POR13, POR12 and POR04 from the eastern side of the Santana Antiform; and RIP03, RIP05, RIP06, RIP07 and RIP09 from the western and southern areas of the same antiform, as well as from one area to the north of Cerro do Godinho Antiform), quartz mylonites from the eastern limb of the Cerro do Godinho Antiform, and (quartz)-muscovite-chlorite schists from the eastern side of Santana Antiform (POR11 and POR06). Also from the eastern Santana Antiform, were collected a fine-grained rock (POR18). Petrography depicts a feldspar-quartz-muscovite-chlorite schist, with deformed plagioclase with grain size <0.2mm, and smaller grains of chlorite and micas in millimeter lenses, with plagioclase porphyroclasts in a biotite-quartz-feldspatic lepidoblastic matrix (Fig.2c and d), also displaying iron oxides.

Other metapelitic samples display quartz lenses of millimeter to centimeter thickness in schist samples of the eastern areas (POR11), with quartz and recrystallized plagioclase occurring in centimetric to millimetric porphyroclasts (see Table 1 for summary on sample descriptions). Quartz boudins are common. Matrix generally displays granoblastic quartz with folded pervasive micas. Some quartz lenses occur parallel to folding, whereas some occur at high angle (90°). Some mica displays augen features with quartz grains. Zircon where commonly found associated with muscovite, and in some cases, small (<25 micra) zircon grains occur associated with quartz. Muscovite displays bookshelves with granoblastic quartz. Parasitic folds occur marked by asymmetric foliation and crenulation. In some samples (POR 04, 06, 11) occur phlogopite in intrafolial fold within the lepidoblastic matrix. The lepidoblastic matrix is composed of thin lenses of < 1mm biotite, interlayered between polygonal granoblastic quartz and plagioclase grains varying from 0.2 to 0.6 mm.

INSERT TABLE 1

5 – METHODS

5.1 – WHOLE-ROCK GEOCHEMISTRY AND ISOTOPIC ANALYTICAL TECHNIQUES

All the isotopic analyses discussed here were carried out at the Isotope Geology Laboratory of Rio Grande do Sul Federal University (UFRGS).

Whole-rock major and minor element geochemistry analyses were carried out in samples POR 04, 06, 11, 12, 13 and 18 using a Rigaku RIX 2000 X Ray Fluorescence (XRF) at the Geochemistry Laboratory of UFRGS. All analyzed samples displayed high loss on ignition values, being indicative that these samples were affected by alteration. More details on the methodology can be obtained in Brown et al (1973).

For Sm-Nd analyses, sample dissolution was carried out in Teflon Savillex beakers, with Sm and Nd extraction from about 0.15g whole-rock powders from each sample. Conventional chromatography cation-exchange methods were used, with dissolution in HNO_3 and HF in

Savillex® vials, with the addition of mixed $^{149}Sm/^{150}Nd$ tracer. REEs were separated in cationic exchange AG- 50W-X8 resin columns (200 to 400 mesh), and Sm was separated from Nd with anionic exchange LN-B50-A resin columns (100 to 200 μm). The analyses were carried out using a Finnigan Neptune ICPMS. Uncertainties on Sm/Nd and $^{143}Nd/^{144}Nd$ ratios are considered better than ± 0.1% (1σ) and ± 0.00001 (1σ), respectively, based in repeated analysis of BHVO-1 standard. $^{143}Nd/^{144}Nd$ was normalized to $^{146}Nd/^{144}Nd$ ratio of 0.7219. The raw data were reduced using Excel macros made in house. Details on sample dissolution and analysis parameters can be found in Gioia & Pimentel (2001). T_{DM} values were calculated using DePaolo (1981) model.

Pb-Pb analyses were carried out with the same sample dissolution, and were analyzed in Finnigan Neptune ICPMS. Uncertainties on $^{207}Pb/^{206}Pb$ are considered better than ± 0.1% (1σ) and ± 0.00001 (1σ), respectively, based repeated analyses of BHVO-1 standard. Details in sample dissolution and analysis parameters can be found at Abre et al (2012).

5.2 - ZIRCON U-Pb GEOCHRONOLOGY

Zircon grains were mounted in epoxy mounts. Images of zircons were obtained using an optical microscope as well as a back-scattered electron detector coupled to a JEOL JSM 5800 electron microscope. Zircon grains were dated with laser ablation microprobe (New Wave UP213) coupled to a MC-ICP-MS (ThermoFinnigan-Neptune) at the Isotope Geology Laboratory of UFRGS. Isotope data where acquired using static mode with spot size of 25 µm, with frequency of 10 Hz and intensity of ~4 J/cm^2. Analyses were made in 40 cycles of 1 s, with laser-induced elemental fractionation and instrumental mass discrimination corrected by GJ-1 (standard zircon) with the measurement of two GJ-1 analyses to every ten sample zircon spots. Details on configuration and other analysis parameters can be found in Chemale et al (2012). The external error was calculated after propagation of the error of the GJ-1 mean and the individual sample zircon. Data were reduced using in-house programs developed at the Isotope Geology Laboratory of UFRGS. Age calculations were carried out with ISOPLOT 3.0 (Ludwig, 2003).

6 – RESULTS

6.1 – WHOLE ROCK GEOCHEMISTRY

CIA (Chemical Index of Alteration) values, which indicates influence of original weathering on sediments composition varied from 65.19 to 85.96. Metasandstone displayed value of 77.35, which is characteristic of middle to highly weathered sediments (Nesbitt and Young, 1982; Taylor and McLennan, 1985). These values could also be representing remobilization, since hydrothermal liquids from metamorphism could lead to alteration of the original composition of these values.

SiO_2 and Al_2O_3 content indicate sedimentary protoliths with granitic composition compared to granite and mafic standards. Values of TiO_2/Zr below 0.33 were found in three of four available samples, indicative of pelitic sources. When compared to other chlorite schists, quartzites and phyllites from Capané Antiform, the values found in Santana da Boa Vista Antiform presents a diversity of protolith composition, with metasandstone (POR18B) composed of immature sediments (pelitic sources) (Fig.5d).

INSERT FIGURE 4

6.2 - Sm-Nd ISOTOPE GEOCHEMISTRY AND GEOCHRONOLOGY

Sm-Nd isotopic data for the PMC are shown in Table 3. $\varepsilon_{Nd}(T)$ values were calculated for ca.750 Ma, which can be used as average age of deposition for all PMC metasediments.

Samples from metasedimentary rocks of the Rincão do Maranhão, Cerro Cambará and Cerro do Facão show less variation in T_{DM} and ε_{Nd} values when compared with those from the Arroio Areião sequence. For the Cerro Cambará rocks, T_{DM} values are of ca. 1.74 Ga in the Santana da Boa Vista Antiform, and range from 1.56 to 1.90 Ga in the Serra dos Pedrosas antiform. Supracrustal rocks from the Serra dos Pedrosas Antiform includes the Rincão do Maranhão schists, which display T_{DM} values between 1.71 and 1.75 Ga, and the Cerro do Facão metasediments, with T_{DM} values varying from 1.64 to 2.00 Ga (Fig. 4-b). Rocks of the Arroio Areião displays a more varied pattern for both model ages and ε_{Nd} values, with T_{DM} varying between 1.40 and 2.58 Ga, and $\varepsilon_{Nd}(T)$ at the age of deposition varying from -11.5 to 0.7 (Fig. 4-c).

ε_{Nd} values of the Arroio Areião near the eastern flank of the Santana da Boa Vista Antiform suggest mafic source-rocks, possibly those from northern part of the belt. Variation of Nd (ppm) X $\varepsilon_{Nd}(T)$ suggests mixture between detrital sedimentary and volcanic rocks (Fig. 4-d).

INSERT FIGURE 5

6.3 – Pb-Pb ISOTOPE GEOCHEMISTRY

Although Pb is a more mobile element than Sm and Nd during secondary processes, comparisons between thorogenic and uranogenic Pb may be used to help distinguishing between different tracts of sialic crust and, therefore, source rocks of detrital sedimentary rocks (Kay et al., 1996; Tosdal, 1996; Loewy et al., 2003 Schwartz and Gromet, 2004; Oyhantçabal et al., 2011).

The samples investigated in this work, from both the Arroio Areião and the Cerro Cambará schists, have uranogenic $^{207}Pb/^{204}Pb$ ratios higher than 15.50, and $^{206}Pb/^{204}Pb$ values higher than 18.55. Samples from Cerro Cambará plot near values for the Kalahari granitoids and Cerro Bori orthogneiss, with values varying from $^{206}Pb/^{204}Pb$ of ca. 19.0 and $^{207}Pb/^{204}Pb$ of ca. 15.75. Both thoro-uranogenic and uranogenic values plot above the H&K (Stacey & Kramers, 1975) curve of evolution of crustal rocks, indicating sources that were highly radiogenic compared to average crust.

Regarding the metasedimentary sequences described, they should be useful as an indicator of possible mixtures between strongly different source-areas. Basements like those of Laurentia display $^{206}Pb/^{204}Pb$ ratios below 19.0, and $^{207}Pb/^{204}Pb$ below 15.5, whereas these values for both Kalahari and La Plata cratons are substantially higher. The analysis of orthogneisses from Cerro Bori (in the Uruguayan eastern domain of DFB) has provided values comparable to those obtained in granitoids from Fafa, Africa (Lenz et al., 2012).

Samples from Arroio Areião do display a broader pattern, plotting between those values typical of the Kalahari and Rio de La Plata cratons (Fig. 5-A). Samples RIP 03 and 05, located west of Santana Antiform, displayed very high radiogenic Pb content. Thoro-uranogenic values suggests a variation on terrain sources from West and East of Santana da Boa Vista Antiform (Fig. 5-B), although these metasediments probably have a common source.

INSERT FIGURE 6

6.4 - GEOCHRONOLOGY

Aiming to constraint possible depositional age and syn-depositional volcanism in the metasedimentary units, ten zircon grains of the sample POR 18 analyzed were selected to be studied here. The Neoproterozoic nine concordant analyses resulted in $^{207}Pb/^{206}Pb$ ages varying from 765 ± 19 Ma to 796 ± 19 Ma (Fig. 6). The concordant analyses yielded a Concordia age of 804 ± 12 Ma (Fig. 5-C). Samples from schists of the same sequence have older zircon grains, ranging from 1113 ± 42 Ma to 2195 ± 31 Ma (Gruber et al., 2011). The prevalence of ages clustered between 821 and 710 Ma possibly indicates a unique source-rock.

INSERT TABLE 2

INSERT TABLE 3

INSERT TABLE 4

INSERT TABLE 5

7 - DISCUSSION

7.1 – Source-areas

Since practically all PMC samples analyzed here and in others works displayed detrital ages of ca. 2.2 and 2.0 Ga, Encantadas should have acted as a main source to all formations in the PMC. This source is also represented in negative εNd values displayed in Fig 4-A.

Similar detrital zircon ages (see Fig. 2-B) occur in both the Arroio Areião and Cerro Cambará schists, although the younger ages obtained are from the first lithodemic unit. Differences in the $^{207}Pb/^{206}Pb$ ratios detailed in the results section can indicate mixture between African sources with Elzeverian zircon ages with reworked La Plata sediments. Mesoproterozoic detrital zircon ages from Cerro Cambará displays the same U-Pb ages compared to Arroio Areião, although ƐNd value of -13 indicates evolved-crustal sources. The Arroio Areião samples displays variable values both in ƐNd X Nd (ppm) and in T_{DM} X ƐNd (t), plotting closer to values obtained in metavolcanic rocks due north of collected samples (Fig. 4-A) (Chemale, 2000). This suggest a tectonic setting where the sediments of Arroio Areião where deposited along volcanic rocks of ca. 800 Ma. The presence of detrital zircon grains with same ages from obtained in zircons from metavolcanics rocks dating of ca. 780 Ma corroborates to the suggestion of Arroio Areião unit being a mixture of the older detritus, probably composed of quartz milonytes, with younger and juvenile volcanic local sources.

Metabasalts with OIB-MORB geochemistry from Capané antiform displays slightly negative ƐNd (Gollmann et al., 2008), and T_{DM} ages varying from Paleo to Mesoproterozoic, compatible with those presented here (Fig. 4-A), which could argue favorable to the hypothesis of these sediments having the same source. If they indeed have same source, the OIB-MORB characteristic of these metabasalts could represent consumption of oceanic crust in a collisional setting. In this case, another source could be argued to the Neoproterozoic sediments, as part of the Dom Feliciano arc (Chemale et al., 2012). These characteristic OIB-MORB metabasalts can argue favorably to an arc or back-arc setting to this PMC section, now localized in the northeastern section of the belt. Comparison between metasediments and metavolcanics from the Capané Antiform (Gollmann et al., 2008) suggests a strong similarity between the metasediment source rocks and Porongos metavolcanics, but volcanic zircon ages obtained in metatuffs from the Capané Antiform displayed younger ages, ranging from 601 ± 2.6 to 578 ± 1.6 Ma (Kohlrausch, 2013), thus indicating that these are not the same sources as the sources in Santana da Boa Vista Antiform.

All samples from east and southeast of Santana da Boa Vista Antiform displays Pb/Pb values comparable to those of Nico Perez and Punta del Este terrains, with $^{206}Pb/^{204}Pb$ varying from ca. 21 to ca.18, and $^{207}Pb/^{204}Pb$ from ca.15.7 to ca.15.9 (see Fig. 5-A), nearer to the La Plata craton. Since there is less indicators of La Plata sources for Mesoproterozoic detrital zircon ages, and evidence for an agglutination of Braziliano terrains of Dom Feliciano and Nico Perez only in Neoproterozoic (Oyhantçabal et al., 2011), sources from or near La

Plata, principally the accreted terrains of Nico Perez and Mar del Plata, are those with younger (<0.9 Ga) ages.

7.2 – Syn-volcanic deposition (ca.780 Ma)

The zircons dated in sample POR-18 could be implying a syn-depositional volcanic event. Following Congo-Kalahari rifting phase (780-740 Ma), Adamastor Ocean begins consumption on its active margins until final stages of Adamastor ocean basin closure (ca. 550 Ma, Gray et al., 2006). The event of rifting could be marking here the initial development of an active margin at RdLP craton.

7.3 – Tectonic setting and evolution

Paleoproterozoic sources from basement, like Encantadas Complex, hardly serves to constraining the minimum timing of deposition. The emplacement age of Encantadas Complex in the PMC supracrustal rocks are estimated as a minimum age of the Braziliano tectonic transcurrency of 540 Ma and maximum age of subduction of oceanic plate in a continental crust and subsequent metamorphism in the Paleoproterozoic (Phillip et al., 2008), more probably at same time of deposition of the PMC lithodemic units in the Santana da Boa Vista Antiform area. Thus, can be considered that PMC’s paleobasin opened at least on ca. 0.9 Ga, in a passive margin or rifting system in the Adamastor ocean. The central section of DFB does have a rifting system active in the Tonian-Cryogenian (ca. 840 Ma, Basei et al., 2008), although these ages are not registered in the southern DFB.

There is a gap between 765-690 Ma in the detrital record for samples to the north and south of the Santana da Boa Vista Antiform, suggesting a non-deposition time span, or absence of source-areas of this age, and therefore can be interpreted as a change in tectonic setting. Since usually collisional settings produces low volumes of magma (Hawkesworth et al., 2010), the final setting of Porongos paleobasin can be considered as a continental orogenic accretionary setting, considering the very low input of ca. 700 Ma or younger detrital zircons. These ages are about the same ages verified in metavolcanics from Santana da Boa Vista Antiform (Porcher et al., 1999; Saalmann et al., 2010), in meta-arenites from Punta Mogotes borehole (Rapela et al., 2011) and in the Cerro Bori orthogneisses, interpreted as a continental volcanic arc (Lenz et al., 2012), which suggests a link between the dates obtained here and the evolution of continental margin in the RdLP craton. It’s important to note that there is registry of ca.780 Ma in SHRIMP U-Pb zircon ages obtained in a 3m-sized tonalitic xenolith (Silva et al., 1997a), with granitic-gneisses intruded in metasedimentary sequences of Pinheiro Machado Complex dated at ca. 631 Ma, interpreted as high grade metamorphism (Silva et al., 1997b). This tonalitic xenolith could be remnant of a ca. 800-780 Ma continental arc in the vicinity of PMC paleobasin.

Profundity of the paleobasin also should have influence on the metamorphism occurring at some portions of PMC while others remain an open basin in the Ediacaran (ca. 0.57 Ga), thus explaining some of the zircons displaying ca. 620-580.

The tectonic evolution is summarized in Fig.7.

INSERT FIGURE 7

8 - CONCLUSIONS

The metasediments from PMC can be divided accordingly to its geochemical and geochronological characteristics: Arroio Areião and Cerro Cambará schists in the east of Santana da Boa Vista Antiform in the Porongos Complex, with juvenile ƐNd factor (Arroio Areião) and sediments trending to those obtained in rocks of La Plata craton, distinct from the second group: Arroio Areião (Southwest of Santana da Boa Vista Antiform), Cerro Cambará (in East and Southeast of Santana da Boa Vista Antiform), Rincão do Maranhão and Cerro do Facão, with negative ƐNd and highly evolved crust in the sources. The quartz mylonites at Santana da Boa Vista Antiform were originally sediments with very negative ƐNd, and Paleoproterozoic to Archean model ages.

Since there is less indicators of a Laurentian-type crust in the source-areas, Porongos paleobasin should be localized somewhere between Kalahari, Congo and La Plata cratons, but Pb-Pb geochemistry suggests that La Plata was not a main source-area in the Mesoproterozoic. More detailed studies in this aspect should provide a better understanding of the boundaries of La Plata craton with DFB.

The PMC tectonic depositional setting of the Santana da Boa Vista Antiform schists (between ca. 780 Ma and ca. 590 Ma, with maximum depositional age of ca. 570 Ma) evolves from a passive margin, probably related to the rifting system of Adamastor Ocean, into an accretionary margin basin, ending with the consumption of Adamastor ocean plate and continental collision between accreted terrains of Kalahari, Congo and La Plata cratons. The clastic immature lithodemic units (metasandstones) were deposited at the same time as the volcanic rocks dated of ca. 780-800 Ma, thus indicating syn-depositional volcanism acting on the vicinity of PMC paleobasin. The absence of these volcanic ages in the central-southern PMC sequences (middle region of Santana da Boa Vista Antiform to south) could be explained by the paleotransport of sediments from south to north, or paleogradients in the paleogeography including topographic highs in the transport system. Younger detrital zircon ages (ca. 620-590 Ma) from Capané Antiform and Cerro do Godinho Antiform indicates another collisional setting (foreland setting), this time with the formation of Dom Feliciano Belt at ca. 570 Ma, thus putting these sequences as the base of Camaquã sedimentary sequences (Pertille et al., 2015b).

In summary, the same age (ca. 780-800 Ma) is registered in other sections of DFB, and were interpreted as the result of a continental volcanic arc. Considering the new detrital record (from PMC and Punta Mogotes fm.) displaying concordance with those volcanic sources, therefore can be interpreted as another evidence for a ca. 780-800 Ma continental arc acting during the pre-Gondwana amalgamation registered in the DFB.

Acknowledges

We would like to thank Agência Nacional do Petróleo, Gás Natural e Biocombustíveis (ANP), Financiadora de Estudos e Projetos (FINEP) and Ministério da Ciência e Tecnologia (MCT), (PRH-ANP/MCT), Petrobras PRH-PB215 for studentship (first author) and LGI-UFRGS staff for providing analysis and technical support.

9 - REFERENCES

Abre, P., Cingolani, C.A., Cairncross, B., Chemale Jr., F. 2012. Siliciclastic Ordovician to Silurian units of the Argentine Precordillera: Constraints on provenance and tectonic setting in the proto-Andean margin of Gondwana. Journal of South American Earth Sciences 40, 1-22.

Almeida, F.F.M., Hasui, Y., Brito Neves, B.B., Fuck, R.A. 1981. Brazilian Structural Provinces: An introduction. Earth Science Reviews 17, 1-29.

Basei, M. A. S., Frimmel, H. E., Nutman, A. P., Preciozzi, F. 2008. West Gonduana amalgamation based on detrital zircon ages from Neoproterozoic Ribeira and Dom Feliciano belts of South America and comparison with coeval sequences from SW Africa. Geological Society, London, Special Publications 2008; v. 294; 239-256

Basei, M.A.S., Campos Neto, M.C., Castro, N.A., Nutman, A.P., Wemmer, K., Yamamoto, M.T., Hueck, M., Osako, L., Siga, O., Passarelli, C.R. 2011. Tectonic evolution of the Brusque Group, Dom Feliciano belt, Santa Catarina, Southern Brazil. Journal of South American Earth Sciences, 32, 24-350.

Borba, A.W., Mizusaki, A.M.P., Silva, D.R.A., Koester, E., Noronha, F.L., Casagrande, J. 2006. Provenance of the Neoproterozoic Maricá Formation (Sul-rio-grandense Shield, Southern Brazil): Petrographic and Sm–Nd isotopic constraints. Gondwana Research 9, 464–474.

Brown, G.C., Hughes, D.J., Esson, J. 1973. New RFX data retrieval techniques and their application to U.S.G.S. standard rocks. Chemical Geology, 11, 223-229.

Chemale, F. 2000. Evolução Geológica do Escudo Sul-rio-grandense. In: Holz, M.; De Ros, L. F. (eds.). Geologia do Rio Grande do Sul. Porto Alegre, CIGO/UFRGS, p. 13-52.

Chemale, F., Mallmann, G., Bitencourt, M.F., Kawashita, K. 2012. Time constraints on magmatism along the Major Gercino Shear Zone, southern

Brazil: Implications for West Gondwana reconstruction. Gondwana Research 22, 184-199.

DePaolo, D.J. 1981. A neodymium and strontium isotopic study of the Mesozoic calc-alkaline granitic batholiths of the Sierra Nevada and Peninsular Ranges. California Journal of Geophysical Research 86, 10470–10488.

Fernandes, L.A.D., Tommasi, A., Porcher, C.C. 1992. Deformation patterns in the southern Brazilian branch of the Dom Feliciano belt: A reappraisal. Journal of South American Earth Sciences 5, 77-96.

Fernandes, L.A.D., Tommasi, A., Vauchez, A., Porcher, C.C., Menegat, R., Koester, E. 1993. Zona de Cisalhamento Transcorrente Dorsal do Cangulu: caracterização e importância na compartimentação tectônica do Cinturão Dom Feliciano. Revista Brasileira de Geociências, 23: 224-233.

Fernandes L.A.D., Menegat R., Costa A.F.U., Koester E., Kramer G., Tommasi A., Porcher, C.C., Ramgrab G.E., Camozzato E. 1995a. Evolução tectônica do Cinturão Dom Feliciano no Escudo Sul-rio-grandense: Parte I - uma contribuição a partir do registro geológico. Revista Brasileira de Geociências, 25:351-374

Fernandes L.A.D., Menegat R., Costa A.F.U., Koester E., Kramer G., Tommasi A., Porcher, C.C., Ramgrab G.E., Camozzato E. 1995b. Evolução Tectônica do Cinturão Dom Feliciano no Escudo Sul-rio-grandense: Parte II- Uma Contribuição a partir do registro geofísico. Revista Brasileira de Geociências, 25:375–384

Foster, D.A., Goscombe, B.D., Newstead, B., Mapani, B., Mueller, P.A., Gregory, L.C., Muvangua, E. 2015. U–Pb age and Lu–Hf isotopic data of detrital zircons from the Neoproterozoic Damara Sequence: Implications for Congo and Kalahari before Gondwana. Gondwana Research, in press, corrected proof.

Frantz J.C., Botelho N.F., Pimentel M.M., Potrel A., Koester E., Teixeira R.S. 1999. Relações isotópicas Rb-Sr e Sm-Nd e idades do magmatismo granítico brasiliano da região leste do Cinturão Dom Feliciano no Rio Grande do Sul: evidências de retrabalhamento de crosta continental paleoproterozóica. Revista Brasileira de Geociências, 29(2):227-232.

Gioia, S.M.C.L., Pimentel, M.M. 2000. The Sm–Nd isotopic method in the Geochronology Laboratory of the University of Brasília. Anais da Academia Brasileira de Ciências 72, 219–245.

Gollmann, K., Marques, J.C., Frantz, J.C., Chemale Jr., F. 2008. Geoquímica e Isotópos de Nd de Rochas Metavulcânicas da Antiforme Capané, Complexo Metamórfico Porongos, RS. Revista Pesquisas em Geociências, 35: 83-95.

Gray, D.R., Foster, D.A., Goscombe, B., Passchier, C.W., Trouw, R.A.J., 2006. $^{40}Ar/^{39}Ar$ thermochronology of the Pan-African Damara orogen, Namibia, with implications for tectonothermal and geodynamic evolution. Precambrian Research 150, 49–72.

Gross, A.O.M.S., Droop, G.T.R., Porcher, C.C., Fernandes, L.A.D. 2009. Petrology and thermobarometry of mafic granulites and migmatites from the Chafalote Metamorphic Suite: new insights into the Neoproterozoic P–T evolution of the Uruguayan–Sul- Rio-Grandense Shield. Precambrian Research, 170:157–174

Gruber, L., Porcher, C. C., Lenz, C., Fernandes, L.A.D. 2011. Proveniência de metassedimentos das sequências Arroio Areião, Cerro Cambará e Quartzo Milonitos no Complexo Metamórfico Porongos, Santana da Boa Vista, RS. Pesquisas em Geociências, Vol 38, n.1: 205-224.

Hartmann, L.A., Santos, J.O.S., McNaughton, N.J., Vasconcellos, M.A.Z., Silva, L.C. 2000. Ion Microprobe (SHRIMP) dates complex granulite from Santa Catarina, southern Brazil. Anais da Academia Brasileira de Ciências 72, 559–572.

Hartmann, L. A. ; Phillip, Ruy P ; Liu, D. ; Wan, Y. ; Wang, Y. ; Santos, João Orestes S ; Vasconcellos, M. A. Z. 2004. Paleoproterozoic magmatic provenance of detrital zircon, Porongos Complex quartzites, southern Brazilian Shield. International Geology Review, 46, 127-157.

Hasui, Y., dal Carneiro, C.R., Coimbra, A.M. 1975. The Ribeira folded belt. Revista Brasileira de Geociências 5, 257-266.

Hawkesworth, C., Dhuime, B., Pietranik, A., Cawood, P., Kemp, T., Storey, C. 2010. The Generation and Evolution of the Continental Crust. Journal of the Geological Society, 167, 229–248.

Herron M.M. 1988. Geochemical classification of terrigenous sands and shales fromcore log data. Journal of Sedimentary Petrology, 58, 820-829.

Jost, H. 1982. Condições do metamorfismo regional de uma parte da faixa de dobramentos de Tijucas no Rio Grande do Sul-RS. Acta Geologica Leopoldensia, 12:3–32

Jost, H., Bitencourt, M.F. 1980. Estratigrafia e tectônica de uma fração da faixa de Dobramentos de Tijucas no Rio Grande do Sul. Acta Geologica Leopoldensia, 4(7):27-60.

Kay, S.M., Orrell, S., Abbruzzi, J.M. 1996. Zircon and whole rock Nd-Pb isotopic evidence for a Grenville age and a Laurentian origin for the basement of the Precordillera in Argentina: Journal of Geology, v. 104, p. 637–648.

Kohlrausch, C.B. 2013. Determinação das idades U-Pb em zircão por LA-ICP-ME nas rochas metavulcânicas da Antiforme Capané, Complexo Metamórfico Porongos. Undergraduate thesis, 61 pp. Universidade Federal do Rio Grande do Sul.

Lena, L., Pimentel, M.M., Phillip, R.P., Armstrong, R., Sato, K. The evolution of the Neoproterozoic São Gabriel juvenile terrane, southern Brazil based on high spatial resolution U-Pb ages and $\delta^{18}O$ data from detrital zircons. Precambrian Research, 247, 126-138. http://dx.doi.org/doi:10.1016/j.precamres.2014.03.010

Lenz, C. 2006. Evolução metamórfica dos metapelitos da antiforme Serra dos Pedrosas: condições e idades do metamorfismo. 111 p. Msc thesis, Universidade Federal do Rio Grande do Sul.

Lenz, C., Fernandes, L.A.D., McNaughton, N.J., Porcher, C.C., Masquelin, H. 2011. U–Pb SHRIMP ages for the Cerro Bori Orthogneisses, Dom Feliciano Belt in Uruguay: Evidences of a ~800 Ma magmatic and ~650 Ma metamorphic event. Precambrian Research, 185:149–163

Lenz, C.C., Porcher, C.C., Fernandes, L.A.D., Masquelin, H., Koester, E., Conceição, R.V. 2012 Geochemistry of the Neoproterozoic (800–767 Ma) Cerro Bori orthogneisses, Dom Feliciano Belt in Uruguay: tectonic evolution of an ancient continental arc. Mineralogy and Petrology, 107(5):785-806.

Loewy, S.L., Connely, J.N., Dalziel, I.W.D., Gower, F.C. 2003. Eastern Laurentia in Rodínia: Constraints from whole-rock Pb and U-Pb geochronology. Tectonophysics v. 375, p. 169-197.

Lopes, C.G., Pimentel, M.M., Phillip, R.P., Gruber, L., Armstrong, R., Junges, S. 2015. Provenance of the Passo Feio Complex: Implications for the age of supracrustal rocks of the São Gabriel Arc, southern Brazil. Journal of South American Earth Sciences, v.58, p. 9-17.

Ludwig, K.R. 2003. Isoplot 3.0 – A geochronological toolkit for Microsoft Excel. Berkley Geochronology Center, Special Publications No. 4.

Marques J.C., Jost H., Roisenberg A., Frantz J.C. 1998a. Eventos ígneos da Suíte Metamórfica Porongos na área da antiforme Capané, Cachoeira do Sul - RS. Revista Brasileira de Geociências, v.28, p.419-430.

Marques J.C., Jost H., Roisenberg A., Frantz J.C. 1998b. Rochas metassedimentares, geologia estrutural e metamorfismo da Suíte Metamórfica Porongos na área da Antiforme Capané, Cachoeira do Sul - RS. Revista Brasileira de Geociências, v.28, p.467-472.

Marques, J. C. ; Roinsenberg, A. ; Jost, H. ; Frantz, J. C. ; Teixeira, R. S. 2003. Geologia e Geoquímica das Rochas Metaultramáficas da Antiforme Capané, Suíte Metamórfica Porongos, RS. Revista Brasileira de Geociências, v. 33, n. 1, p. 95-107.

Nesbitt, H.W.M., Young, G.M. 1982. Early Proterozoic climates and plate motions inferred from major element chemistry of lutites. Nature 299, 715-717.

Oyhantçabal P., Siegesmund S., Wemmer K., Layer P. 2010. The Sierra Ballena Shear Zone in the southernmost Dom Feliciano Belt (Uruguay): evolution, kinematics and deformation conditions. International Journal of Earth Sciences (Geol. Rundschau) v. 99: 1227–1246.

Oyhantçabal, P., Siegesmund, S., Wemmer, K. 2011. The Rio de la Plata Craton: a review of units, boundaries, ages and isotopic signature. International Journal of Earth Science, 100, 201–220.

Pertille, J., Hartman, L.A., Phillip, R.P. 2015a. Zircon U-Pb age constraints on the Paleoproterozoic sedimentary basement of the Ediacaran Porongos Group, Sul-Riograndense Shield, southern Brazil. Journal of South American Earh Sciences 63, pp.334-345.

Pertille, J., Hartmann, L.A., Phillip, R.P., Petry, T.S., Lana, C.C. 2015b. Origin of the Ediacaran Porongos Group, Dom Feliciano Belt, southern Brazilian Shield, with emphasis on whole rock and detrital zircon geochemistry and U-Pb, Lu-Hf isotopes. Journal of South American Earth Sciences 64, pp. 69-93.

Petry, T.S. 2014. Evolução do Complexo Porongos na Antiforme Capané com base em mapeamento geológico, petrografia, geoquímica e datação U-Pb em zircão detrítico no USP-SHRIMP IIe. Undergraduate thesis. UFRGS, Porto Alegre, 88 pgs.

Philipp, R.P. & Machado, R. 2005. The Neoproterozoic to Cambrian Granitic Magmatism of Pelotas Batholith, Southern Brazil. Journal of South American Earth Sciences 19, 461-478.

Philip, R.P., Lusa, M., Nardi, L. 2008. Petrology of dioritic, tonalitic and trondhjemitic gneisses from Encantadas Complex, Santana da Boa Vista, southernmost Brazil: Paleoproterozoic continental-arc magmatism. Anais da Academia Brasileira de Ciências v.80, n.4.

Porcher, C.C. 1990. Caracterização das condições de fluxo em uma zona de cisalhamento tangencial na região de Santana da Boa Vista (RS). Msc thesis, Porto Alegre, RS –UFRGS.

Porcher, C.C., Fernandes, L.A.D. 1990. Relações embasamento/"cobertura" na porção ocidental do cinturão Dom Feliciano: um esboço estrutural. Pesquisas, 17 (l/2):72-96.

Porcher, C. C., Macnaughton, N. J., Leite, J. A. D., Hartmann, L. A., Fernandes, L.A.D. 1999. Idade SHRIMP do vulcanismo ácido do Complexo Metamórfico Porongos, RS.. In: 1º SIMPÓSIO SOBRE VULCANISMOS E AMBIENTES ASSOCIADOS, 1999, Gramado. Resumos... 1999. Sociedade Brasileira de Geologia.

Porcher, C. C., Fernandes, L.A.D., Lenz, C., Gruber, L., Vignol, L., Jourdan, F. Metamorphic ages from Porongos Metamorphic Complex: Rb-Sr and Ar-Ar in muscovite and apatite fission track results. In: VII SSAGI, 2010, Brasília. VII SSAGI, 2010, Brasília. Abstracts...VII SSAGI, 2010., 2010. v. Único. p. 121-124.

Rapela, C.W., Fanning, C.M., Casquet, C., Pankhurst, R.J., Poiré, L.S.D. Baldo, E.G. 2011. The Rio de la Plata craton and the adjoining Pan-African/brasiliano terranes: Their origins and incorporation into south-west Gondwana, Gondwana Research, (20):4, p. 673-690.

Remus M.V.D., Tedesco MA, Philipp RP, Faccini UF. 1987. Evolução estrutural da unidade Porongos a sul do Rio Camaquã, RS. In: Anais Simpósio Sul-Brasileiro de Geologia 3, SBG, Curitiba, Sociedade Brasileira de Geologia Rio de Janeiro, pp 223–244.

Remus, M. V. D., Philipp, R. P., Faccini, U. F. & Junges, S. L. 1990. Contribução ao estudo geológico-estrutural dos Gnaisses Encantadas e das relacões com as supracrustais Porongos na região de Santana da Boa Vista/RS. In Congresso Brasileiro de Geologia 36, Natal (ed. Sociedade Brasileira de Geologia Rio de Janeiro), pp. 2356–70. Anais do Congresso Brasileiro de Geologia 36, SBG 5. Sociedade Brasileira de Geologia Rio de Janeiro.

Remus M.V.D., Hartmann L.A., Ribeiro, M. 1991. Nota sobre a geologia dos metamorfitos de pressão intermediária e granitóides associados da região de Pinheiro Machado/RS. Acta Geologica Leopoldensia, 34:175–190.

Saalmann, K., Remus, M. V. D., Hartmann, L.A. 2006. Structural evolution and tectonic setting of the Porongos belt, southern Brazil. Geological Magazine, 143 (1), 59–88.

Saalmann, K., Remus, M. V. D., Hartmann, L.A, Koester, E., Conceição, R.V. 2005. Sm–Nd isotope geochemistry of metamorphic volcano-sedimentary successions in the São Gabriel Block, southernmost Brazil: evidence for the existence of juvenile Neoproterozoic oceanic crust to the east of the Rio de la Plata craton. Precambrian Research 136 (2005) 159–175.

Saalmann, K., Gerdes, A., Lahaye, Y., Hartmann, L.A., Remus, M.V.D., Läufer, A. 2010. Multiple accretion at the eastern margin of the Rio de la Plata craton: the prolonged Brasiliano orogeny in southernmost Brazil. International Journal of Earth Sciences, (100) 355-378.

Schwartz, J. J., Gromet, L. P. 2004. Provenance of a late proterozoic early Cambrian basin, Sierras de Córdoba, Argentina. Precambrian Research 129:1–21.

Silva, L.C., McNaughton, N.J., Hartmann, L.A., Fletcher, I.R. 1997a. U-Pb SHRIMP geochronology in the Camboriú Complex and other gneisses from the basement of the Neoproterozoic (Brasiliano) southern Brazilian granitic province. In II International Symposium on Granites and Associated Mineralizations, Salvador, Brazil, extended abstracts, 1997a, pp. 278-279.

Silva, L.C., McNaughton, J., Hartmann, L.A., Fletcher, I.R., Gresse, P., Scheepers, R., 1997b. U-Pb (SHRIMP) isotopic constraints for the evolution of the southern Brazilian Granitic Province (SBGP) and some correlated South African, Pan-African plutons. In II International Symposium on Granites and Associated Mineralizations, Salvador, Brazil, extended abstracts, 1997b, pp. 276-277.

Stacey, J.S., Kramers, J.D. 1975. Approximation of terrestrial lead isotope evolution by a two-stage model. Earth and Planetary Science Letters 26, 207– 221.

Taylor, S.R., McLennan, S.M. 1985. The continental crust: its composition and evolution. Blackwell, Oxford, 312 pp.

Tosdal, R.M. 1996. The Amazon-Laurentia connection as viewed from the Middle Proterozoic rocks in the central Andes, western Bolivia and northern Chile. Tectonics, v. 15, p. 827–842.

FIGURE CAPTIONS

Figure 1 – A – Reconstruction of the Rio de La Plata, Kalahari and Congo cratons (Modified from Fernandes et al., 1995a); B: Geological sketch map of the Dom Feliciano Belt, including PMC position; C: Schematic geological map displaying the Pan-African belts in the Congo-Kalahari-La Plata convergion on the Gondwana formation.

Figure 2 – A - Schematic geological map of the Porongos Complex (modified from Porcher and Fernandes, 1990) with locations of analyzed samples; $^{207}Pb/^{206}Pb$ zircon ages from metasedimentary rocks are displayed in the map (from Gruber et al., 2011); B - Detritic zircon distribution ($^{207}Pb/^{206}Pb$ ages) of Porongos metasedimentary sequences (from Gruber et al., 2011). All analysis displayed are less than 10% discordant, with age uncertainties smaller than 20% (2□). The age of volcanism is from Porcher et al. (1999) and Saalmann et al. (2010). Analytical methods used in this analysis can be obtained in Simon et al. (2004) and Chemale

et al. (2012); C, D - Petrographic features of sample POR 18, showing quartz and plagioclase aggregates with interlayered mica (Polarized light); B, D: Cross-polars photograph for the same sample, displaying interlobed contact between quartz grains.

Figure 3 – Comparison of zircon magmatic and metamorphic ages from the main cratons and mobile belts associated with DFB and PMC. Modified from Rapella et al., 2011, with added data from Lenz et al., 2011 and 2012, Lena et al., 2014; Lopes et al., 2015, Foster et al., 2015 and references therein.

Figure 4 – A - ƐNd X time diagram of the analyzed samples. Metabasalts Arroio Capané data from Gollmann et al. (2008); Encantadas complex from Chemale (2000); B – Plot of the T_{DM} ages for ƐNd (T=0) for analyzed samples; samples from Arroio Areião metasediments have a stronger dispersion, whereas metasediments from Cerro Cambará, Rincão do Maranhão and Cerro do Facão have T_{DM} and ƐNd less variations; in comparison, metavolcanics of Capané Antiform displays a trend similar to the metasediments of Arroio Areião, with the exception of sample POR 18; C - Variation of T_{DM} ages for ƐNd (T=750Ma), with Arroio Areião metasediments showing a broader occurrence of ƐNd(t), with the more juvenile sample being the metapelitic sample from east of Santana da Boa Vista Antiform (POR 18); metasediments from other units displays negative ƐNd values, with the more negative being sample from quartz mylonite localized at south of Santana da Boa Vista Antiform; D - Diagram of Nd (ppm) against ƐNd(t), where Arroio Areião samples displays again large variations; samples from Cerro Cambará and Cerro do Facão displays almost the same quantities of Nd. Rincão do Maranhão and Cerro do Facão data from Lenz (2006); data on metavolcanics of Capané Antiform from Gollmann et al. (2008).

Figure 5 – A- Uranogenic $^{207}Pb/^{204}Pb$ X $^{206}Pb/^{204}Pb$ diagram displaying large compositional variation for samples from the Arroio Areião sequence, while samples of the Cerro Cambará display values within a narrower range; comparison with possible source cratons shows that there is no participation of sediments with Laurentian affinity (Eastern North America and Canada) and strong resemblance with African and La Plata sources, particularly Nico Perez and Punta del Este terrains. Modified from Oyhantçabal et al. (2011). Data from Cerro Bory presented by Lenz et al. (2012); B – Thoro-uranogenic $^{208}Pb/^{204}Pb$ X $^{206}Pb/^{204}Pb$, displaying metasediments from east and west of Santana da Boa Vista antiform; C - Concordia diagram for sample POR 18 (A); D - Sedimentary rock classification (Herron, 1988), with faded fields indicating data from Petry, 2014).

Figure 6 - BSE images from analyzed zircon grains presenting less than 10% discordance, $^{207}Pb/^{206}Pb$ ages are displayed in the positions where the spots were made.

Figure 7 – Top view displaying schematic plate reconstruction and tectonic evolution between ca. 0.90 to 0.57 Ga: A – 1: Opening of Adamastor Ocean; 2 – initial rifting of Damara orogeny – ca. 780 Ma continental volcanism (formation of Khomas ocean) (Gray et al., 2006); 3 – African continental terranes; 4 – Alkaline magmatism; 5 – São Gabriel Orogen (after the Passinho Oceanic Arc; ca. 0.9 Ga); B – derivation of the Passinho Arc into the RdLP craton; C – Collision of RdLP

and Congo-Kalahari cratons; D – lateral view at ca. 900 Ma, displaying installation of Passinho Intraoceanic Arc; E – At ca. 780 Ma, Passinho is already agglutinated at RdLP margin, and continental arc magmatism starts with consumption of the Adamastor ocean; F – rifting of South Adamastor ocean thrusts a continental-like terrain or block into the direction of La Plata craton; deposition of the first sequence of terrigenous sediments of the PMC (quartzites); G – Agglutination of the cratons, with final pulses of sedimentation of ca. <580 Ma. Modified from Rapela et al., 2011, with data from Lena et al., 2014, Lenz et al., 2012, and references therein.
Abbreviations: SBSZ – Sierra Balena Shier Zone; SYSZ – Sarandí del Yí Shear Zone; P – possible location of Paranapanema craton; NP – Nico Perez terrain; PMC – Porongos Metamorphic Complex; K – Kalahari; RPC – Rio de La Plata Craton; A – Angola block

TABLE CAPTIONS

Table 1 - Summary of samples; samples marked with * means analysis published in Gruber et al (2011). ESA – East of Santana da Boa Vista Antiform; WSA – West of Santana da Boa Vista Antiform; ECG – East of Cerro do Godinho Antiform; SDP – Serra dos Pedrosas Antiform.

Table 2 - Laser Ablation ICP-MS U–Pb analyses.

Table 3 – Whole-rock Sm-Nd analyses.

Table 4 – Whole-rock Pb-Pb analyses.

Table 5 - Whole-rock geochemical analyses. CIA calculated according to Nesbitt and Young, 1982 and Taylor and McLennan, 1985; LOI – loss on ignition.

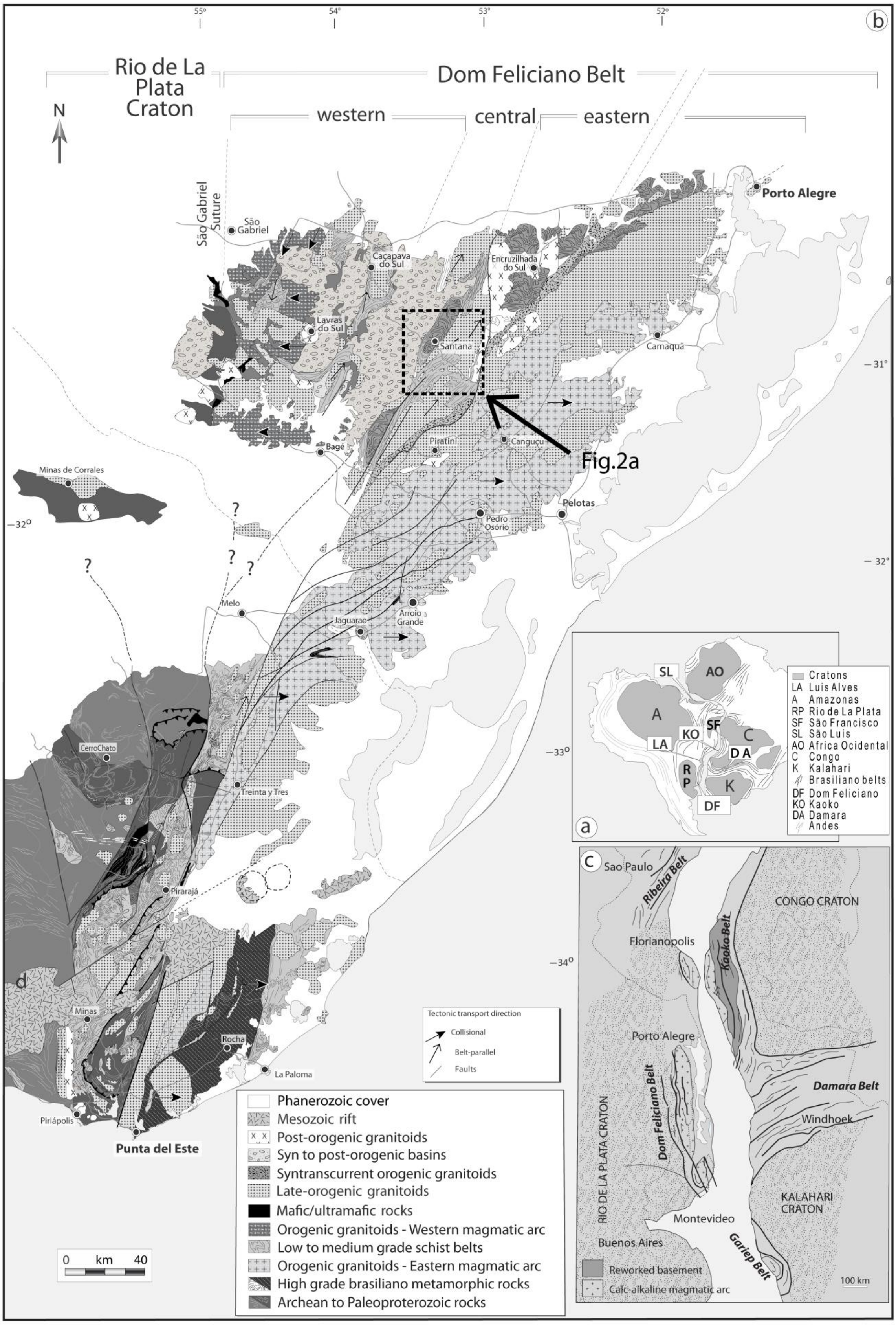

Rio de La Plata Craton
Dom Feliciano Belt
western
central
eastern
N
São Gabriel Suture
São Gabriel
Caçapava do Sul
Encruzilhada do Sul
Porto Alegre
Lavras do Sul
Santana
Camaquã
Bagé
Piratini
Canguçu
Fig.2a
Minas de Corrales
Pelotas
Pedro Osório
Melo
Jaguarão
Arroio Grande
CerroChato
Treinta y Tres
Pirarajá
Minas
Rocha
La Paloma
Piriápolis
Punta del Este
55°
54°
53°
52°
31°
32°
33°
34°
Cratons
LA Luis Alves
A Amazonas
RP Rio de La Plata
SF São Francisco
SL São Luis
AO Africa Ocidental
C Congo
K Kalahari
Brasiliano belts
DF Dom Feliciano
KO Kaoko
DA Damara
Andes
Sao Paulo
Ribeira Belt
Florianopolis
Porto Alegre
Dom Feliciano Belt
RIO DE LA PLATA CRATON
Montevideo
Buenos Aires
CONGO CRATON
Kaoko Belt
Damara Belt
Windhoek
KALAHARI CRATON
Gariep Belt
Reworked basement
Calc-alkaline magmatic arc
100 km
Tectonic transport direction
Collisional
Belt-parallel
Faults
Phanerozoic cover
Mesozoic rift
Post-orogenic granitoids
Syn to post-orogenic basins
Syntranscurrent orogenic granitoids
Late-orogenic granitoids
Mafic/ultramafic rocks
Orogenic granitoids - Western magmatic arc
Low to medium grade schist belts
Orogenic granitoids - Eastern magmatic arc
High grade brasiliano metamorphic rocks
Archean to Paleoproterozoic rocks
0 km 40

Figure 1

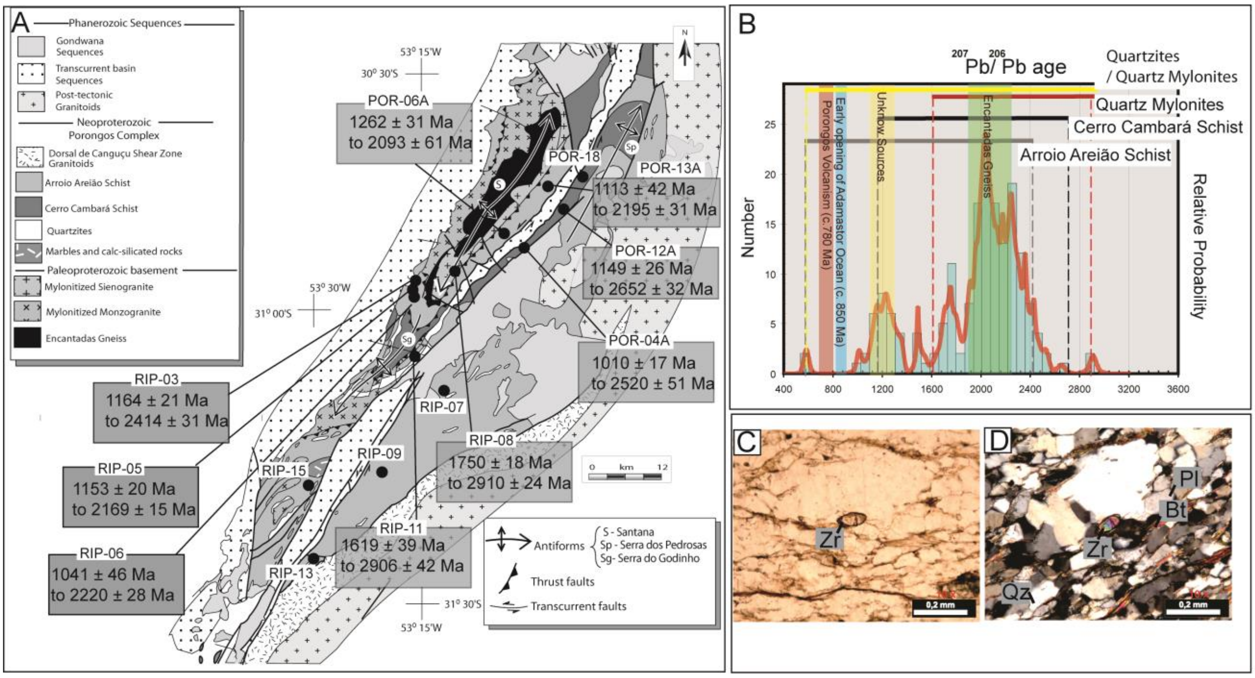
A
Phanerozoic Sequences
Gondwana Sequences
Transcurrent basin Sequences
Post-tectonic Granitoids
Neoproterozoic Porongos Complex
Dorsal de Canguçu Shear Zone Granitoids
Arroio Areião Schist
Cerro Cambará Schist
Quartzites
Marbles and calc-silicated rocks
Paleoproterozoic basement
Mylonitized Sienogranite
Mylonitized Monzogranite
Encantadas Gneiss
53° 15'W
30° 30'S
53° 30'W
31° 00'S
31° 30'S
53° 15'W
N
POR-06A
1262 ± 31 Ma
to 2093 ± 61 Ma
POR-18
POR-13A
1113 ± 42 Ma
to 2195 ± 31 Ma
POR-12A
1149 ± 26 Ma
to 2652 ± 32 Ma
POR-04A
1010 ± 17 Ma
to 2520 ± 51 Ma
RIP-03
1164 ± 21 Ma
to 2414 ± 31 Ma
RIP-05
1153 ± 20 Ma
to 2169 ± 15 Ma
RIP-06
1041 ± 46 Ma
to 2220 ± 28 Ma
RIP-07
RIP-08
1750 ± 18 Ma
to 2910 ± 24 Ma
RIP-09
RIP-11
1619 ± 39 Ma
to 2906 ± 42 Ma
RIP-13
RIP-15
S
Sp
Sg
0 km 12
Antiforms
S - Santana
Sp - Serra dos Pedrosas
Sg- Serra do Godinho
Thrust faults
Transcurrent faults
B
207Pb/206Pb age
Quartzites / Quartz Mylonites
Quartz Mylonites
Cerro Cambará Schist
Arroio Areião Schist
Porongos Volcanism (c. 780 Ma)
Early opening of Adamastor Ocean (c. 850 Ma)
Unknow Sources
Encantadas Gneiss
Number
Relative Probability
0
5
10
15
20
25
400
800
1200
1600
2000
2400
2800
3200
3600
C
Zr
0,2 mm
D
Pl
Bt
Zr
Qz
0,2 mm

Figure 2

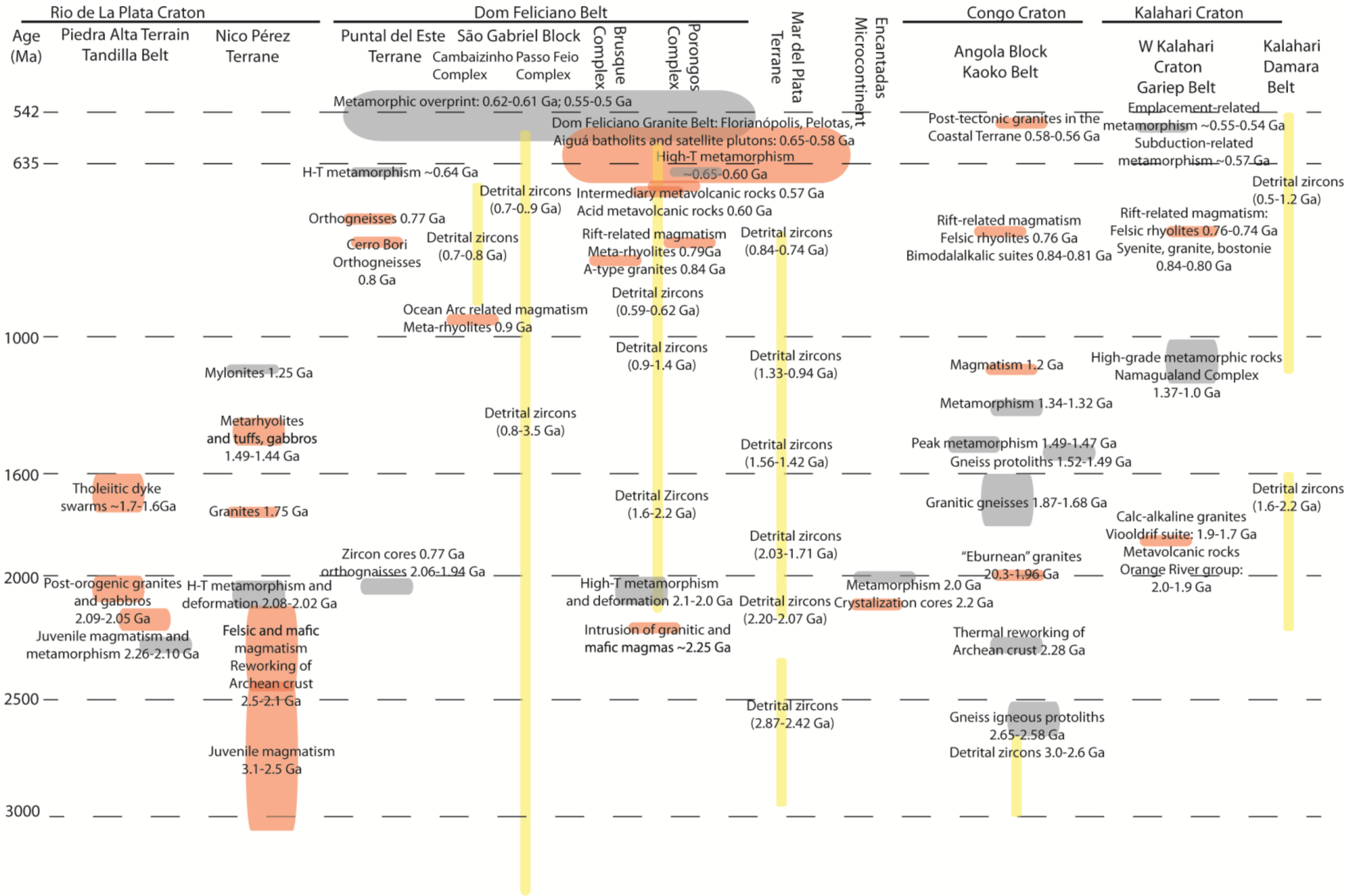

Rio de La Plata Craton
Dom Feliciano Belt
Congo Craton
Kalahari Craton
Age (Ma)
Piedra Alta Terrain Tandilla Belt
Nico Pérez Terrane
Puntal del Este Terrane
São Gabriel Block
Cambaizinho Complex
Passo Feio Complex
Brusque Complex
Porongos Complex
Mar del Plata Terrane
Encantadas Microcontinent
Angola Block Kaoko Belt
W Kalahari Craton Gariep Belt
Kalahari Damara Belt
542
635
1000
1600
2000
2500
3000
Metamorphic overprint: 0.62-0.61 Ga; 0.55-0.5 Ga
Dom Feliciano Granite Belt: Florianópolis, Pelotas, Aiguá batholits and satellite plutons: 0.65-0.58 Ga
High-T metamorphism ~0.65-0.60 Ga
H-T metamorphism ~0.64 Ga
Detrital zircons (0.7-0..9 Ga)
Intermediary metavolcanic rocks 0.57 Ga
Acid metavolcanic rocks 0.60 Ga
Orthogneisses 0.77 Ga
Cerro Bori Orthogneisses 0.8 Ga
Detrital zircons (0.7-0.8 Ga)
Rift-related magmatism Meta-rhyolites 0.79Ga A-type granites 0.84 Ga
Detrital zircons (0.84-0.74 Ga)
Detrital zircons (0.59-0.62 Ga)
Ocean Arc related magmatism Meta-rhyolites 0.9 Ga
Detrital zircons (0.9-1.4 Ga)
Detrital zircons (1.33-0.94 Ga)
Mylonites 1.25 Ga
Detrital zircons (0.8-3.5 Ga)
Metarhyolites and tuffs, gabbros 1.49-1.44 Ga
Detrital zircons (1.56-1.42 Ga)
Tholeiitic dyke swarms ~1.7-1.6Ga
Granites 1.75 Ga
Detrital Zircons (1.6-2.2 Ga)
Detrital zircons (2.03-1.71 Ga)
Zircon cores 0.77 Ga orthognaisses 2.06-1.94 Ga
Post-orogenic granites and gabbros 2.09-2.05 Ga
H-T metamorphism and deformation 2.08-2.02 Ga
High-T metamorphism and deformation 2.1-2.0 Ga
Detrital zircons (2.20-2.07 Ga)
Metamorphism 2.0 Ga Crystalization cores 2.2 Ga
Juvenile magmatism and metamorphism 2.26-2.10 Ga
Felsic and mafic magmatism Reworking of Archean crust 2.5-2.1 Ga
Intrusion of granitic and mafic magmas ~2.25 Ga
Detrital zircons (2.87-2.42 Ga)
Juvenile magmatism 3.1-2.5 Ga
Post-tectonic granites in the Coastal Terrane 0.58-0.56 Ga
Rift-related magmatism Felsic rhyolites 0.76 Ga Bimodalalkalic suites 0.84-0.81 Ga
Magmatism 1.2 Ga
Metamorphism 1.34-1.32 Ga
Peak metamorphism 1.49-1.47 Ga
Gneiss protoliths 1.52-1.49 Ga
Granitic gneisses 1.87-1.68 Ga
"Eburnean" granites 20.3-1.96 Ga
Thermal reworking of Archean crust 2.28 Ga
Gneiss igneous protoliths 2.65-2.58 Ga
Detrital zircons 3.0-2.6 Ga
Emplacement-related metamorphism ~0.55-0.54 Ga
Subduction-related metamorphism ~0.57 Ga
Detrital zircons (0.5-1.2 Ga)
Rift-related magmatism: Felsic rhyolites 0.76-0.74 Ga Syenite, granite, bostonie 0.84-0.80 Ga
High-grade metamorphic rocks Namagualand Complex 1.37-1.0 Ga
Detrital zircons (1.6-2.2 Ga)
Calc-alkaline granites Vioolddrif suite: 1.9-1.7 Ga
Metavolcanic rocks Orange River group: 2.0-1.9 Ga

Figure 3

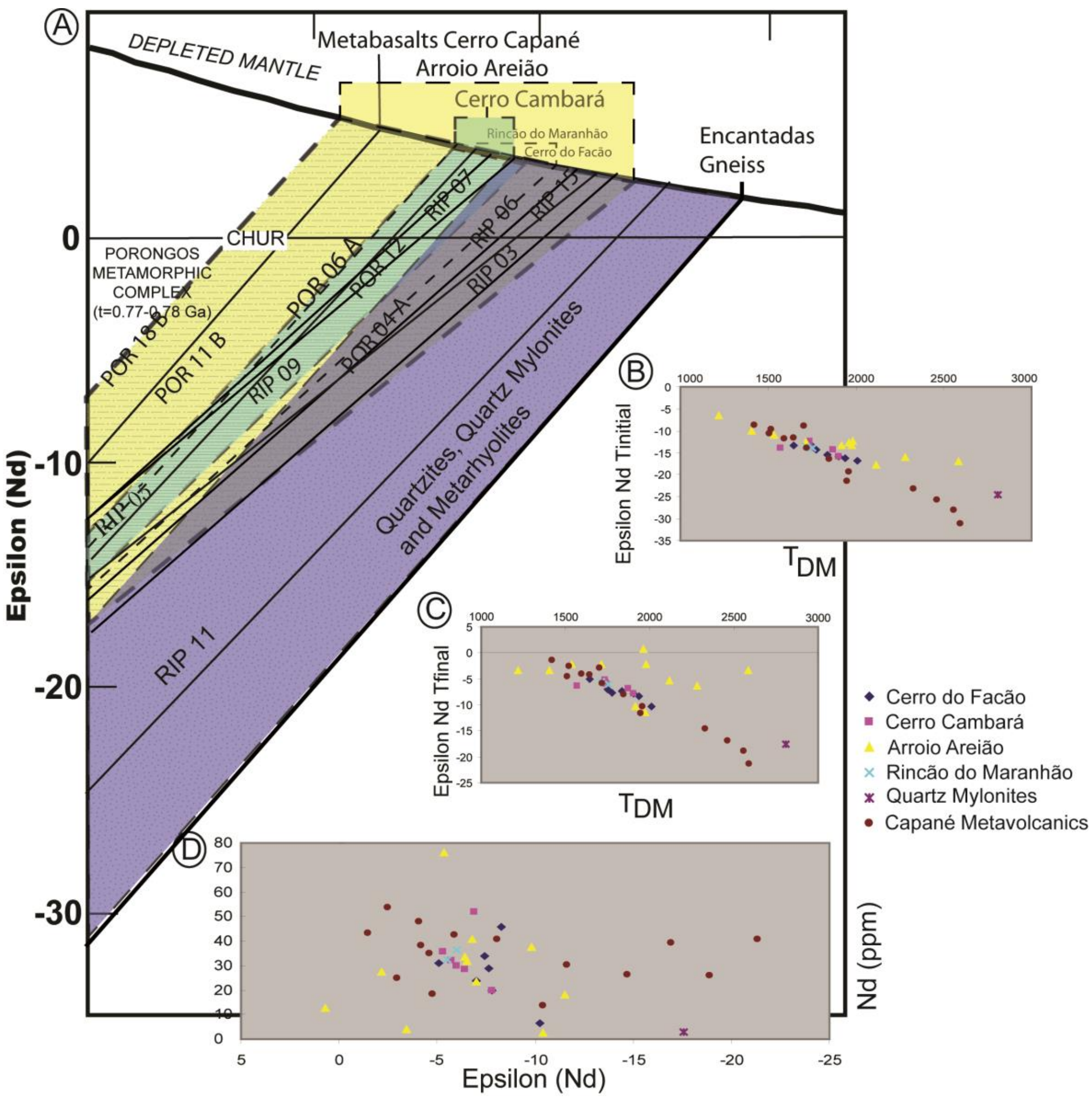
A
DEPLETED MANTLE
Metabasalts Cerro Capané
Arroio Areião
Cerro Cambará
Rincão do Maranhão
Cerro do Facão
Encantadas
Gneiss
CHUR
PORONGOS
METAMORPHIC
COMPLEX
(t=0.77-0.78 Ga)
POR 18 B
POR 11 B
POR 06 A
POR 12
POR 04 A
RIP 07
RIP 06
RIP 15
RIP 03
RIP 09
RIP 05
RIP 11
Quartzites, Quartz Mylonites
and Metarhyolites
Epsilon (Nd)
B
Epsilon Nd Tinitial
TDM
C
Epsilon Nd Tfinal
TDM
D
Nd (ppm)
Epsilon (Nd)
Cerro do Facão
Cerro Cambará
Arroio Areião
Rincão do Maranhão
Quartz Mylonites
Capané Metavolcanics

Figure 4

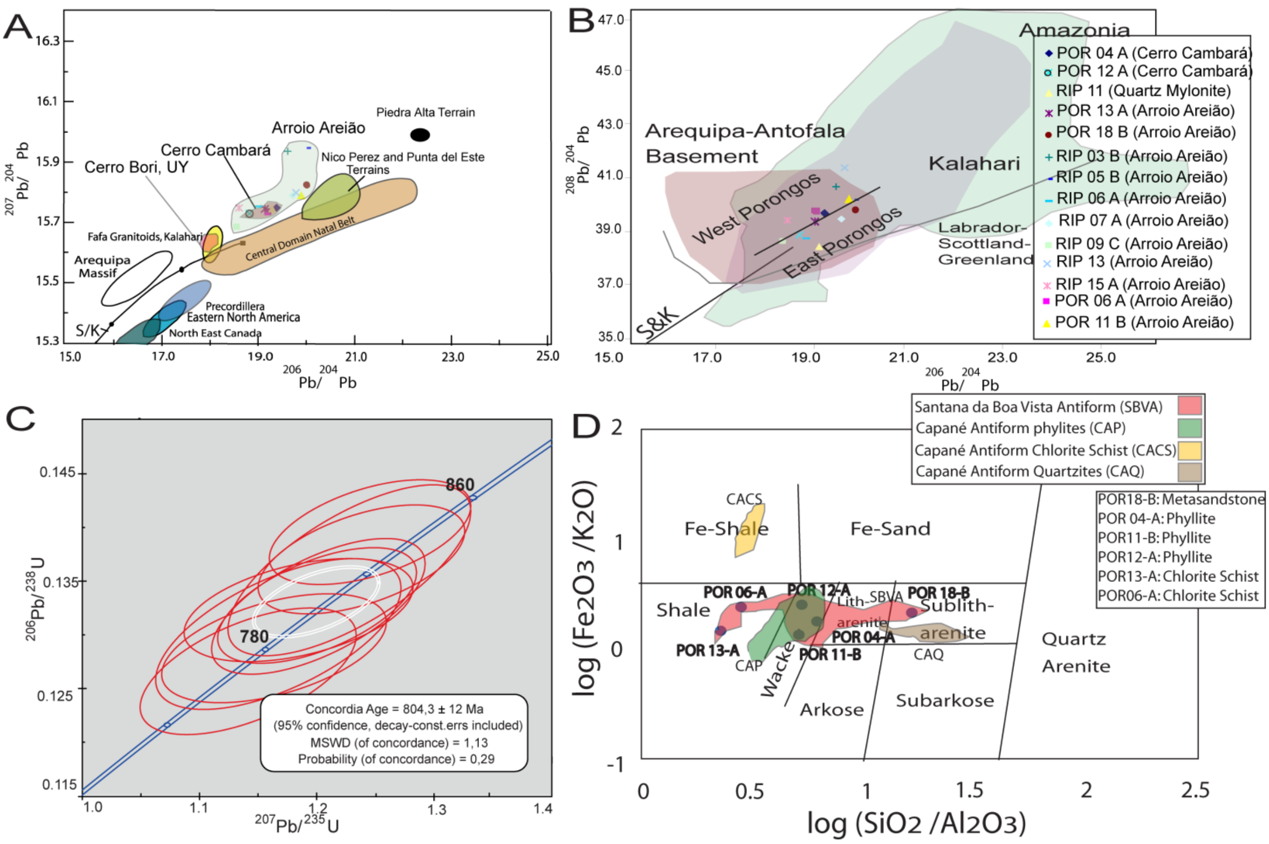
A
Piedra Alta Terrain
Arroio Areião
Cerro Cambará
Nico Perez and Punta del Este Terrains
Cerro Bori, UY
Fafa Granitoids, Kalahari
Central Domain Natal Belt
Arequipa Massif
Precordillera
Eastern North America
North East Canada
S/K
B
Amazonia
Arequipa-Antofala Basement
Kalahari
West Porongos
East Porongos
Labrador-Scottland-Greenland
S&K
POR 04 A (Cerro Cambará)
POR 12 A (Cerro Cambará)
RIP 11 (Quartz Mylonite)
POR 13 A (Arroio Areião)
POR 18 B (Arroio Areião)
RIP 03 B (Arroio Areião)
RIP 05 B (Arroio Areião)
RIP 06 A (Arroio Areião)
RIP 07 A (Arroio Areião)
RIP 09 C (Arroio Areião)
RIP 13 (Arroio Areião)
RIP 15 A (Arroio Areião)
POR 06 A (Arroio Areião)
POR 11 B (Arroio Areião)
C
860
780
Concordia Age = 804,3 ± 12 Ma
(95% confidence, decay-const.errs included)
MSWD (of concordance) = 1,13
Probability (of concordance) = 0,29
D
Santana da Boa Vista Antiform (SBVA)
Capané Antiform phylites (CAP)
Capané Antiform Chlorite Schist (CACS)
Capané Antiform Quartzites (CAQ)
POR18-B: Metasandstone
POR 04-A: Phyllite
POR11-B: Phyllite
POR12-A: Phyllite
POR13-A: Chlorite Schist
POR06-A: Chlorite Schist
Fe-Shale
Fe-Sand
Shale
Wacke
Arkose
Subarkose
Sublith-arenite
Quartz Arenite
log (Fe2O3 /K2O)
log (SiO2 /Al2O3)

Figure 5

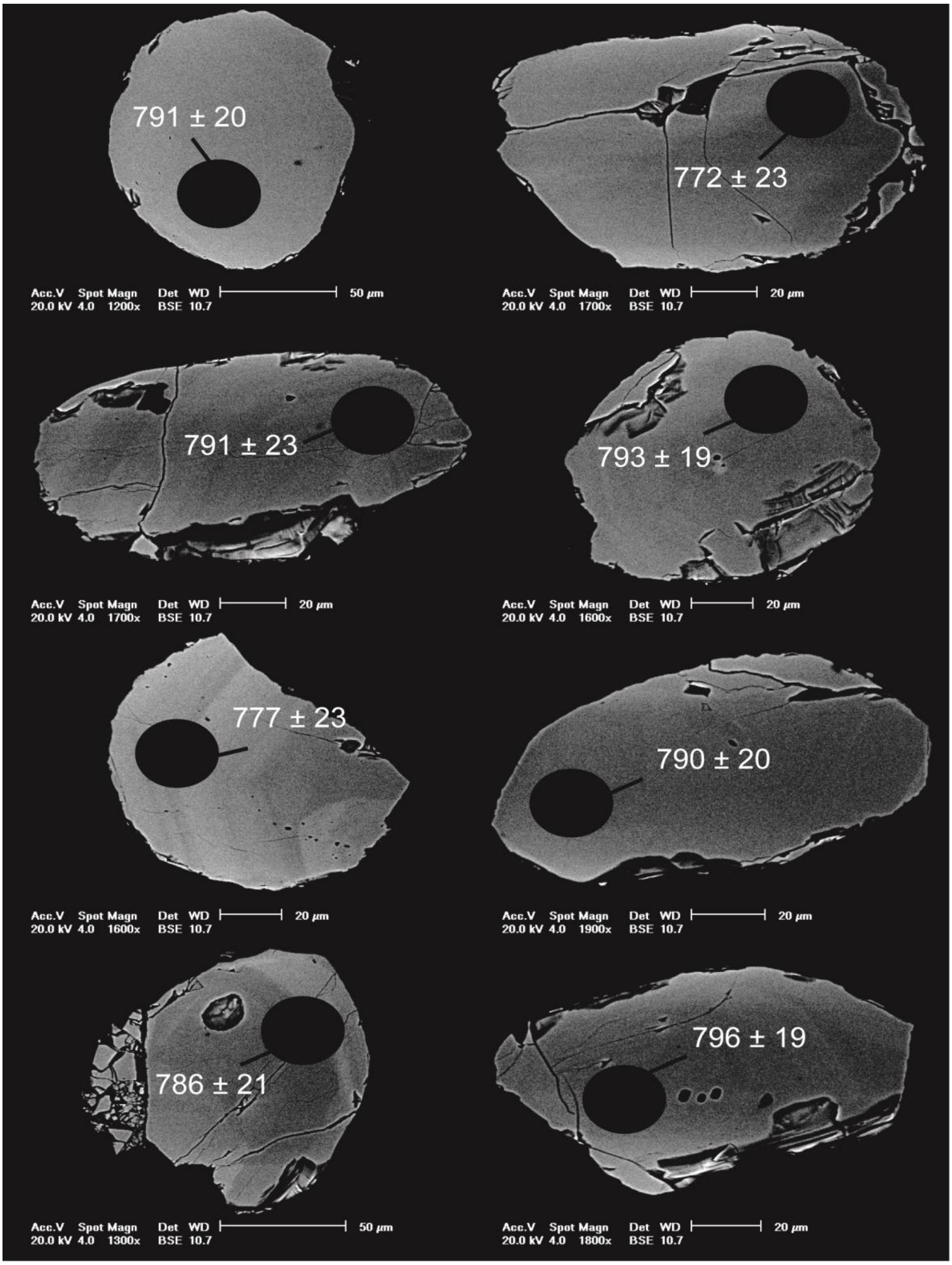
791 ± 20
Acc.V Spot Magn Det WD 50 µm
20.0 kV 4.0 1200x BSE 10.7
772 ± 23
Acc.V Spot Magn Det WD 20 µm
20.0 kV 4.0 1700x BSE 10.7
791 ± 23
Acc.V Spot Magn Det WD 20 µm
20.0 kV 4.0 1700x BSE 10.7
793 ± 19
Acc.V Spot Magn Det WD 20 µm
20.0 kV 4.0 1600x BSE 10.7
777 ± 23
Acc.V Spot Magn Det WD 20 µm
20.0 kV 4.0 1600x BSE 10.7
790 ± 20
Acc.V Spot Magn Det WD 20 µm
20.0 kV 4.0 1900x BSE 10.7
786 ± 21
Acc.V Spot Magn Det WD 50 µm
20.0 kV 4.0 1300x BSE 10.7
796 ± 19
Acc.V Spot Magn Det WD 20 µm
20.0 kV 4.0 1800x BSE 10.7

Figure 6

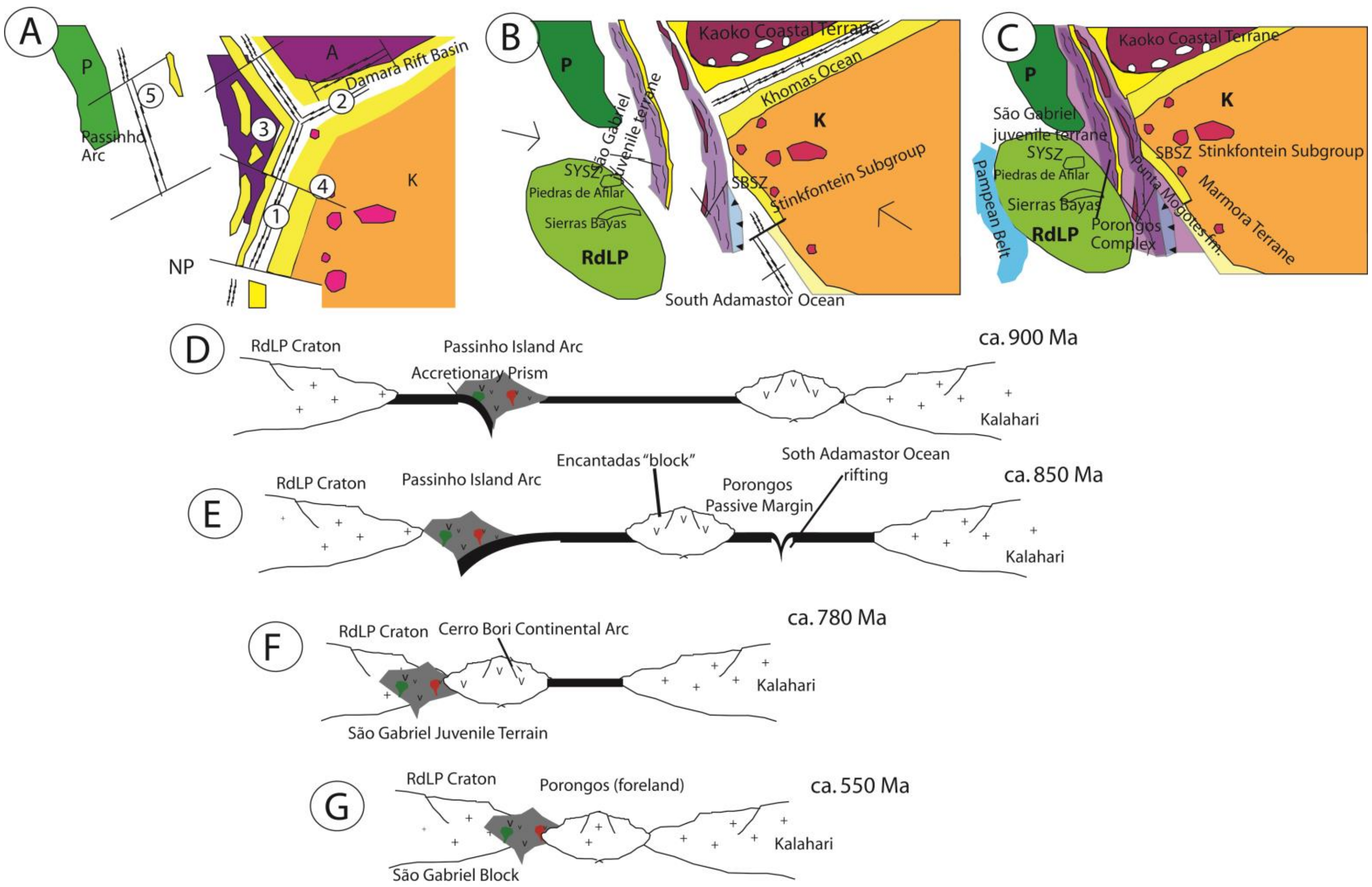
A
P
Passinho Arc
5
A
Damara Rift Basin
2
3
4
1
K
NP
B
P
São Gabriel Juvenile terrane
SYSZ
Piedras de Afilar
Sierras Bayas
RdLP
Kaoko Coastal Terrane
Khomas Ocean
K
SBSZ
Stinkfontein Subgroup
South Adamastor Ocean
C
P
Kaoko Coastal Terrane
K
São Gabriel juvenile terrane
SYSZ
Piedras de Afilar
Sierras Bayas
RdLP
Pampean Belt
Porongos Complex
Punta Mogotes fm.
SBSZ
Stinkfontein Subgroup
Marmora Terrane
D
RdLP Craton
Passinho Island Arc
Accretionary Prism
ca. 900 Ma
Kalahari
E
RdLP Craton
Passinho Island Arc
Encantadas "block"
Porongos Passive Margin
Soth Adamastor Ocean rifting
ca. 850 Ma
Kalahari
F
RdLP Craton
Cerro Bori Continental Arc
ca. 780 Ma
Kalahari
São Gabriel Juvenile Terrain
G
RdLP Craton
Porongos (foreland)
ca. 550 Ma
Kalahari
São Gabriel Block

Figure 8

Table 1

Sample	UTM	Lithodemic Unit	Rock	Mineralogy	Analysis
POR 04 A	0295050 m E 6570950 m S	Cerro Cambará (ESA)	Chlorite-muscovite schist	Chlorite, Muscovite, Plagioclase, Quartz	Pb-Pb, Sm-Nd, U-Pb (zircon)*
POR 06 A	0294500 m E 6577850 m S	Arroio Areião (ESA)	Chlorite-muscovite schist	Chlorite, Muscovite, Plagioclase, Quartz	Pb-Pb, Sm-Nd, U-Pb (zircon)*
POR 11 B	0299250 m E 6580202 m S	Arroio Areião (ESA)	Chlorite-muscovite schist	Chlorite, Muscovite, Plagioclase, Quartz	Pb-Pb, Sm-Nd
POR 12 A	0303845 m E 6580950 m S	Cerro Cambará	Quartz-muscovite schist	Muscovite, Quartz	Pb-Pb, Sm-Nd, U-Pb (zircon)*
POR 13 A	0304250 m E 6585050 m S	Arroio Areião (ESA)	Muscovite schist	Muscovite, Quartz	Pb-Pb, Sm-Nd, U-Pb (zircon)*
POR 18 B	0303100 m E 6585650 m S	Arroio Areião (ESA)	Feldspar-quartz-chlorite schist	Muscovite, Biotite, Quartz, Plagioclase	Pb-Pb, Sm-Nd, U-Pb (zircon)
RIP 03 B	0285108 m E 6575214 m S	Arroio Areião (WSA)	Chlorite-muscovite schist	Chlorite, Muscovite, Plagioclase, Quartz ± Carbonate	Pb-Pb, Sm-Nd, U-Pb (zircon)*
RIP 05 B	0285835 m E 6573864 m S	Arroio Areião (WSA)	Chlorite-muscovite schist	Chlorite, Muscovite, Plagioclase, Quartz ± Carbonate	Pb-Pb, Sm-Nd, U-Pb (zircon)*
RIP 06 A	0285952 m E 6572869 m S	Arroio Areião (WSA)	Chlorite-muscovite schist	Chlorite, Muscovite, Plagioclase, Quartz ± Carbonate	Pb-Pb, Sm-Nd, U-Pb (zircon)*
RIP 07 A	0285999 m E 6572527 m S	Arroio Areião (ECG)	Chlorite-muscovite schist	Chlorite, Muscovite, Plagioclase, Quartz	Pb-Pb, Sm-Nd, U-Pb (zircon)*
RIP 09 C	0287367 m E 6564841 m S	Arroio Areião (ECG)	Chlorite-muscovite schist	Chlorite, Muscovite, Plagioclase, Quartz	Pb-Pb, Sm-Nd
RIP 11	0286715 m E 6562808 m S	Quartz Mylonite (ECG)	Quartz mylonite	Quartz, Plagioclase, Muscovite	Pb-Pb, U-Pb (zircon)*
RIP 13	0275535 m E 6530189 m S	Arroio Areião (ECG)	Quartz-muscovite schist	Muscovite, Quartz	Pb-Pb
RIP 15 A	0275555 m E 6527489 m S	Arroio Areião (ECG)	Chlorite-muscovite phyllite	Chlorite, Muscovite, Plagioclase, Quartz	Pb-Pb

Table 2

Sample POR 18			**Isotope ratios**							**Ages (Ma)**						
Spot number	**$^{206}Pb/^{204}Pb$**	**Th/U**	**$^{207}Pb/^{235}U$**	**1 s [%]**	**$^{206}Pb/^{238}U$**	**1 s [%]**	**Rho**	**$^{207}Pb/^{206}Pb^{d}$**	**1 s [%]**	**$^{206}Pb/^{238}U$**	**1 s abs**	**$^{207}Pb/^{235}U$**	**1 s abs**	**$^{207}Pb/^{206}Pb$**	**1 s abs**	**% Conc**
Zr-111-F-VI-01	2992	0.02	1.23789	2.90	0.13704	1.51	0.52	0.06552	2.47	828	13	818	24	791	20	105
Zr-111-F-VI-02	3147	0.32	1.18410	3.36	0.13227	1.48	0.44	0.06493	3.02	801	12	793	27	772	23	104
Zr-111-F-VI-03	2818	0.23	1.16344	3.36	0.12876	1.60	0.48	0.06553	2.95	781	12	784	26	791	23	99
Zr-111-F-VI-04	5802	0.34	1.01296	3.27	0.11067	2.13	0.65	0.06638	2.49	677	14	710	23	818	20	83
Zr-111-F-VI-05	5319	0.25	1.20014	2.89	0.13274	1.65	0.57	0.06557	2.37	803	13	801	23	793	19	101
Zr-111-F-VI-07	9343	0.36	1.16708	3.65	0.13007	2.21	0.61	0.06508	2.90	788	17	785	29	777	23	101
Zr-111-F-VI-08	3977	0.24	1.24506	2.81	0.13953	1.42	0.50	0.06472	2.43	842	12	821	23	765	19	110
Zr-111-F-VI-09	5169	0.57	1.22760	3.45	0.13599	2.39	0.69	0.06547	2.48	822	20	813	28	790	20	104
Zr-111-F-VI-10	3318	0.32	1.14121	3.30	0.12662	1.90	0.57	0.06537	2.70	769	15	773	26	786	21	98
Zr-111-F-VI-11	3462	0.34	1.20104	3.10	0.13263	1.94	0.63	0.06568	2.42	803	16	801	25	796	19	101

Table 3

Sample	Sm(ppm)	Nd(ppm)	$^{147}Sm/^{144}Nd$	$^{143}Nd/^{144}Nd$	error (ppm)	Epsilon Nd (0)	Epsilon Nd (t)	T_{DM}	$^{143}Nd/^{144}Nd$ (t=750)
POR 04 A	6.37	32.03	0.12031	0.51197	43	-13.0	-5.7	1.73	0.51138
POR 06 A	0.74	3.81	0.11822	0.51208	56	-10.9	-3.5	1.53	0.51149
POR 11B	5.18	27.45	0.11398	0.51212	40	-10.1	-2.2	1.40	0.51156
POR 12 A	7.26	35.58	0.12343	0.51201	39	-12.3	-5.3	1.73	0.51140
POR 13 A	15.15	75.93	0.12061	0.51199	13	-12.6	-5.4	1.71	0.51140
POR 18 B	2.52	12.53	0.12165	0.51231	65	-6.5	0.7	1.21	0.51171
RIP 03 B	4.14	18.12	0.13809	0.51176	13	-17.1	-11.5	2.58	0.51108
RIP 05 B	7.42	33.49	0.13399	0.51200	35	-12.4	-6.4	1.98	0.51134
RIP 06 A	0.51	2.58	0.11923	0.51173	24	-17.8	-10.4	2.11	0.51114
RIP 07 A	6.97	31.88	0.13212	0.51199	94	-12.7	-6.5	1.96	0.51134
RIP 09 C	5.02	23.40	0.12983	0.51195	13	-13.4	-7.0	1.97	0.51131
RIP11	0.55	2.70	0.12307	0.51138	3	-24.7	-17.54	2.80	0.51077
RIP 13	8.19	37.44	0.13219	0.51182	83	-15.97	-9.80	2281	0.51117
RIP 15 A	8.56	40.65	0.12731	0.51195	57	-13.41	-6.77	1916	0.51132

Table 4

Sample Name	**$^{206}Pb/^{204}Pb$**	**SE (%)**	**$^{207}Pb/^{204}Pb$**	**SE (%)**	**$^{208}Pb/^{204}Pb$**	**SE (%)**	**$^{208}Pb/^{206}Pb$**	**SE (%)**	**$^{207}Pb/^{206}Pb$**	**SE (%)**
POR 04 A	19.37561	0.0083	15.74699	0.0075	39.83039	0.0075	2.05567	0.0023	0.81272	0.0016
POR 06 A	19.19231	0.0042	15.73182	0.0054	39.89286	0.0040	2.07867	0.0017	0.81973	0.0015
POR 11B	19.88524	0.0078	15.78905	0.0062	40.35159	0.0072	2.02918	0.0038	0.79399	0.0014
POR 12 A	18.81813	0.0049	15.72727	0.0049	39.05199	0.0051	2.07522	0.0010	0.83575	0.0007
POR 13 A	19.13910	0.0009	15.74474	0.0018	39.54444	0.0024	2.06614	0.0019	0.82263	0.0015
POR 18 B	20.01847	0.0258	15.82259	0.0260	39.95011	0.0246	1.99565	0.0030	0.79038	0.0040
RIP 03 B	19.61483	0.0029	15.93771	0.0026	40.84595	0.0042	2.08257	0.0003	0.81244	0.0002
RIP 05 B	20.01148	0.0018	15.94995	0.0016	40.31886	0.0026	2.01493	0.0002	0.79694	0.0002
RIP 06 A	19.01235	0.0017	15.74994	0.0016	38.79429	0.0025	2.04064	0.0002	0.82814	0.0002
RIP 07 A	19.71898	0.0017	15.78861	0.0015	39.60218	0.0025	2.00847	0.0002	0.80058	0.0002
RIP 09 C	18.55247	0.0013	15.68252	0.0012	38.68988	0.0020	2.08561	0.0002	0.84525	0.0001
RIP 11	19.27950	0.0018	15.74303	0.0017	38.48995	0.0027	1.99657	0.0002	0.81649	0.0001
RIP 13	19.78336	0.0030	15.79877	0.0027	41.59954	0.0044	2.10292	0.0003	0.79849	0.0002
RIP 15 A	18.60428	0.0015	15.74809	0.0014	39.55200	0.0022	2.12615	0.0002	0.84641	0.0001

Table 5

Sample	POR-04-A	POR-06-A	POR-11-B	POR-12-A	POR-13-A	POR-18-B
SiO_2	73,39	55,3	68,02	70,7	52,62	88,74
Al_2O_3	13,36	20,4	13,56	13,74	23,27	5,33
TiO_2	0,91	1,38	0,69	0,9	1,32	0,36
Fe_2O_3 (total)	5,28	9,74	4,34	7,03	8,36	3,12
MnO	0,02	0,18	0,1	0,16	0,06	0,04
MgO	1	2,17	1,62	0,3	2,02	0,3
CaO	0,02	0,37	2,5	nd	0,02	0,02
Na_2O	0,01	0,86	1,74	nd	0,57	0,09
K_2O	2,43	4,1	3	2,84	5,49	1,45
P_2O_5	0,05	0,14	0,08	0,09	0,1	0,01
LOI*	3,73	4,7	4,02	4,29	6,05	1,46
Total	**100,19**	**99,34**	**99,68**	**100,05**	**99,88**	**100,93**
Y	-	-	34	55	129	16
Pb	-	-	15	49	31	6
Ni	-	-	6	56	34	nd
Co	-	-	nd	75	37	nd
Cu	-	-	12	50	64	16
Ga	-	-	15	21	41	7
Sr	-	-	103	61	115	20
Zr	-	-	232	400	200	309
Zn	-	-	52	265	212	26
Nb	-	-	14	24	44	5

Rb	-	-	195	226	466	92
As	-	-	2	20	11	nd
Cr	-	-	139	144	205	142
Ba	-	-	715	697	1917	466
CIA	85.96	79.28	65.19	79.28	79.28	77.35

MSc Leonardo Gruber:

Thank you for submitting the manuscript, "Geochronology (U-Pb) and isotope geochemistry (Sr/Sr and Pb/Pb) applied to the Varzea do Capivarita Metamorphic Suite, Dom Feliciano Belt, Southern Brazil: Insights and paleogeographical implications to West Gondwana evolution" to Geochimica Brasiliensis. With the online journal management system that we are using, you will be able to track its progress through the editorial process by logging in to the journal web site:

Manuscript URL:
http://www.geobrasiliensis.org.br/ojs/index.php/geobrasiliensis/author/submission/446
Username: leonardogruber

If you have any questions, please contact me. Thank you for considering this journal as a venue for your work.

Geochronology (U-Pb) and isotope geochemistry (Sr/Sr and Pb/Pb) applied to the Varzea do Capivarita Metamorphic Suite, Dom Feliciano Belt, Southern Brazil: Insights and paleogeographical implications to West Gondwana evolution

Leonardo Gruber[1], Carla Cristine Porcher[2], Humberto Geller[1], Luís Alberto D'Ávilla Fernandes[2], Edinei Koester[2]

1 - Programa de Pós-graduação em Geociências, Universidade Federal do Rio Grande do Sul (Instituto de Geociências, Av. Bento Gonçalves, 9500. Porto Alegre, RS, Brasil - CEP 91501-970. leonardo.gruber@ufrgs.br;
2 - Departamento de Geologia, UFRGS. Av. Bento Gonçalves, 9500. Porto Alegre, RS, Brasil - CEP 91501-970.

ABSTRACT

Geochronological and isotope geochemistry analysis on the marbles and pelitic gneisses outcropping in the Várzea do Capivarita Metamorphic Suite in the Dom Feliciano Belt (DFB), southern Brazil, confirms its origin during the agglutination of Congo-Kalahari-La Plata cratons into the Gondwana Supercontinent, in the Tonian-Cryogenian periods. Detrital ages displayed provenance from local sources (2.2 - 2.0 Ga), from development of rifting processes (1.7 Ga) to agglutination of terrains in the Neoproterozoic (0.7 Ga), and constraints the sediments deposition within minimum detrital age of 714.3 ± 3.9 Ma and metamorphic age of 618 ± 7.3 Ma. $^{206}Pb/^{204}Pb$ and $^{207}Pb/^{204}Pb$ analysis displayed variations from ratios near those obtained to stromatolitic dolomites in Gariep Belt (Kalahari) and some o of the less radiogenic ratio are similar to signatures of Neoproterozoic (ca. 800 Ma) volcanic arcs (Cerro Bori Continental Arc) in the Rio de La Plata craton. Comparison with others marble-schists sequences from DFB, Marmora Terrane and African sequences lead to the interpretation of these sediments representing small-area basins developing along little shallow bays in the agglutination of terrains between Kalahari and La Plata cratons in the Neoproterozoic. $^{87}Sr/^{86}Sr$ ratio of 0.70609 found in marbles could also be considered a West Gondwana extension of the Sturtian glacial epoch.

Key Words: Isotope Geochemistry; Geochronology; Sturtian Glacial Epoch; West Gondwana

1. INTRODUCTION

The evolution of Gondwana west margin can be summarized as the result of interactions between five recognized cratons (Amazonia, West African, Rio de La Plata, Kalahari, São Francisco - Congo) and others elusive cratons, such as Paranapanema and cratonic fragments, as the Luis Alvez Terrain (Cordani *et al.*, 2013).

The Pan-African-Brasiliano orogeny marks the supercontinent's agglutination on its western side, with consumption of oceanic plates, possibly the Adamastor ocean between La Plata-Kalahari/Congo, and Khomas between Kalahari/Congo at the end of the Neoproterozoic (e.g Frimmel *et al.*, 2008; Basei *et al.*, 2011; Rapela *et al.*, 2011). In this context, the Dom Feliciano Belt (DFB) in the Southern Brazil is the southernmost portion of the Mantiqueira Province, and is a crucial belt to understand evolution of the Gondwana formation on its western side and its role in the major glacial epochs that marks this period.

Trying to contextualize the DFB in the Stuartian-Cryogenian-Marinoan glaciations, we used U-Pb in detrital and metamorphic rims of zircon grains of paragneisses, as well as Pb/Pb and $^{87}Sr/^{86}Sr$ in marbles, aiming to correlate the studied samples with the global registers of Snow Ball Earth (Sturtian Glaciation) and comparison with other sections of DFB and African carbonates.

2. GEOLOGY

The Várzea do Capivarita Metamorphic Suite (VCMS) outcrops in the eastern portion of the central region in this belt (Fig.1-b). The DFB can be subdivide in three major units separated by suture zones (Fernandes *et al.*, 1995a,b): *i*, Eastern Domain, with alkaline post tectonic granitic intrusions produced mainly in the Neoproterozoic, interpreted as an active continental-margin magmatic registered in the Pelotas Batolith (Philipp and Machado, 2005); *ii*, the Central Domain, whose main feature are schists belts with provenance ages from ca. 0.5 to 2.8 Ga, with major peaks of U-Pb detrital zircon ages of 2.2 – 2.0 Ga (Basei *et al.*, 2011; Gruber et al., 2011; Pertille et al., 2015a), and TTG-type suite of calc-alkaline gneisses, like Encantadas Complex, interpreted as an active continental arc in the

Paleoproterozoic (Philipp *et al.*, 2008), along roof pendants of granulite facies (Encruzilhada Bock) and metasediments occurring on the roof pendants (VCMS) intruded by calc-alcaline granitoids trespassed by mid-crustal mega transcurrent shear zones (Fernandes and Koester, 1999b); and *iii*, the Western Domain, which is represented by an ophiolite assemblage in a Neoproterozoic juvenile magmatic arc of ca. 750 Ma (Leite *et al.*, 1998; Chemale 2000; Saalmann *et al.*, 2005; Lena *et al.*, 2014), with remnants of older crust present in megaxenoliths dated at ca. 0.9 Ga (Hartmann *et al.*, 2008) and younger volcanic rocks of post-collisional affinity (Gastal *et al.*, 2005).

The VCMS is a sequence of metapelites, pure and impure marbles, calc-silicated rocks and mafic gneisses metamorphosed at high-anfibolite to granulite facies (Fernandes *et al.*, 1990; Silva et al., 2002; Gross *et al.*, 2006). Three sections were mapped and classified accordingly to field description, metamorphic association and structural analysis. The three sections are the Arroio Canhão, Cerro Partido and Várzea do Capivarita roof pendants.

The Várzea do Capivarita roof pendant is composed of pure and impure dolomitic marbles. Impure marbles displays compositional bands of centimeter to meter mafic (phlogopite + olivine) and felsic (calcite ± dolomite) layers. Boudins composed of diopside + pargasite interlayered with bands of phlogopite and olivine are common. Pure marbles displays massive structures, in some cases with original S0 preserved through the continuity of interlayered calcitic beds with dolomitic siliceous, quartz-feldspar pelitic gneisses and calc silicate gneisses (Silva *et al.*, 2002; Bom *et al.*, 2014). Boudins marked by forsterite encircling dolomite are interpreted as the result of reaction zones generated by hydrothermal fluid percolation (Silva *et al.*, 2002).

The Arroio Canhão roof pendant is represented by calc-silicate rocks, with a main mineralogy varying from felsic bands of calcite, quartz, plagioclase, scapolite and k-feldspar, interlayered by mafic bands composed of clinopiroxen, biotite and garnet (Silva *et al.*, 2002; Gross *et al.*, 2006).

The roof pendant of Cerro Partido displays outcrops of pelitic gneisses and migmatitic metapelites. The minimum conditions of metamorphism were determined in this section by Gross *et al* (2006) based on three groups: (*i*) garnet–cordierite–spinel–sillimanite–biotite–plagioclase–Kfeldspar in SiO_2-poor layers; (*ii*) garnet–quartz–biotite–cordierite–plagioclase–K-feldspar in SiO_2-rich layers, and (*iii*) quartz–garnet–biotite–K-feldspar in leucosome layers. Later, the peak conditions were determined as granulite facies (800-850°C, intermediate pressure and ultra-high temperature series) to the leucogranitic injections in the paragneisses (Bom *et al.*, 2014).

The metapelites and marbles of VCMS are understood as record of a passive margin, associated with a continental shelf in the Neoproterozoic (Fragoso-César, 1991; Fernandes *et al.*, 1992), deposited before the amalgamation of the cratons Rio de La Plata and Kalahari/Congo. Previous analysis of the metasedimentary units described the pure and impure marbles from VCMS as composed of interlayered bands of calcite and dolomite. Low-Mg calcite and high-Mg dolomites, the later displaying intergrowth with tremolite (Gross *et al.*, 2006), usually interpreted as hydrothermal interaction of fluids enriched in H_2O (Silva *et al.*, 2002).The high influx of fluids by break of biotite and muscovite (Bom *et al.*, 2002) and magmatic calc-alkaline intrusions (Cordilheira Granite) suggests that the metapelites and marbles had the peak conditions of metamorphism with ultra-high temperature (850-1000º C), possibly as result of a magmatic arc tectonic setting in a collisional belt event (Silva *et al.*, 2002; Bom *et al.*, 2014).

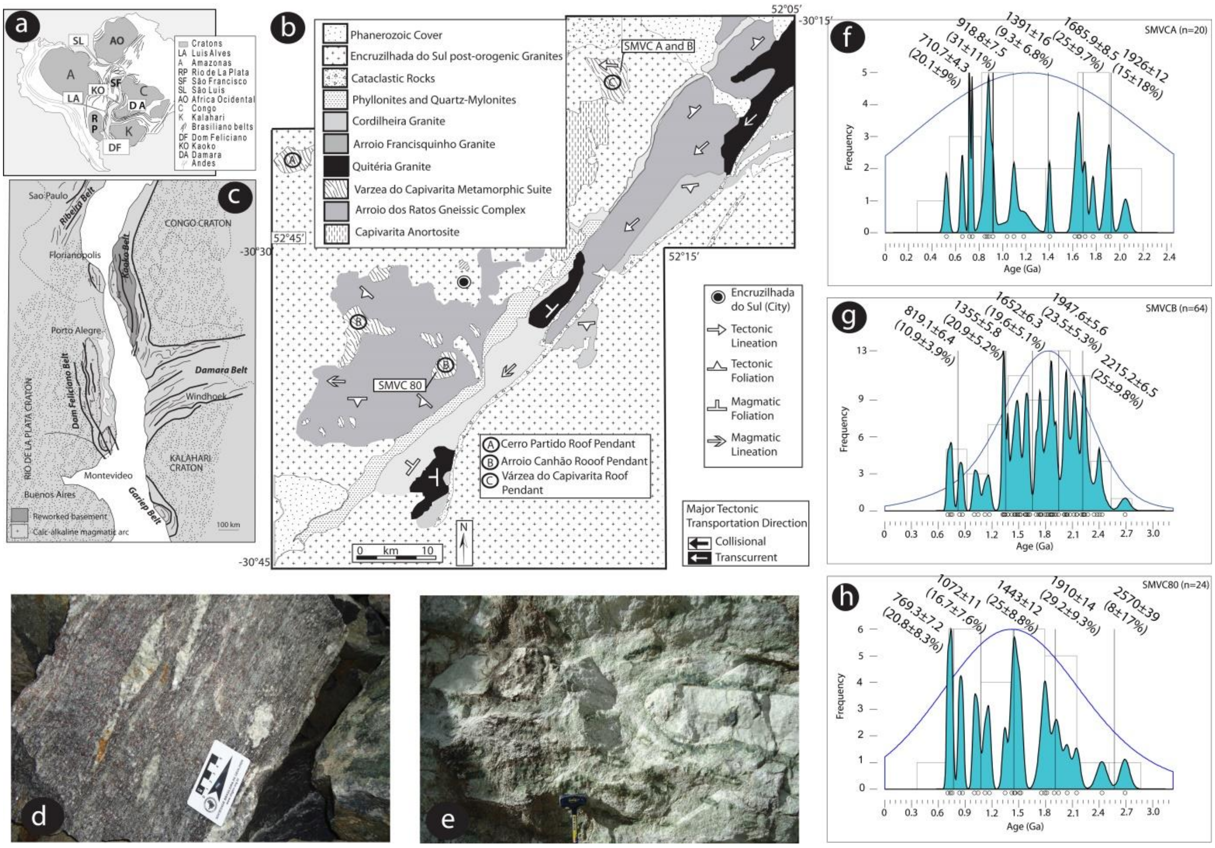

Figure 1 – VCMS is part of the DFB, in the MP (a), and its basin was developed among Kalahary, Congo and Rio de La Plata cratons during Rodínia breakup and Gondwana assembly (b); Geological sketch (modified from Silva *et al.*, 2002) (c) of the studied area, showing main occurrences of the VCMS outcrops in the Cerro Partido, Arroio Canhão and Várzea do Capivarita roof pendants and localization of selected samples and outcroppings in the VCMS (A); (d) detail of the pelitic gneiss; and (e) detail of the marbles (Várzea do Capivarita Roof Pendant); U-Pb data: plots of Kernel Density Estimates distributions on the $^{238}U/^{206}Pb$ zircon ages found on samples SMVCA (f) and B (g) and SMVC80 (h).

3. MATERIALS AND METHODS

Samples (four marbles and three metapelites) were collected in the Arroio Canhão and Várzea do Capivarita roof pendants (Fig.1-b), mainly from a limestone quarry characterized by ca. 40 meter walls of marbles and interlayered with pelitic gneiss (samples in Fig.1-d and e). Gneiss banding is well marked on outcrop and thin sections in the pelitic gneisses, with uneven levels of granoblastic quartz-feldspar alternating bands with biotite in preferred orientation forming an equigranular lepidoblastic texture. Interlobbed-contact in quartz grains occurs in the pelitic gneisses.

$^{87}Sr/^{86}Sr$ was analyzed in TIMS model VG SECTOR 54 equipment localized at Laboratório de Geologia Isotópica from UFRGS (LGI-UFRGS). Samples were crushed and pulverized, weighted for ca. 0.01 gr in Savilex^{tm} beaks before chemical aperture with lixiviation by HCL 0.25 N at room temperature. Anionic chemical columns LN-B50-A (100 - 200 mesh) and cationic AG-50W-X8 (200 – 400 mesh) were used to separate Rb and Sr, by lixiviation of HCl 2.5N and HNO_3 in a step-leeching process. Details in this methodology can be obtained in Baylei *et al* (2000). Data displayed in table 1.

For Pb/Pb analysis, conventional chromatography cation-exchange methods were used, with dissolution in HNO_3 and HF in Savillex® vials. A

Finnigan Neptune ICPMS were used for ratio analysis. Uncertainties on ^{207}Pb/^{206}Pb are considered better than ± 0.1% (1σ) and ± 0.00001 (1σ), respectively, based repeated analyses of BHVO-1 standard. Details in sample dissolution and analysis parameters can be found at Abre *et al* (2012).Data is presented in Table 2.

Zircon concentrates were extracted from 5-10 kg of rock samples. Samples were crushed in a jaw crusher to a 500 μm size, followed by panning. Zircons were separated by use of standard gravitational techniques and Frantz Isodynamic® separator, and handpicked under binocular microscope. The zircon concentrates were cast in epoxy. Cathodoluminescence images performed prior U-Pb analyses were used to indicate possible metamorphic rims on the crystal structures (selected images on Figure 2).

U-Pb ages (sample SMVC80) were obtained in the SHRIMP II in the facilities of Universidade de São Paulo (USP). All analytical procedures used are the same described in Williams (1998). To each zircon grain analyzed, four scans through the mass stations were made for every age determination. Standard Temora 2 with ^{206}Pb/^{238}U age of 416.18 ± 0.33 Ma was used to calibrate the ^{206}Pb/^{238}U ratios. Decay constants are the same recommended by Steiger and Jager (1977). Common lead correction was made with measured ^{204}Pb in each analysis, and data reduction with Squid and Isoplot Excel™ programs (Ludwig, 2003) (Data presented in Tables 3 and 4).

Samples SMVCA and B were dated with laser ablation microprobe (New Wave UP213) coupled to a MC-ICP-MS (ThermoFinnigan-Neptune) at LGI-UFRGS. Isotope data where acquired using static mode with spot size of 25 um, with frequency of 10 Hz and intensity of ~4 J/cm^2. Analyses were made in 40 cycles of 1 s, with laser-induced elemental fractionation and instrumental mass discrimination corrected by GJ-1 (standard zircon) with the measurement of two GJ-1 analyses to every four sample zircon spots. The external error was calculated after propagation of the error of the GJ-1 mean and the individual sample zircon. Data were reduced using in-house programs developed at the LGI-UFRGS (Data is presented on tables 5 and 6).

Probability Density Plots and Kernel Density Estimates were made with DensityPlotter (Vermeesh, 2012), with grains with concordance better than 70%, only non-recrystallized nucleus and rims. ^{206}Pb/^{238}U ratios were used for Neoproterozoic detrital zircon ages, and ^{206}Pb/^{207}Pb to the older grains.

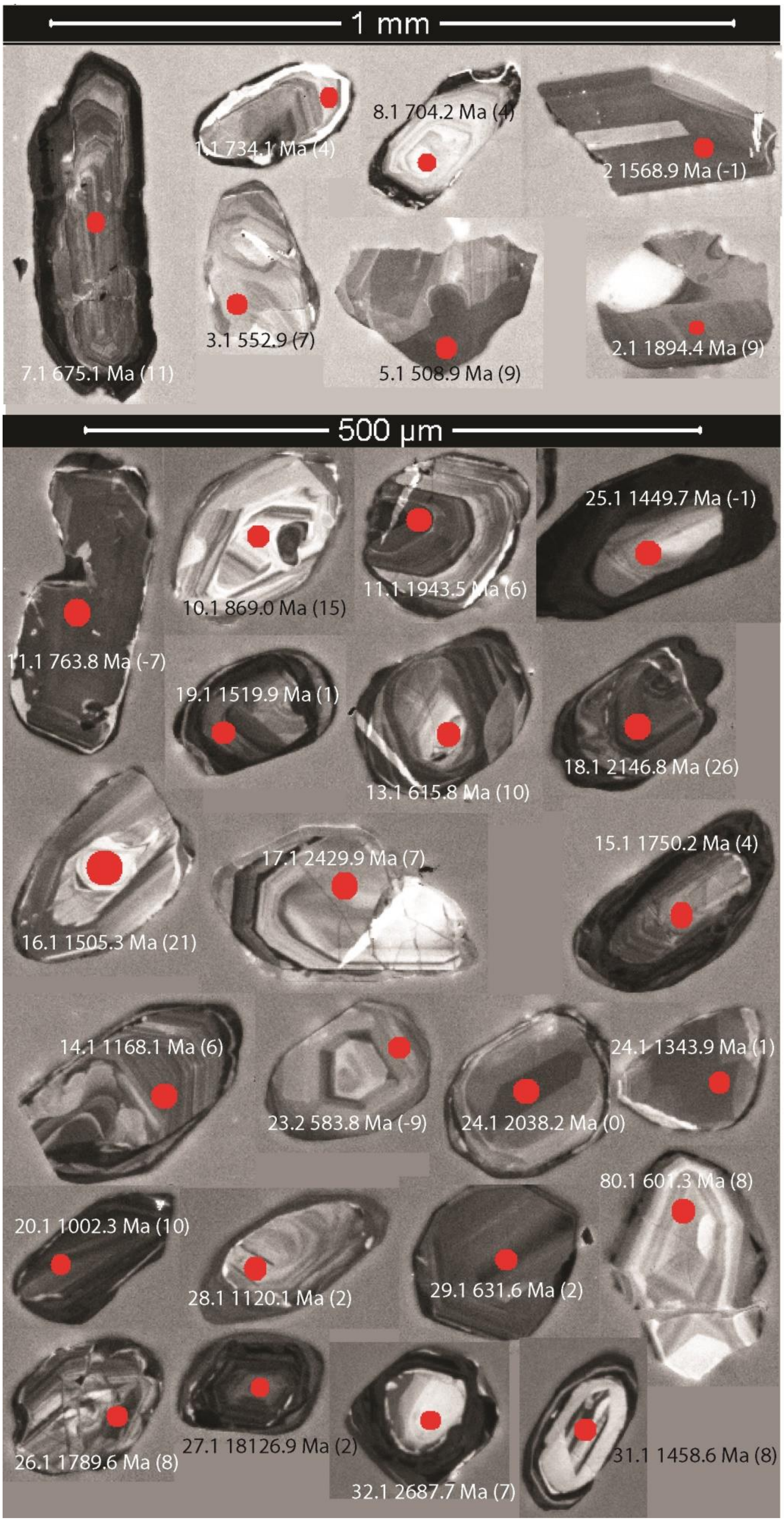

Fig. 2 - selected cathodoluminescence images for sample SMVC80 (red circle indicates beam position; includes ages and analysis number for reference). Cathodoluminescence imaging was carried out using a scanning electron microscope at the Universidade de São Paulo, Brazil.

Table 1 - $^{87}Sr/^{86}Sr$ Data.

Sample	$^{87}Sr/^{86}Sr$	error (%)	N. of Analysis
VC 13-1	0.71527912	0.0021	80
13-Mar	0.71268259	0.0014	100
VC 12-03	0.71204570	0.0028	80
PO 21	0.70609164	0.0006	100

Table 2 – Pb/Pb Data.

Sample Name	$^{206}Pb/^{204}Pb$	SE (%)	$^{207}Pb/^{204}Pb$	SE (%)	$^{208}Pb/^{204}Pb$	SE (%)
VC13-1	19.4212	0.003483	15.651667	0.002915	37.613468	0.006895
13/mar	17.9252	0.003756	15.567244	0.003200	37.573106	0.007532
VC12-03	20.3793	0.003914	15.790098	0.003454	38.046486	0.008872
PO21	25.0805	0.009486	16.131532	0.006070	37.743674	0.014223

Table 3 - SHRIMP Data (sample SMVC80).

Spot	$^{204}Pb/^{206}Pb$	% err	$^{207}Pb/^{206}Pb$	% err	$^{208}Pb/^{206}Pb$	% err	% comm 206	ppm U	ppm Th	$^{232}Th/^{238}U$
1-1.1	7.6E-4	26	.075	2.6	.142	3.0	1.42	186	75	0.42
1-2.1	3.1E-4	33	.132	0.9	.173	1.1	0.59	145	82	0.58
1-3.1	3.0E-4	50	.064	1.7	.157	1.5	0.56	294	135	0.47
1-4.1	4.3E-4	25	.065	1.6	.462	0.9	0.81	344	492	1.48
1-5.1	3.3E-4	24	.063	1.4	.106	1.5	0.61	506	161	0.33
1-6.1	3.2E-4	25	.068	2.2	.086	1.8	0.61	376	86	0.24
1-7.1	6.9E-4	18	.074	1.5	.204	1.2	1.30	335	192	0.59
1-8.1	4.2E-4	31	.070	1.4	.116	1.5	0.78	303	102	0.35
1-9.1	6.2E-5	43	.128	0.6	.232	0.7	0.12	312	239	0.79
1-10.1	4.4E-4	24	.079	1.4	.078	1.9	0.82	297	44	0.15
1-11.1	2.9E-4	26	.067	1.4	.300	1.0	0.55	355	341	0.99
1-12.1	1.7E-4	79	.104	1.1	.171	1.2	0.32	288	83	0.30
2-13.1	5.3E-4	25	.070	2.6	.276	1.8	0.99	264	208	0.81
3-14.1	3.0E-4	23	.086	1.1	.083	2.4	0.55	262	65	0.26
3-15.1	1.5E-4	32	.113	1.2	.189	1.4	0.28	179	112	0.65
3-16.1	6.3E-4	21	.120	1.0	.272	0.9	1.18	187	150	0.83
3-17.1	2.7E-4	24	.178	0.8	.164	1.1	0.51	126	71	0.59
3-18.1	1.1E-4	29	.187	0.7	.139	1.5	0.21	326	152	0.48
3-19.1	1.8E-4	23	.098	0.7	.099	1.0	0.33	473	151	0.33
4-20.1	5.7E-5	15	.077	1.0	.065	1.7	0.11	424	83	0.20
4-21.1	2.7E-4	29	.103	2.4	.035	7.8	0.51	189	12	0.06
4-21.2	1.1E-4	23	.116	0.6	.024	2.3	0.20	548	60	0.11
4-22.1	5.4E-5	60	.127	0.9	.209	0.7	0.10	299	212	0.73
4-23.1	1.7E-4	97	.068	2.7	.236	2.3	0.32	163	115	0.73
4-24.1	1.2E-4	43	.089	1.0	.384	0.7	0.23	279	349	1.29
4-23.2	5.1E-4	49	.065	3.0	.202	1.7	0.96	194	116	0.62

4-25.1	7.2E-4	25	.101	1.7	.389	1.3	1.35	74	92	1.29
5-26.1	2.2E-4	20	.122	0.7	.279	1.4	0.41	277	248	0.93
5-27.1	1.1E-4	32	.115	0.6	.201	0.7	0.21	396	259	0.67
5-28.1	2.5E-4	27	.081	1.2	.159	1.2	0.46	244	110	0.46
5-29.1	2.0E-4	27	.064	1.1	.410	0.7	0.37	569	739	1.34
5-30.1	4.0E-4	24	.067	1.6	.223	1.2	0.75	327	218	0.69
6-31.1	4.0E-4	16	.103	0.8	.252	0.9	0.75	294	191	0.67
6-32.1	1.4E-4	60	.206	1.0	.282	2.0	0.26	63	61	1.00

Table 4 - SHRIMP ages (sample SMVC80).

Spot	**^{204}corr ^{206}Pb /^{238}U Age**	**1s err**	**^{207}corr ^{206}Pb /^{238}U Age**	**1s err**	**^{208}corr ^{206}Pb /^{238}U Age**	**1s err**	**^{204}corr ^{207}Pb /^{206}Pb Age**	**1s err**	**^{204}corr ^{208}Pb /^{232}Th Age**	**1s err**	**% Dis-cor-dant**
1-1.1	731.4	15.7	730.8	16.0	736.1	16.8	750	124	656	53	3
1-2.1	1894.4	36.6	1862.1	42.5	1899.2	39.8	2071	27	1833	65	9
1-3.1	552.9	12.2	552.1	12.3	552.9	13.1	594	90	553	27	7
1-4.1	568.9	12.0	569.0	12.2	571.8	15.8	563	77	558	14	-1
1-5.1	508.9	11.7	508.2	11.8	511.0	12.3	554	58	468	21	9
1-6.1	578.8	12.0	576.2	12.2	578.7	12.5	705	68	582	31	22
1-7.1	675.1	14.0	673.1	14.3	676.0	15.5	753	85	665	27	11
1-8.1	704.2	14.6	703.4	14.9	706.5	15.4	732	76	661	39	4
1-9.1	1943.5	35.9	1919.9	42.1	1941.0	40.2	2066	12	1966	45	6
1-10.1	869.0	17.8	864.0	18.4	862.9	18.4	1002	59	1145	90	15
1-11.1	753.8	15.4	755.4	15.9	759.0	18.2	699	53	722	19	-7
1-12.1	1043.3	21.2	1007.1	22.0	1006.6	22.6	1649	41	1876	76	58
2-13.1	615.8	13.1	614.5	13.4	613.5	15.1	675	99	633	22	10
3-14.1	1168.1	23.3	1163.8	24.6	1170.7	24.3	1240	36	1098	56	6
3-15.1	1750.2	45.6	1741.0	51.8	1753.3	50.1	1815	25	1716	59	4
3-16.1	1505.3	33.7	1471.4	36.8	1500.5	38.6	1815	41	1545	54	21
3-17.1	2429.9	57.7	2361.5	77.5	2439.7	62.4	2600	17	2300	81	7
3-18.1	2146.8	39.1	1982.6	52.3	2148.2	41.8	2700	12	2123	59	26
3-19.1	1519.9	29.0	1517.8	31.9	1522.6	30.4	1541	19	1462	44	1
4-20.1	1002.3	19.9	997.8	20.7	1001.6	20.5	1098	21	1029	29	10
4-21.1	835.3	17.7	801.2	18.4	833.3	17.9	1611	52	1048	162	93
4-21.2	1421.1	27.0	1375.4	29.2	1429.8	27.4	1870	12	848	51	32
4-22.1	2038.2	37.3	2036.7	45.3	2040.3	41.3	2046	16	2018	47	0
4-23.1	607.0	13.3	602.4	13.4	605.3	15.0	807	97	621	27	33
4-24.1	1343.9	26.2	1342.7	28.3	1346.2	32.4	1359	26	1333	31	1
4-23.2	583.8	15.2	584.9	15.4	585.6	16.7	529	164	566	36	-9
4-25.1	1449.7	31.3	1451.0	34.1	1460.9	38.7	1436	72	1395	48	-1
5-26.1	1789.6	33.9	1766.8	38.6	1786.4	39.1	1936	17	1813	48	8
5-27.1	1812.6	34.8	1807.1	40.1	1810.6	38.4	1848	14	1834	45	2
5-28.1	1120.1	27.4	1119.1	28.9	1114.5	29.6	1138	37	1202	41	2
5-29.1	631.6	12.8	631.4	13.1	635.1	16.2	643	40	617	14	2
5-30.1	601.3	13.1	600.3	13.4	602.3	14.8	647	69	593	19	8
6-31.1	1458.6	28.0	1446.8	30.5	1430.7	31.6	1582	29	1742	46	8
6-32.1	2687.7	52.8	2579.3	81.1	2683.1	60.8	2864	18	2723	91	7

Table 5 - Laser Ablation ICP-MS U–Pb data (MT110 – SMVCA; MT109 – SMVCB).

Sample	f(206)%	Th/U	6/4 ratio	7/6 ratio	1s(%)	7/5 ratio	1s(%)	6/8 ratio	1s(%)	Rho
03_mt110_1	0.09	0.38	181375	0.06373	6.2	0.9432	6.6	0.10734	2.2	0.33
04_mt110_2	0.02	0.29	295326	0.13377	1.8	6.2664	2.3	0.33975	1.4	0.61
05_mt10_3	0.04	0.43	113172	0.06212	2.6	0.8561	2.8	0.09996	1.1	0.37
06_mt110_04	0.02	0.21	256747	0.06266	3.8	0.8716	3.9	0.10089	1.1	0.45
09_mt110_05	0.01	0.43	1576	0.13751	2.1	7.0993	2.8	0.37443	1.8	0.65
10_mt110_6	0.03	0.64	4077	0.05808	3.2	0.8043	3.5	0.10044	1.3	0.36
11_mt110_7	0.01	0.51	11368	0.12476	1.8	5.0388	2.2	0.29292	1.2	0.53
12_mt110_08	0.02	0.47	1104	0.06235	3.7	0.8278	3.9	0.09629	1.2	0.45
15_mt110_09	0.02	0.36	4799	0.11813	4.0	2.3975	4.3	0.14719	1.5	0.34
16_mt110_10	0.06	0.29	570	0.13114	1.4	5.7211	1.9	0.31640	1.2	0.63
17_mt110_11	0.03	0.27	5505	0.05763	2.5	0.8339	3.0	0.10495	1.7	0.54
18_mt110_12	0.07	0.09	12113	0.06142	11.8	0.9036	12.0	0.10671	2.3	0.35
22_mt110_13	0.00	0.38	181375	0.09734	1.2	1.9344	2.4	0.14413	2.1	0.86
23_mt110_14	0.01	0.29	295326	0.10370	1.4	2.1844	2.2	0.15278	1.8	0.78
18_mt110_15	0.01	0.43	113172	0.09991	11.6	2.4082	16.7	0.17482	12.0	0.72
25_mt110_16	0.01	0.21	256747	0.10151	2.1	2.5974	2.9	0.18559	1.9	0.85
26_mt110_17	0.00	0.43	1576	0.13366	1.1	5.3695	1.9	0.29136	1.6	0.81
29_mt110_18	0.02	0.64	4077	0.05947	1.5	0.8287	1.8	0.10107	1.0	0.53
30_mt110_19	0.00	0.51	11368	0.13061	3.1	3.6168	6.7	0.20084	5.9	0.89
30_mt110_20	0.01	0.47	1104	0.07356	1.5	1.1965	1.8	0.11797	1.0	0.72
34_mt110_21	0.01	0.36	4799	0.11003	1.0	3.6822	1.6	0.24272	1.2	0.76
29_mt110_18	0.01	0.29	570	0.13054	0.9	5.4477	1.4	0.30267	1.1	0.75
36_mt110_23	0.00	0.27	5505	0.07847	1.3	1.3201	1.6	0.12201	1.0	0.59
37_mt110_24	0.01	0.09	12113	0.06828	8.1	0.7941	8.9	0.08435	3.6	0.66
40_mt110_25	0.00	0.38	181375	0.13220	0.9	6.3027	1.4	0.34579	1.0	0.73
41_mt110_26	0.01	0.29	295326	0.08731	2.7	1.6930	4.7	0.14064	3.9	0.82
42_mt110_27	0.01	0.43	113172	0.06035	0.9	0.8677	1.4	0.10429	1.0	0.71
43_mt110_28	0.00	0.21	256747	0.13704	2.5	5.3860	2.9	0.28505	1.5	0.73
11_mt109_5	0.04	0.35	29560	0.06426	0.9	0.8800	1.2	0.09932	0.8	0.64
12_mt109_6	0.05	0.13	37098	0.13570	0.8	7.3937	1.2	0.39517	0.9	0.74
14_mt109_8	0.01	0.25	9987	0.15660	0.7	7.4745	1.1	0.34617	0.9	0.86
17_mt109_9	0.01	0.45	83536	0.13101	0.5	4.6915	1.7	0.25971	1.6	0.94
19_mt109_11	0.01	0.30	24008	0.12739	0.6	5.0234	2.4	0.28599	2.4	0.97
20_mt109_12	0.02	0.30	33258	0.12581	0.8	5.2948	1.6	0.30523	1.3	0.92
23_mt109_13	0.20	0.40	33753	0.06019	2.5	0.7821	2.9	0.09425	1.5	0.50
24_mt109_14	0.01	0.23	31043	0.13767	0.5	7.0410	0.9	0.37095	0.7	0.81
25_mt109_15	0.04	0.20	33824	0.13388	0.6	7.6517	1.4	0.41453	1.3	0.92
35_mt109_21	0.03	0.21	38344	0.06112	1.0	0.8927	1.1	0.10593	0.6	0.51
36_mt109_22	0.03	0.22	56341	0.13275	0.6	6.7264	1.2	0.36749	1.1	0.88
41_mt109_25	0.03	0.31	30808	0.12468	0.6	6.6758	1.2	0.38832	1.0	0.85
43_mt109_27	0.03	0.32	47022	0.13322	0.6	7.7572	1.7	0.42232	1.5	0.93
44_mt109_28	0.03	0.23	38594	0.13019	1.7	5.5539	2.0	0.30940	1.0	0.73
47_mt109_29	0.02	0.33	32670	0.12526	0.5	5.7846	1.1	0.33493	1.0	0.89
53_mt109_33	0.02	0.18	20079	0.12980	0.6	7.0792	2.3	0.39557	2.2	0.97
54_mt109_34	0.21	0.23	82526	0.05970	1.8	0.9601	2.5	0.11664	1.8	0.70
55_mt109_35	0.02	0.31	55610	0.11663	0.6	3.6503	1.6	0.22699	1.5	0.94
56_mt109_36	0.01	0.30	14914	0.11378	1.0	3.7389	1.3	0.23833	0.9	0.81
60_mt109_37	0.02	0.35	29560	0.11755	1.2	3.8465	3.9	0.23733	3.7	0.95
61_mt109_38	0.01	0.13	37098	0.06834	1.6	0.9902	2.7	0.10508	2.2	0.80
62_mt109_39	0.07	0.13	18379	0.06013	1.0	0.8802	1.5	0.10616	1.1	0.72
63_mt109_40	0.02	0.25	9987	0.16595	0.8	10.3187	1.2	0.45097	1.0	0.87
66_mt109_42	0.03	0.31	27997	0.13780	0.6	7.8436	1.1	0.41282	0.9	0.84

67_mt109_43	0.03	0.30	24008	0.13689	0.5	7.7536	1.5	0.41080	1.4	0.93
73_mt109_47	0.04	0.20	33824	0.13063	0.6	6.0723	1.5	0.33715	1.4	0.92
74_mt109_48	0.04	0.25	68167	0.13216	1.0	7.0739	1.3	0.38820	0.9	0.82
78_mt109_50	0.05	0.25	30257	0.10357	0.8	4.2852	1.2	0.30008	0.9	0.76
79_mt109_51	0.01	0.23	48280	0.11069	0.5	4.3217	1.1	0.28318	1.0	0.88
80_mt109_52	0.06	0.32	40790	0.05872	6.1	0.7942	7.6	0.09809	4.5	0.82
86_mt109_56	0.02	0.30	57776	0.12346	0.6	5.5794	1.5	0.32777	1.4	0.92
89_mt109_57	0.03	0.36	51106	0.12145	0.8	3.8525	1.4	0.23006	1.1	0.88
89_mt109_57	0.03	0.31	30808	0.12161	0.6	3.8478	1.3	0.22947	1.1	0.86
91_mt109_59	0.02	0.32	47022	0.14218	1.7	6.5227	3.7	0.33273	3.3	0.89
95_mt109_61	0.04	0.33	32670	0.12704	0.6	5.8914	1.2	0.33633	1.0	0.87
97_mt109_63	0.04	0.34	43095	0.06023	0.8	0.8574	1.2	0.10324	0.9	0.73
98_mt109_64	0.01	0.27	39232	0.12567	1.4	4.4589	2.7	0.25733	2.3	0.94
102_mt109_65	0.03	0.18	20079	0.12451	0.6	4.7964	1.4	0.27938	1.3	0.89
103_mt109_66	0.05	0.23	82526	0.12034	0.5	5.1493	1.4	0.31035	1.3	0.92
104_mt109_67	0.02	0.31	55610	0.12764	0.5	6.5324	1.9	0.37119	1.8	0.96
105_mt109_68	0.02	0.30	14914	0.12647	0.9	6.6125	1.4	0.37922	1.1	0.87
108_mt109_69	0.01	0.35	29560	0.14461	1.7	8.1139	4.0	0.40694	3.7	0.91
109_mt109_70	0.04	0.13	37098	0.12236	0.6	6.1634	1.6	0.36532	1.5	0.93
114_mt109_72	0.01	0.45	83536	0.12484	0.8	4.7699	2.0	0.27712	1.8	0.91
115_mt109_74	0.02	0.31	27997	0.12851	0.5	4.8857	1.3	0.27573	1.2	0.91
116_mt109_75	0.01	0.30	24008	0.16286	0.5	9.3016	1.7	0.41424	1.6	0.96
120_mt109_77	0.01	0.40	33753	0.13323	0.7	8.0394	3.3	0.43765	3.3	0.98
121_mt109_78	0.01	0.23	31043	0.14248	1.2	8.7441	3.1	0.44511	2.9	0.92
123_mt109_80	0.23	0.25	68167	0.06681	4.2	0.9601	4.5	0.10422	1.6	0.59

Table 6- Laser Ablation ICP-MS U–Pb ages (MT110 – SMVCA; MT109 – SMVCB).

Sample	7/6 age	1s(Ma)	7/5 age	1s(Ma)	6/8 age	1s(Ma)	Conc (%)
03_mt110_1	732.7	132.0	674.6	32.6	657.3	13.7	89.71
04_mt110_2	2148.1	30.8	2013.8	19.7	1885.4	22.9	87.77
05_mt10_3	678.1	55.5	628.0	13.2	614.2	6.3	90.56
06_mt110_04	696.7	80.0	636.4	18.6	619.6	6.8	88.94
09_mt110_05	2196.1	36.6	2124.0	24.8	2050.2	31.9	93.36
10_mt110_6	532.6	70.2	599.2	15.6	617.0	7.6	115.84
11_mt110_7	2025.4	32.5	1825.9	18.5	1656.1	17.3	81.76
12_mt110_08	686.2	78.5	612.4	17.8	592.7	6.7	86.37
15_mt110_09	1928.1	71.7	1241.8	30.6	885.2	12.3	45.91
16_mt110_10	2113.3	25.3	1934.6	16.4	1772.1	19.0	83.86
17_mt110_11	515.7	55.4	615.8	13.9	643.3	10.1	124.74
18_mt110_12	653.8	253.8	653.7	58.1	653.6	14.1	99.97
22_mt110_13	1573.8	23.3	1093.1	16.3	868.0	17.0	55.15
23_mt110_14	1691.3	25.5	1176.1	15.6	916.5	15.1	54.19
18_mt110_15	1622.4	216.2	1245.1	119.9	1038.6	115.2	64.02
25_mt110_16	1651.8	38.7	1299.9	21.0	1097.4	19.7	66.44
26_mt110_17	2146.6	19.5	1880.0	16.6	1648.3	23.1	76.79
29_mt110_18	584.3	31.7	612.9	8.1	620.7	5.8	106.22
30_mt110_19	2106.2	54.4	1553.2	53.2	1179.8	63.9	56.02
30_mt110_20	1029.3	30.7	799.0	9.9	718.9	6.5	69.84
34_mt110_21	1799.9	18.2	1567.5	12.5	1400.8	15.2	77.83
29_mt110_18	2105.2	15.8	1892.4	12.0	1704.5	15.9	80.97
36_mt110_23	1158.9	25.2	854.6	9.3	742.1	6.9	64.04
37_mt110_24	877.1	168.3	593.5	40.0	522.1	18.1	59.52
40_mt110_25	2127.3	15.9	2018.8	11.9	1914.5	16.7	89.99

41_mt110_26	1367.4	51.9	1005.9	30.3	848.3	31.0	62.04
42_mt110_27	616.0	20.3	634.3	6.4	639.5	6.0	103.81
43_mt110_28	2190.1	43.2	1882.6	25.1	1616.7	22.1	73.82
11_mt109_5	750.3	18.6	641.0	5.6	610.4	4.6	81.35
12_mt109_6	2173.0	14.0	2160.2	11.1	2146.8	17.2	98.79
14_mt109_8	2419.3	11.4	2169.9	9.9	1916.3	14.6	79.21
17_mt109_9	2111.6	9.6	1765.7	13.8	1488.4	20.7	70.48
19_mt109_11	2062.3	10.4	1823.3	20.7	1621.5	34.0	78.62
20_mt109_12	2040.2	14.9	1868.0	13.4	1717.2	20.0	84.17
23_mt109_13	610.3	53.1	586.7	12.7	580.6	8.1	95.14
24_mt109_14	2198.0	8.2	2116.6	7.7	2033.9	12.7	92.53
25_mt109_15	2149.4	9.7	2190.9	12.8	2235.6	24.7	104.01
35_mt109_21	643.6	20.4	647.8	5.5	649.1	4.0	100.84
36_mt109_22	2134.7	9.9	2076.1	10.8	2017.6	18.8	94.52
41_mt109_25	2024.3	11.0	2069.4	10.8	2115.0	18.9	104.48
43_mt109_27	2140.8	10.3	2203.3	14.8	2271.0	29.5	106.08
44_mt109_28	2100.5	29.9	1909.0	17.0	1737.7	15.4	82.73
47_mt109_29	2032.5	8.3	1944.1	9.5	1862.2	15.9	91.62
53_mt109_33	2095.2	10.2	2121.4	20.2	2148.6	40.2	102.55
54_mt109_34	592.8	38.1	683.4	12.4	711.2	11.9	119.97
55_mt109_35	1905.2	10.1	1560.6	12.9	1318.7	18.2	69.21
56_mt109_36	1860.6	17.2	1579.7	10.3	1378.0	10.7	74.06
60_mt109_37	1919.3	21.4	1602.5	31.3	1372.8	45.6	71.53
61_mt109_38	878.9	32.9	698.8	13.6	644.1	13.3	73.28
62_mt109_39	608.3	22.6	641.1	7.3	650.4	7.0	106.93
63_mt109_40	2517.2	12.9	2463.8	11.4	2399.6	19.3	95.33
66_mt109_42	2199.8	9.6	2213.2	9.7	2227.8	17.3	101.27
67_mt109_43	2188.2	9.5	2202.8	13.4	2218.6	25.9	101.39
73_mt109_47	2106.4	10.4	1986.3	13.3	1872.9	22.9	88.91
74_mt109_48	2126.8	16.9	2120.8	11.9	2114.5	16.5	99.42
78_mt109_50	1689.1	13.9	1690.5	9.9	1691.7	14.0	100.16
79_mt109_51	1810.7	9.4	1697.5	9.2	1607.3	14.0	88.77
80_mt109_52	556.9	133.5	593.6	34.0	603.2	25.7	108.31
86_mt109_56	2006.8	10.4	1912.9	13.0	1827.5	22.1	91.07
89_mt109_57	1977.6	15.0	1603.8	11.4	1334.8	13.6	67.50
89_mt109_57	1980.0	11.1	1602.8	10.3	1331.7	13.4	67.26
91_mt109_59	2253.9	28.9	2049.0	32.5	1851.6	53.0	82.15
95_mt109_61	2057.4	9.9	1960.0	10.3	1869.0	17.0	90.84
97_mt109_63	611.9	17.7	628.7	5.8	633.4	5.6	103.52
98_mt109_64	2038.3	25.5	1723.4	22.7	1476.2	30.7	72.42
102_mt109_65	2021.9	11.3	1784.3	11.9	1588.2	17.7	78.55
103_mt109_66	1961.2	9.7	1844.3	12.0	1742.4	19.9	88.84
104_mt109_67	2065.7	8.6	2050.3	16.3	2035.0	31.2	98.51
105_mt109_68	2049.4	16.3	2061.0	12.4	2072.6	18.7	101.13
108_mt109_69	2283.1	28.6	2243.8	36.5	2200.9	68.7	96.40
109_mt109_70	1990.9	10.4	1999.3	14.0	2007.3	25.7	100.82
114_mt109_72	2026.5	14.2	1779.6	16.6	1576.8	25.2	77.81
115_mt109_74	2077.7	9.1	1799.8	10.8	1569.8	16.3	75.56
116_mt109_75	2485.5	8.4	2368.2	15.8	2234.3	31.0	89.89
120_mt109_77	2141.0	12.6	2235.5	30.1	2340.1	63.9	109.30
121_mt109_78	2257.5	20.6	2311.7	28.3	2373.5	56.9	105.14
123_mt109_80	832.0	87.8	683.3	22.4	639.1	9.6	76.81

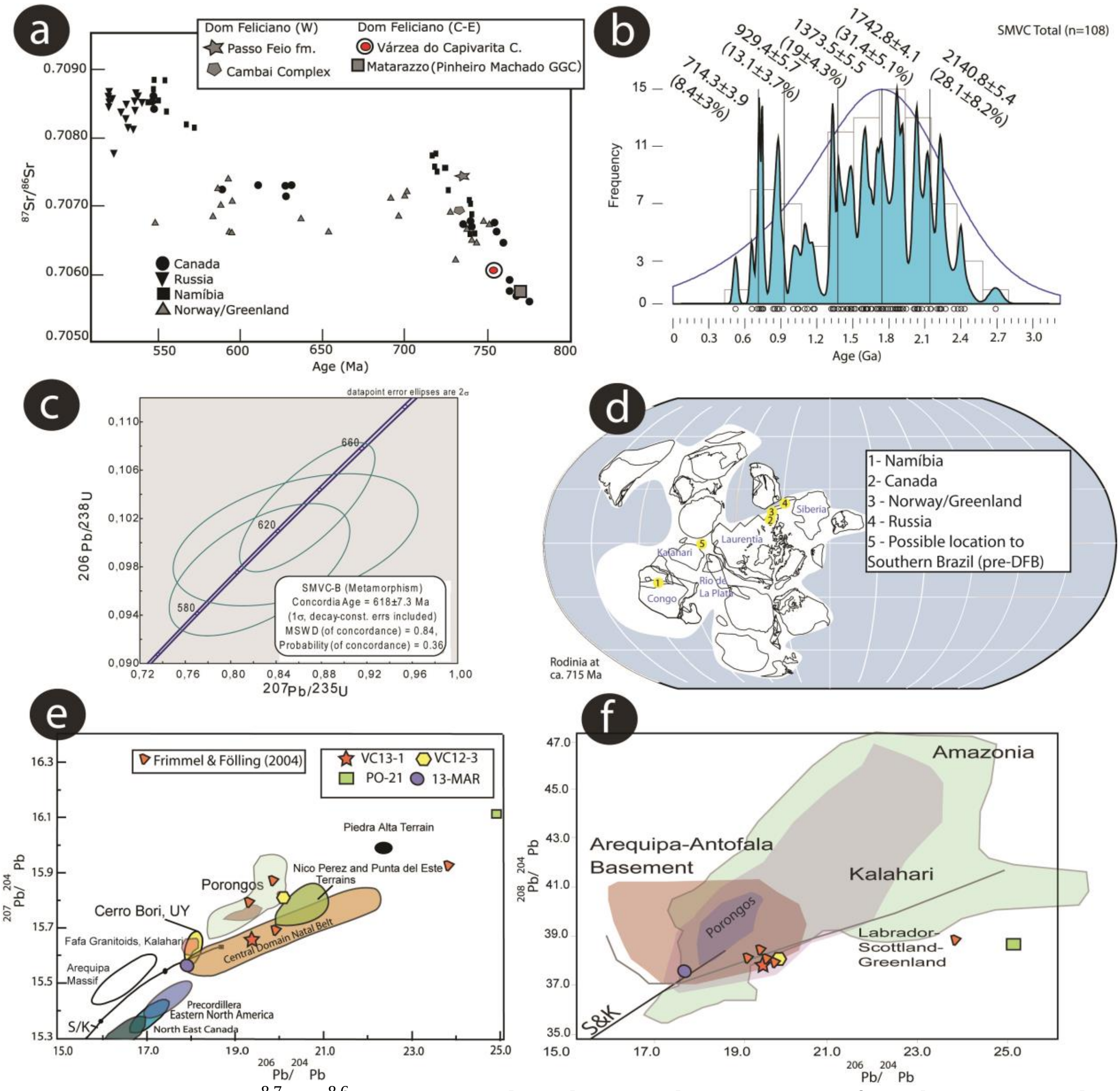

Figure 3 – (a) - $^{87}Sr/^{86}Sr$ temporal and spatial variation of carbonates and evaporites from various units used to define the principal glaciations of the Neoproterozoic (modified from Jacobsen and Kaufman, 1998; Frimmel 2008, Goulart *et al*., 2011, Neis 2014); Stacked distribution ages for VCMS (b); metamorphic Concordia age for the sample SMVCB found in zircons with typical metamorphic textures with SHRIMP (c), with selected examples of cathodoluminescense images from zircons displaying typical metamorphic overgrowth in ca. 580-601 Ma. Age calculations were carried out with ISOPLOT 3.0 (Ludwig, 2003) (d) Reconstruction of Rodínia supercontinent at ca. 715 Ma (modified from Rooney *et al*., 2015, using the reconstruction of Li et al., 2013). Considering that DFB were developed between Rio de La Plata and Kalahari cratons, we estimated a possible position of the VCMS pelagic basin in the Rodínia breakup scheme; (e) Uranogenic $^{207}Pb/^{204}Pb$ X $^{206}Pb/^{204}Pb$ analysis plotted in comparison with samples from Kalahari, Congo, N. America, Cerro Bori Continental Arc (localized in the Dom Feliciano Belt, Uruguay); Porongos Metamorphic Complex schists and quartzites, Punta Del Este and Piedra Alta Terrain, and stromatolitic

dolomites from Marmora Terrain, in the Pan-African Gariep Bel; samples from VCMS displays similar patterns to some of the dolomites of the Gariep belt, as well as some relation to metassediments of Porongos Metamorphic Complex and Nico Pérez Terrain. The high variability of VCMS marbles could be interpreted as varied degree of metassomatism affecting the samples; nonetheless, they all plot near values obtained to DFB and its African counterpart; (f) Thorogenic $^{208}Pb/^{204}Pb$ X $^{206}Pb/^{204}Pb$, displaying a congruence between the analysed samples and samples from Gariep Belt; in this case, Porongos Metamorphic Complex schists didn't displayed proximal values to those found to VCMS. Modified from Oyhantçabal *et al*. (2011). Data from Cerro Bory presented by Lenz *et al*. (2012), data from Porongos Metamorphic Complex from Gruber *et al* (submitted) and Gariep Belt samples from Frimmel & Föelling (2004).

4. RESULTS AND DISCUSSION

4.1. $^{87}Sr/^{86}Sr$

The $^{87}Sr/^{86}Sr$ ratios determined for three of the four marble samples are influenced by their Rb contents and the addition of radiogenic ^{87}Sr (0.7120–0.7152), and therefore are of no further interest to determine depositional features, since these values are affected by post-depositional fluids, forming the paragenesis of Calcite + Dolomite + Olivine (Silva *et al*., 2002). The ratio of 0.70609 obtained in sample PO-21 is used here by comparing the ratios obtained in other sections of DFB marbles and carbonates, and also from carbonates and dolomites from African sequences, aiming to determine an approximation to the depositional age of the carbonates. Considering these $^{87}Sr/^{86}Sr$ ratios and minimum detrital zircon age (see 4.3), the marbles analyzed here could have been deposited at a slighter older age, up to ca. 750 Ma (Fig. 3-a). Values of 0.7048 to 0.7063 were obtained by Neis (2014) in the Matarazzo and Fida marbles in Arroio Grande, near the Pinheiro Machado Complex, with granitoids dated of ca. 575 Ma (Philipp *et al*., 2002) and sin-transcurrent granitoids of ca. 570 Ma (Koester *et al*., 1997). These $^{87}Sr/^{86}Sr$ ratios were interpreted as having a depositional age of ca. 850 Ma.

In the other hand, marbles and carbonates analyzed in the Passo Feio Formation and in the Cambaí Complex (medium to high grade sequences) near Caçapava granitic intrusion of ca. 560 Ma (Remus *et al*., 2000a) reveled values of 0.7074 ($^{87}Sr/^{86}Sr$), -0,26‰ and 2.44‰ ($\delta^{13}C_{PDB}$) and -5.68‰ ($\delta^{18}O_{PDB}$) (Passo Feio) 0.7069 ($^{87}Sr/^{86}Sr$), 5.75‰ ($\delta^{13}C_{PDB}$) and -11,64‰ ($\delta^{18}O_{PDB}$) (Cambai Complex). These data confirmed depositional age of 770 - 730 Ma to Passo Feio Formation and 740 - 730 Ma to Cambai Complex (Goulart *et al*., 2013).

Reconstructions of the Rodínia to Gondwana supercontinent cycles configure La Plata craton in correlation to Kalahari and Congo cratons in the Mesoproterozoic (McMenamin and McMenamin, 1990) and in the Neoproterozoic (Hartnady *et al*., 1985; Frimmel *et al*., 2008; Li *et al*., 2008). A ^{206}Pb-^{207}Pb age of 728 ± 32 Ma obtained in marbles of the Pickelhaube fm. indicated deposition of ca. 750 Ma, coincident with the glaciation marked in the underlying Stinkinfontein Subgroup (Fölling *et al*., 2000). This is registered as the post-rift evolution in the Gariep Belt, and can be used as parameter to compare marbles from La Plata side of the pre-Gondwana assemble to African side, notably those found on Damara, Namaqua-Natal and Gariep belts. $^{87}Sr/^{86}Sr$ ratios of the Widouw Formation (Namaqua-Natal Belt) were found varying from 0.7082 to 0.7085 in the Bloeddrif Member and 0.7080 to 0.7087 in the Kombuis (Frimmel 2008), all of those higher than that found in this work and in other comparable sections of DFB.

Geodynamical reconstruction of Rodínia configuration is displayed in Fig.4-d, to show possible correlation of the sea level and isotopic variations at ca. 715-750 Ma. Considering the preliminary data presented here, the main values of marbles from Cambaí Complex (São Gabriel Block or western DFB), Passo Feio Formation (Western DFB) and Matarazzo and Fida marbles (Eastern DFB) can be used as a proxy to the depositional age of VCMS marbles. The estimative of a pre-Cryogenian age to the deposition of these marbles could represent a correlation with others marble and carbonate sequences originated in the Sturtian glacial epoch (Rooney *et al.*, 2015). The marbles underwent high-temperature and low-pressure metamorphism (see section 2), obliterating any petrological or facies association to recognize cap carbonates typical from glaciation periods (e.g. Hoffman *et al.*, 1998; Fairchild, 1993).

4.2. Pb-Pb

The analyzed samples displayed values of $^{207}Pb/^{204}Pb$ varying from 25.08 to 17.92, $^{206}Pb/^{204}Pb$ varying from 15.56 to 16.13 and $^{208}Pb/^{206}Pb$ varying from 37.57 to 38.04. The uranogenic values varied within the domains of typical samples of Pan-African signatures and La Plata signatures (Oyhantçabal *et al.*, 2011), some even close to those obtained in the Cerro Bori orthogneisses (Lenz *et al.*, 2012) and Porongos Metamorphic Complex schists (Gruber *et al.*, submitted) (Fig. 3-e), and this variation on the values obtained could be due to metasomatism affecting the samples. Alternatively, the terrigenous materials in the marbles could record a varied degrees of dispersion of the uranogenic values, so it’s not reasonable to predict source-areas in this manner. Nonetheless, thorogenic values showed samples plotting near those obtained in the Gariep samples of Frimmel & Föelling (2004) (Fig.3-f), which could be interpreted as indication of relationship of the original ocean composition. In this manner, it becomes a possibility to interpret the uranogenic values as proximal to the depositional system (or a middle-point between the metasomatism and original values), probably indicating a close relationship of VCMS marbles and ocean between Rio de La Plata and Kalahari cratons in the Neoproterozoic, thus reaffirming the suggested paleogeography of the samples original ocean (Fig.3-d) as suggested by Fragoso-César (1991). This ocean can be represented by the Adamastor Ocean (Hartnady *et al.*, 1995), or a series of small seas between arcs and terrains, as constrained in models from Frimmel *et al.* (2011). Considering the reported Sr/Sr ratios and U-Pb ages (see 4.3), it’s possible to admit this sea with the initial rifting phase of Brazilides Ocean.

4.3. U-Pb

Three samples (SMVC A and B, SMVC80) were analyzed and have its results presented and discussed here. All samples displayed ages varying from 2687.7 ± 52.8 Ma to 714.3 ± 3.9 Ma. From the 20 grains in SMVCA and 64 grains of SMVCB, 28.1 ± 8.2 % of the total have an estimated age of 2140.8 ± 54 Ma. Sample SMVC80 displayed roughly the same patterns.

Including all samples, probability density plot presented optimal five clusters (detrital zircons dated only): 1 – A cluster with 8.4 ± 3% of detrital zircon grains presented a maximum depositional age of 714.3 ± 3.9 Ma, that can be roughly related to the estimated depositional age for the marbles, and correlates well with ages obtained for the Pickelhaube Formation and Stinkinfontein Subgroup (see item above) and the base of the glaciogenic Grand Conglomerate on Congo craton (Rooney *et al.*, 2015). Since the marbles analyzed here occurs as banding gneisses within the marbles, the S0 from the metapelites can be understood as a minimum depositional age for the marbles as well; 2 – A second cluster displays the same pattern of dates found in PMC's schists (Basei *et al.*, 2011; Gruber *et al.*, 2011; Pertille *et al.*, 2015a and b) were registered in the cluster of ages that can be correlated to Tonian sources. This cluster represents 13.1 ± 3.7% of the total detrital record, with an estimated age of 929.4 ± 5.7 Ma; 3 - another cluster (19 ± 4.3%) represents an age of 1373.5 ± 5.5 Ma, and could have been originated in the Capivarita Anorthosite and from other Pan-African sources with ages between 1.3-1.5 Ga, related to extensional settings on the margin of Congo craton (Mayer *et al.*, 2004; Chemale *et al.*, 2011); 4 - another local unknown source of 1742.8 ± 4.1 Ma is represented by a cluster of 31.4 ± 5.1%, although could represent long-distance transport from other terrains; and 5 - finally, the older zircon ages obtained can be clustered in the proxy to Encantadas complex (2.2 – 2.0 Ga). The histograms of stack probability density age distribution are shown in Figure 1-f, g and h.

Metamorphic rims were detected in zircon ribbons, and were used to calculate a Concordia age of 618 ± 7.3 Ma (Fig. 3-c) to SMVCB and 618 ± 22 Ma to SMVCA, and better constraint the high-temperature and low-pressure metamorphism S1 placed by Sm-Nd garnet-whole rock ages of 626-604 Ma obtained in the same rocks by Gross *et al* (2006). Also, zircon high temperature of crystallization can be a record of the collisional-type UTH metamorphism (ultra-high temperature) and IDT (isothermal decompression) described by Bom *et al* (2014). Also, this metamorphic zircon age is in the same range of ages obtained in zircon's rims from metagranitoids with partial melting in the Florianópolis Batolith, the northern tip of DFB (Silva *et al.*, 2005), and could represent another evidence for the extension of DFB orogeny's continental mature arc setting in the Neoproterozoic.

5. CONCLUSIONS

The metamorphic record is constrained at 618 ± 7.3 Ma, marking a collisional event likely related to the collision of the reworked margins of Rio de La Plata and Kalahari. Comparison with Porongos Metamorphic Complex metasediments and the basement rocks in the DFB indicates that some provenance compatibility is registered with VCMS metasediments to Paleoproterozoic and Mesoproterozoic clusters, but doesn't hold the same ages for the younger cluster. PMC is understood as an Ediacaran basin (Pertille et al., 2015b), so they could not represent the same depositional setting. The origin of the same clusters can be interpreted as reworked sediments of the same source-terrains in the transition from passive margin to collisional setting at ca. 600 Ma. Also, the same source-terrains could be reworked in more than one collision. Since there is some degree of comparison of detrital zircon ages, and Pb-Pb ratios, the Cerro Bori Arc and the Dom Feliciano Orogeny are certainly two Neoproterozoic accretions recorded by VCMS metasediments.

VCMS pelitic gneisses have a maximum depositional age of 714.3 ± 3.9 Ma to the original pelitic sequences and ca. 715-750 Ma to the marble sequences, which could be interpreted as being a register of the Sturtian glacial epoch between Kalahari and Rio de La Plata cratons. The minimum age of deposition for the marbles is 714.3 ± 3.9 Ma (younger detrital zircon grain of the metapelitic gneisses).It remains speculative if these marbles indeed represents protoliths composed of cap carbonates.

In the context of Pos-Rodínia breakup, development of intraoceanic and continental arcs in the margins of La Plata and Kalahari could have created a setting of closed bays and small seas before the agglutination of West Gondwana and the Pan-African orogenesis. This setting can have been active in the margins of the Sturtian Glaciation. The original body water between these terrains remains constrained to a plataformal sequence, admitting both "one big ocean" Adamastor or a series of small seas and oceans like the Brazilides Ocean.

Acknowledges

We would like to thank Agência Nacional do Petróleo, Gás Natural e Biocombustíveis (ANP), Financiadora de Estudos e Projetos (FINEP) and Ministério da Ciência e Tecnologia (MCT), (PRH-ANP/MCT), Petrobras PRH-PB215 for studentship (first author) and LGI-UFRGS staff for providing analysis and technical support.

6. REFERENCES

Abre, P., Cingolani, C.A., Cairncross, B., Chemale Jr., F. 2012. Siliciclastic Ordovician to Silurian units of the Argentine Precordillera: Constraints on provenance and tectonic setting in the proto-Andean margin of Gondwana. *Journal of South American Earth Sciences* 40, 1-22.

Bailey, T.R., McArthur, J.M., Prince, H., Thirlwall, M.F. 2000. Dissolution methods for strontium isotope stratigraphy: whole rock analysis. *Chemical Geology*, **167 (3-4)**, 313-319

Basei, M.A.S., Campos Neto, M.C., Castro, N.A., Nutman, A.P., Wemmer, K., Yamamoto, M.T., Hueck, M., Osako, L., Siga, O., Passarelli, C.R. 2011. Tectonic evolution of the Brusque Group, Dom Feliciano belt, Santa Catarina, Southern Brazil. *Journal of South American Earth Sciences*, **32**, 24-350.

Bom, F.M., Philipp, R.P., Zvirtes, G. 2014. Evolução metamórfica e estrutural do Complexo Várzea do Capivarita, Cinturão Dom Feliciano, Encruzilhada do Sul, RS. *Pesquisas em Geociências*, **41 (2)**, 131-153.

Chemale, F. 2000. Evolução Geológica do Escudo Sul-rio-grandense. In: Holz, M.; De Ros, L. F. (eds.). *Geologia do Rio Grande do Sul*. Porto Alegre, CIGO/UFRGS, p. 13-52.

Chemale, F., Philipp, R.P., Dussin, I.A., Formoso, M.L.L., Kawashita, K., Bertotti, A.L. 2011. Lu-Hf and U-Pb age determination of Capivarita Anorthosite in the Dom Feliciano Belt, Brazil. *Precambrian Research*, **186**, 117-126.

Fairchild, I.J., 1993. Balmy shores and ice wastes: the paradox of carbonates associated with glacial deposits in Neoproterozoic times. *Sedimentology Review* **1**, 1-16.

Fernandes, L.A.D., Tommasi, A., Porcher, C.C. 1990. Esboço estrutural de parte do Batólito de Pelotas - região de Quitéria-Capivarita. *Acta Geologica Leopoldensia*, **13**, 117–138.

Fernandes L.A.D., Tommasi A., Porcher C.C. 1992. Deformation patterns in the Southern Brazilian Branch of the Pan-African Dom Feliciano belt. *Journal of South American Earth Sciences.*, 5:77-96

Fernandes L.A.D., Menegat R., Costa A.F.U., Koester E., Kramer G., Tommasi A., Porcher, C.C., Ramgrab G.E., Camozzato E. 1995a. Evolução tectônica do Cinturão Dom Feliciano no Escudo Sul-rio-grandense: Parte I - uma contribuição a partir do registro geológico. *Revista Brasileira de Geociências*, **25**, 351-374

Fernandes, L.A.D., Menegat, R., Costa, A.F.U., Porcher, C.C., Tommasi, A., Kraemer, G., Rambgrab, G.E., Camozzato, E. 1995b. Evolução tectônica do Cinturão Dom Feliciano no Escudo Sul-riograndense: uma contribuição a partir das assinaturas geofísicas. *Revista Brasileira de Geociências*, **25**, 375–384.

Fernandes, L.A.D., Koester, E. 1999. The Neoproterozoic Dorsal de Canguçu Strike-Slip Shear Zona: its nature and role in the tectonic evolution of southern Brazil. *Journal of African Earth Sciences*, **29**, 3-24.

Fragoso-César, A. R. S. 1991. **Tectônica de Placas no Ciclo Brasiliano: As Orogenias dos Cinturões Dom Feliciano e Ribeira no Rio Grande do Sul.** Tese de Doutorado, USP, São Paulo. 367 p.

Frimmel, H.E., Basei, M.S., Gaucher, C. 2011. Neoproterozoic geodynamic evolution of SW Gondwana: a southern African perspective. *Int J Earth Sci (Geol Rundsch)*, **100**, pp. 323–354.

Frimmel, H.E. 2008. An evaporitic facies in Neoproterozoic post-glacial carbonates: The Gifberg Group, South Africa. *Gondwana Research,* **13**, 453–468

Frimmel, H.E. and Föelling, P.G. 2004. Late Vendian Closure of the Adamastor Ocean: Timing of Tectonic Inversion and Syn-orogenic Sedimentation in the Gariep Basin *Gondwana Research*, **7**, pp. 685-699.

Fölling, P.G., Zartman, R.E., Frimmel, H.E., 2000. A novel approach to doublespike Pb–Pb dating of carbonate rocks: examples from Neoproterozoic sequences in southern Africa. *Chemical Geology,* **171,** 97–122.

Gastal, M.C.P., Lafon, J.M., Hartmann, L.A., Koester, E., 2005. Sm–Nd isotopic com-positions as a proxy for magmatic processes during the Neoproterozoic of thesouthern Brazilian shield. *Journal of South American Earth Sciences,* **18**, 255–276.

Goulart, R.V., Remus, M.V.D., Reis, R. S. 2013. Composição isotópica de Sr, C e O e geoquímica de ETRs das rochas carbonáticas do Bloco São Gabriel, Rio Grande do Sul. *Pesquisas em Geociências*, **40 (1)**: 75-97.

Gross, A.O.M.S., Porcher C.C., Fernandes L.A.D., Koester E. 2006. Neoproterozoic low pressure/high-temperature collisional metamorphic evolution in the Varzea do Capivarita Metamorphic Suitee, SE Brazil: thermobarometric and Sm/Nd evidence. *Precambrian Research,* **147**, 41–64.

Gruber, L., Porcher, C. C., Lenz, C., Fernandes, L.A.D. 2011. Proveniência de metassedimentos das sequências Arroio Areião, Cerro Cambará e Quartzo Milonitos no Complexo Metamórfico Porongos, Santana da Boa Vista, RS. *Pesquisas em Geociências*, **38**, n.1: 205-224.

Hartnady, C., Joubert, P., Stowe, C. 1985. Proterozoic crustal evolution in southwestern Africa. *Episodes* **8**:236–244.

Hoffman, P.F., Kaufman, A.J., Halverson, G.P. & Schrag, D.P., 1998. A Neoproterozoic snowball Earth. *Science* **281**, 1342-46.

Jacobsen, S.B and Kaufman, A.J. 1999. The Sr, C and O isotopic evolution of Neoproterozoic seawater. Chemical *Geology*, **161**: 37–57.

Koester, E., Soliani, E. Jr., Fernandes, L.A.D., Kraemer, G., Tommasi, A. 1997. Geocronologia Rb/Sr e K/Ar dos granitóides sintectônicos á Zona de Cisalhamento Transcorrente Dorsal de Canguçu na região de Encruzilhada do Sul (RS). *Pesquisas*, **24**:67–77.

Leite, J.A.D., Hartmann, L.A., Fernandes, L.A.D., McNaughton, N.J., Soliani Jr., E., Koester, E., Santos, J.O.S., Vasconcellos, M.A.Z., 1998. Zircon U–Pb zircon geochronology of Neoproterozoic juvenile and crustal reworked terranes in southernmost Brazil. *Int. Geol. Rev*. **40**, 688–705.

Lena, L., Pimentel, M.M., Philipp, R.P., Armstrong, R., Sato, K. The evolution of the Neoproterozoic São Gabriel juvenile terrane, southern Brazil based on high spatial resolution U-Pb ages and δ18O data from detrital zircons. *Precambrian Research*, **247**, 126-138.

Lenz, C.C., Porcher, C.C., Fernandes, L.A.D., Masquelin, H., Koester, E., Conceição, R.V. 2012 Geochemistry of the Neoproterozoic (800–767 Ma) Cerro Bori orthogneisses, Dom Feliciano Belt in Uruguay: tectonic evolution of an ancient continental arc. *Mineralogy and Petrology*, 107(5):785-806.

Li, Z.X., Bogdanova, S.V., Collins, A.S., Davidson, A., De Waele, B., Ernst, R.E., Fitzsimons ICW, Fuck, R.A., Gladkochub, D.P., Jacobs, J., Karlstrom, K.E., Lu, S., Natapov, L.M., Pease, V., Pisarevsky, S.A., Thrane, K., Vernikovsky, V. 2008. Assembly, configuration, and break-up of Rodinia: a synthesis. *Precambrian Research*, **160**:179–210

Li, Z.X., Evans, D.A.D., and Halverson, G.P. 2013. Neoproterozoic glaciations in a revised global paleogeography from the breakup of Rodinia to the assembly of Gondwanaland: *Sedimentary Geology*, **294**, 219–232, doi:10.1016/j.sedgeo.2013.05.016.

Ludwig, K.R. 2003. Isoplot 3.0 – A geochronological toolkit for Microsoft Excel. Berkley Geochronology Center, *Special Publications* **No. 4**.

Mayer, A., Hoffmann, A.W., Sinigoi, S., Morais, E. 2004. Mesoproterozoic Sm-Nd and U-Pb ages for the Kunene Anorthosite Complex of SW Angoa. *Precambrian Research*, **133** (3-4), 187-206.

McMenamin, M.A.S., McMenamin, D.L.S. 1990. **The emergence of animals: the Cambrian breakthrough**. Columbia University Press, New York

Neis,L. 2013. Geoquímica de metacarbonatos do escudo Sul-Rio-Grandense na região de Caçapava do Sul e Arroio Grande, RS. . Unpublished undergraduate dissertation, 61 pp. Universidade Federal do Rio Grande do Sul.

Oyhantçabal P., Siegesmund S., Wemmer K., Layer P. 2010. The Sierra Ballena Shear Zone in the southernmost Dom Feliciano Belt (Uruguay): evolution, kinematics and deformation conditions. *International Journal of Earth Sciences (Geol. Rundschau)* **v. 99**: 1227–1246.

Oyhantçabal, P., Siegesmund, S., Wemmer, K. 2011. The Rio de la Plata Craton: a review of units, boundaries, ages and isotopic signature. *International Journal of Earth Science*, 100, 201–220.

Pertille, J., Hartman, L.A., Philipp, R.P. 2015a. Zircon U-Pb age constraints on the Paleoproterozoic sedimentary basement of the Ediacaran Porongos Group, Sul-Riograndense Shield, southern Brazil. *Journal of South American Earh Sciences* 63, pp.334-345.

Pertille, J., Hartmann, L.A., Philipp, R.P., Petry, T.S., Lana, C.C. 2015b. Origin of the Ediacaran Porongos Group, Dom Feliciano Belt, southern Brazilian Shield, with emphasis on whole rock and detrital zircon geochemistry and U-Pb, Lu-Hf isotopes. *Journal of South American Earth Sciences* 64, pp. 69-93.

Philipp, R.P., Machado, R., Nardi, L. V. S., Lafon, J.M. 2002. O magmatismo granítico Neoproterozóico do Batólito Pelotas no Sul do Brasil: Novos dados e revisão da geocronologia regional. *Revista Brasileira de Geociências*, **32** (2), pp. 277-290.

Philipp, R.P. & Machado, R. 2005. The Neoproterozoic to Cambrian Granitic Magmatism of Pelotas Batholith, Southern Brazil. *Journal of South American Earth Sciences* 19, 461-478.

Philipp, R.P., Lusa, M., Nardi, L. 2008. Petrology of dioritic, tonalitic and trondhjemitic gneisses from Encantadas Complex, Santana da Boa Vista, southernmost Brazil: Paleoproterozoic continental-arc magmatism. *Anais da Academia Brasileira de Ciências*, **80**, n.4.

Rapela, C.W., Fanning, C.M., Casquet, C., Pankhurst, R.J., Poiré, L.S.D. Baldo, E.G. 2011. The Rio de la Plata craton and the adjoining Pan-African/brasiliano terranes: Their origins and incorporation into south-west Gondwana, *Gondwana Research*, **(20):4**, p. 673-690.

Remus, M.V.D., Hartmann, L.A., McNaughton, N.J., Groves, D.I., Fletcher, I.R., 2000a. The link between hydrothermal epigenetic copper mineralization and the Cac¸apava Granite of the Brasiliano Cycle in southern Brazil. *Journal of South American Earth Sciences*, **13**, 191– 216.

Rooney, A.D., Strauss, J.V., Brandon, A.D., Macdonald, F.A. 2015. A Cryogenian chronology: Two long-lasting synchronous Neoproterozoic glaciations. *Geology*, **43**, 459-462. doi:10.1130/G36511.1.

Saalmann, K., Hartmann, L.A., Remus, M.V.D., Koester, E., Conceição, R.V., 2005. Sm–Nd isotope geochemistry of metamorphic volcanosedimentary successions in the São Gabriel Block, southernmost Brazil: evidence for the existence ofjuvenile Neoproterozoic oceanic crust to the east of the Rio de la Plata craton. *Precambrian Research*, **136**, 159–175.

Saalmann, K., Gerdes, A., Lahaye, Y., Hartmann, L.A., Remus, M.V.D., Läufer, A., 2011. Multiple accretion at the eastern margin of the Rio de la Plata craton: the prolonged Brasiliano orogeny in southernmost Brazil. *International Journal of Earth Sciences,* **100**, 355–378.

Silva, A.O.M.S., Porcher, C.C., Fernandes, L.A.D., Droop, G.T.R. 2002. Termobarometria da Suíte Metamórfica Várzea do Capivarita (RS): Embasamento do Cinturão Dom Feliciano. *Revista Brasileira de Geociências*, **32 (4)**: 419-432.

Silva, L.C., McNaughton, N.J., Flecther, I.R. 2005. SHRIMP U-Pb geochronology of Neoproterozoic crustal granitoids (Southern Brazil): A case of discrimination of emplacement and inherited ages. *Lithos*, **82**, 503-525.

Steiger., R.H., Jäger, E. 1977. Subcommission on geochronology: convention on the use of decay constants in geo- and cosmochronology. *Earth and Planetary Science Letters* **36**, 359–362.

Vermeesch, P., 2012. On the visualisation of detrital age distributions. *Chemical Geology*, **v.312-313**, 190-194, doi: 10.1016/j.chemgeo.2012.04.021

Williams, I.S. 1998. U-Th-Pb Geochronology by Ion Microprobe. In McKibben, M. A., Shanks III, W. C., and Ridley, W. I. (eds.): Applications of microanalytical techniques to understanding mineralizing processes. *Reviews in Economic Geology,* **7**. 1-35.

27-Jan-2016

Dear Mr. Gruber:

Your manuscript entitled "Comparison between U-Pb zircon ages and Hf isotopic signatures of Porongos Metamorphic Complex and Várzea do Capivarita Metamorphic Suit in Dom Feliciano Belt, South America: Implications to West Gondwana evolution" has been successfully submitted online and is presently being given full consideration for publication in the Brazilian Journal of Geology.

Your manuscript ID is BJGEO-2016-0020.

Please mention the above manuscript ID in all future correspondence or when calling the office for questions. If there are any changes in your street address or e-mail address, please log in to ScholarOne Manuscripts at https://mc04.manuscriptcentral.com/bjgeo-scielo and edit your user information as appropriate.

You can also view the status of your manuscript at any time by checking your Author Center after logging in to https://mc04.manuscriptcentral.com/bjgeo-scielo.

Thank you for submitting your manuscript to the Brazilian Journal of Geology.

Sincerely,
Brazilian Journal of Geology Editorial Office

Comparison between U-Pb zircon ages and Hf isotopic signatures of Porongos Metamorphic Complex and Várzea do Capivarita Metamorphic Suit in Dom Feliciano Belt, South America: Implications to West Gondwana evolution

Leonardo Gruber[1], Carla C. Porcher[2], Edinei Koester[2], Anelise L. Bertotti[3], Luís A. D'ávilla Fernandes[2]

[1] Programa de Pós-graduação em Geociências da Universidade Federal do Rio Grande do Sul - Instituto de Geociências, Av. Bento Gonçalves, 9500. Porto Alegre, RS, Brasil - CEP 91501-970. Email: leonardo.gruber@ufrgs.br;

[2] Departamento de Geologia, UFRGS. Av. Bento Gonçalves, 9500. Porto Alegre, RS, Brasil. Email: carla.porcher@ufrgs.br; edinei.koester@ufrgs.br; aneber79@gmail.com; ladfernandes@gmail.com

[3] Núcleo de Geologia, UFS - Cidade Universitária Prof. José Aloísio de Campos, Av. Marechal Rondon, s/n Jardim Rosa Elze - CEP 49100-000 - São Cristóvão, SE, Brasil. Email addres; aneber79@gmail.com

ABSTRACT

The agglutination of West Gondwana involved at least three cratons (Rio de La Plata, Congo and Kalahari), volcanic arcs and terrains after the breakup of Rodínia. The Rio de La Plata Craton is surrounded by sets of belts characterized by basement orthogneisses with igneous crystallization ages from Archean to Paleoproterozoic (2.6 to 2.1-1.8 Ga), adjoined to juvenile terrains marked by subduction of oceanic crust, and its margins includes, in the Dom Feliciano Belt, the Porongos Metamorphic Complex, with minimum depositional ages of ca. 0.6 Ga and felsic metavolcanics varying from ca. 800 to 660 Ma, and the Várzea do Capivarita Metamorphic Suit. Both recorded the same juvenile sources, as indicated by positive εHf at 1.4 and 2.2 Ga. Ectasian and Estenian ages are represented by mixed sources of zircons with negative and positive εHf, while Neoproterozoic zircons exhibit negative εHf values, which is similar to Damara Belt signatures in Congo Craton, but not the same pattern of Damara Belt at Kalahari side. The agglutination of a basement could have generated a continental volcanic arc of ca. 800 Ma (Cerro Bori). Partial melting record at ca. 660 Ma is presented here, indicating generation of the felsic metavolcanics during West Gondwana assembly.

KEYWORDS: Provenance; LA-ICP-MS Zircon Ages; SHRIMP Zircon Ages; Hf Isotopes; Crustal Evolution

RESUMO

A aglutinação do Gondwana Ocidental envolveu pelo menos três cratons (Rio de La Plata, Congo e Kalahari), além de terrenos e arcos após o rompimento do Rodínia. O Cráton Rio de La Plata é circundado por conjuntos de cinturões constituídos de embasamentos caracterizados por ortognaisses com idade de cristalização ígnea Arqueana a Paleoproterozóica (variando de 2.6 a cerca de 2-1.8 Ga), adjunta a terrenos juvenis marcados por subducção de crosta oceânica, e sua margem retrabalhada inclui, no Cinturão Dom Feliciano, o Complexo Metamórfico Porongos, com idades mínimas de deposição de 0.6 Ga e vulcanismo félsico variando de 800 a 660 Ma, e a Suíte Metamórfica Várzea do Capivarita. Ambos registraram as mesmas fontes juvenis como indicado por εHf positivo em 1.4 e 2.2 Ga. Idades Ectasianas e Estenianas são representadas por fontes mistas de zircões com εHf negativos e positivos, enquanto zircões Neoproterozóicas exibem valores de εHf negativos, o que é semelhante para assinaturas do cinturão Damara no Congo, mas não é o mesmo padrão do Damara no Kalahari. A colagem de um embasamento pode ter gerado vulcanismo continental de arco de 800 Ma (Cerro Bori). O registro de um evento de fusão parcial de crosta de 660 Ma é apresentado aqui, indicando geração de metavulcanicas félsicas durante a aglutinação do Gondwana Oeste.

PALAVRAS-CHAVE: Proveniência; Idades LA-ICP-MS em zircão; Idades SHRIMP em zircão; Isótopos de Háfnio; Evolução Crustal

INTRODUCTION

The Gondwana is usually suggested as the result of amalgamation of various building blocks of different origins, generally starting with the breakup of Rodínia (Cordani *et al*., 2013; Li *et al*., 2008). The cycle of supercontinents assembly and breakup is registered in southeastern South America in the Mantiqueira Province, with two main tectonic cycles registered widely in the province: Paleoproterozoic, associated with Ryacian Orogeny (2.2 Ga) pulses, and Neoproterozoic, commonly associated with Brasiliano Orogeny pulses. The latter are registered in three belts: Dom Feliciano Belt (DFB) in the south, Ribeira in the central portion and Araçuaí in the north (e.g. Almeida 1981; Neves *et al*., 2014). In the DFB context, it's usually accepted that the Precambrian terrains and arcs that now compose its geology were generated at the same time and crust of typical African terrains, like Angola block, Marmora Terrain, Cuchilla-Dionísio-Pelotas Terrain, Encantadas Microcontinent (e.g. Basei *et al*., 2011; Frimmel *et al*., 2011; Rapela *et al*., 2011; Chemale *et al*., 2012).

To help to test these hypotheses, we used U-Pb and Lu-Hf isotope geochronology in detrital and volcanic zircon grains from metasedimentary and metavolcanic units located in the central-eastern domain of the DFB, aiming to compare and constraint age and chemical maturity with the possible sources from African terrains.

GEOLOGY OF THE DOM FELICIANO BELT

In Southern Brazil, DFB can be separated in three domains formed in various orogenic collage systems – Western Domain, which is formed mainly by the São Gabriel Block (SGB), comprising Paleoproterozoic sialic crust with Neoproterozoic juvenile metavolcanic and plutonic rocks interpreted as result of an oceanic arc adjoining Rio de La Plata (RdLP) Craton on the west; Central Domain to east of SGB presents reworked Paleoproterozoic basement and collisional Neoproterozoic granitois and metavolcanosedimentary belts resulted from continental arc collisions, with ages varying from Archean to Paleoproterozoic sources (ca. 3.4-2.2 Ga) and Neoproterozoic deposition age (ca. 600 Ma) (Lopes *et al*., 2015), alongside post tectonic basins developed after Gondwana amalgamation (Camaquã Basin) (e.g. Hartman 1991, Fernandes *et al*., 1995a,b, Basei *et al*., 2010, Chemale *et al*., 2012) and the Eastern Domain, comprised by Pelotas Batholith, representing the final stages of collision of the Brasiliano Cycle in southern Brazil at ca. 0.6 Ga, with the development of a continental magmatic arc, voluminous syn- to post-collisional magmatism, which resulted in extensive reworking of older continental crust (Silva *et al*., 1999; Frantz *et al*., 1999) (Fig. 1A). Others main geological events are distinguished in the DFB by a rifting process at 1.5 Ga, related to fragmentation of a Mesoproterozoic supercontinent (Chemale *et al*., 2011) and crustal building events in Tonian, Cryogenian and Cambrian. These terrain collages occurred between Kalahari, Congo and RdLP cratons when the initial stages of West Gondwana assemble developed along the accretionary margin of RdLP. This initial accretionary margin was probably developed from Mesoproterozoic to Tonian, starting with the oceanic arc system Passinho (Saalmann *et al*., 2006), accreting in the RdLP margin at ca. 0.8 Ga (Leite *et al*., 1998; Saalmann *et al*., 2006; with proximal detrital zircon ages presented in pelitic schists of Cambaizinho Complex, varying from 840 to 660 Ma (Lena *et al*., 2014). Subsequently, there was the Mar del Plata terrain, rifted from Angola block, with a collage in RdLP registered at Punta Mogotes Formation at ca. 780 Ma (Rapela *et al*., 2011). Another possible accretion to RdLP margin is the Encantadas microcontinent, consisting of a Paleoproterozoic sialic crust, with collage age in the RdLP Craton estimated between 1000 to 680 Ma (Chemale *et al*., 2012). The post-collisional system of the Dom Feliciano Arc that originates the Pelotas Batolith is followed by intrusions of granitic and volcanic rocks associated both with collision and subduction of oceanic plate, and orogenic metasedimentary complexes - the Porongos Metamorphic Complex (PMC) and Várzea do Capivarita Metamorphic Suit (VCMS).

INSERT FIGURE 1

Background geology of studied samples

Samples analyzed were collected along PMC and VCMS in the DFB, Southern Brazil. PMC displays three main Antiforms (Fig. 1B), characterized by metapelitic and metavolcanic schists interlayered with phyllites, quartz-mylonites and marble lenses, with main events of D1 and D2 presented in all complex (Fernandes *et al*., 1992) and M1 indicating a green schist to amphibolite facies (Porcher & Fernandes., 1994). VCMS (Fig. 1C) is a low pressure/ultra-high temperature collisional metamorphic suit with M1 at 618 ± 7.3 Ma (Gruber *et al*., submitted) and retrogressional static M2 in the final stages of Gondwana amalgamation marked by E-W mineral trending and stretching lineations (Gross *et al*., 2006; Bom *et al*., 2014). It's assemblages consists mostly of para- and ortho- gneisses and marbles, outcropping as roof pendants in the Arroio dos Ratos Gneissic Complex, considered as a register of a Neoproterozoic volcanic arc (Fernandes *et al*., 1990).

Porongos Metamorphic Complex samples RIP16 (UTM 6531450m; N 265900m E) and RIP12 (6527050m; N 276115m E) were collected in small outcrops along Santana da Boa Vista and Cerro do Godinho antiforms. Both are phyllites composed mainly of chlorite, quartz, plagioclase and biotite (main mica). RIP12 displays above average quartz-plagioclase/chlorite ratio. VCMS samples were collected in the Várzea do Capivarita roof pendant, mainly from a limestone quarry characterized by ca. 40 meter walls of marbles and calc silicate rocks interlayered with pelitic gneiss, with granitic to granodioritic igneous rock intrusions (UTM 6645425m N; 371935m E). Gneiss banding is well marked on outcrop and thin sections in the pelitic gneisses, with uneven levels of granoblastic quartz-feldspar alternating bands with biotite in preferred orientation forming an equigranular lepidoblastic texture. Some poikiloblastic garnet occurs as well, developed in the contact metamorphism analysed by Gross *et al* (2006). Samples PPC-6046 and CMP 82 and CMP85 are from metavolcanic rocks interlayered in the metasediments of PMC. PPC-6046 is a metasienite (UTM 6629000m; N

324000m E), characterized by equigranular feldpsar, primarily pertitic orthoclase, with <5% of biotite.

Sample CMP85 is a k-feldspar gneiss from Capané Antiform. Sample CMP82 is a felsic metavolcanic chlorite-muscovite schist, from the same antiform. Sample CMP41 is a chlorite muscovite-biotite-garnet schist (quartz-muscovite-biotite-chlorite-garnet-staurolite-plagioclase-ilmenite) (6597828m N; 326332m E), outcropping in the Cerro do Facão Antiform.

METHODS

Samples of metavolcanic (3) and metapelitic (6) rocks from PMC and VCMS were collected (locations on Fig. 1A and B) and analyzed here. From those, 3 samples were already presented in other works (Gruber *et al*., 2011; Gruber *et al*., submitted), but analyzed here with Lu-Hf systematics in the same domains dated by U-Pb.

U-Pb Methodology

U-Pb on zircons were analyzed in laser ablation–inductively coupled plasma–mass spectrometry (LA-ICP-MS) (Table 1) at Laboratório de Geologia Isotópica from UFRGS (LGI-UFRGS), and Sensitive High Resolution Ion Microprobe (SHRIMP II) at Laboratório de Geocronologia from USP (LG-USP) (Table 2), with cathodoluminescense images obtained prior to grain analysis. Zircon concentrates were extracted from 5-10 kg of rock samples. Samples were crushed in a jaw crusher to a 500 µm size, followed by panning. Zircons were separated by use of standard gravitational techniques and Frantz Isodynamic® separator, and handpicked under binocular microscope. The zircon concentrates were cast in epoxy.

LA-ICP-MS

LA-ICP-MS data were obtained in a laser ablation microprobe (New Wave UP213) coupled to a MC-ICP-MS (ThermoFinnigan-Neptune) at LGI-UFRGS. Isotope data where acquired using static mode with spot size of 25 um, with frequency of 10 Hz and intensity of ~4 J/cm2. Analysis were made in 40 cycles of 1 s, with laser-induced elemental fractionation and instrumental mass discrimination corrected by GJ-1 (standard zircon) with the measurement of two GJ-1 analyses to every four sample zircon spots. The external error was calculated after propagation of the error of the GJ-1 mean and the individual sample zircon. Data were reduced using in-house programs developed at the LGI-UFRGs and the Laboratório de Geocronologia from UnB.

SHRIMP

All analytical procedures used for SHRIMP U-Pb ages are the same described in Williams (1998). To each zircon grain analyzed, four scans through the mass stations were made for every age determination. Standard Temora 2 with $^{206}Pb/^{238}U$ age of 416.18 ± 0.33 Ma was used to calibrate the $^{206}Pb/^{238}U$ ratios. Decay constants are the same recommended by Steiger and Jager (1977). Common lead correction was made with measured ^{204}Pb in each analysis, and data reduction was made with Squid and Isoplot excel programs (Ludwig, 2003).

Zircons from metavolcanic rocks had a Concordia age calculated with the Isoplot 3.0 ExcelTM macro from Ludwig (2003). Gaussian histograms were made using Density Plotter (Vermeesh, 2012), using data from PMC obtained in this work and others (Gruber *et al*., 2011). $^{207}Pb/^{206}Pb$ ages were chosen to zircons older than Neoproterozoic or with discordant analysis (<70%), while $^{206}Pb/^{238}U$ preferred to Neoproterozoic ages.

Lu-Hf Methodology

Zircon Hf isotope geochemistry was performed at the LGI-UFRGS using laser and ICP-MS routines similar to those used for U-Pb geochronology (for analytical protocols, see Bertotti *et al*., 2014) (Table 3). In situ Hf isotope measurements were conducted on 77 dated zircons. Initial $^{176}Hf/^{177}Hf$ ratios are reported as εHf(t), which represents the isotopic composition at the time of crystallization relative to the chondritic uniform reservoir. The εHf(t) values were calculated using the ^{176}Lu decay constant of Scherer *et al*. (2001) and the chondritic values of Bouvier *et al*. (2008). Hf model ages were approximated to the time of crystallization using $^{176}Lu/^{177}Hf$ = 0.015 for the present-day crust (Goodge and Vervoort, 2006). Hf model ages provide an estimate for the timing of extraction of source rocks from a depleted mantle reservoir. Some samples had U-Pb ages determined in Gruber *et al* (2011) (case of samples RIP3-5-6, 11; SMVC-A).

INSERT TABLE 1

INSERT TABLE 2

INSERT TABLE 3

INSERT FIGURE 2

RESULTS

U-Pb DATA

Zircon grains are generally euhedral to subhedral, with prismatic and acicular prisms, characteristic of igneous-volcanic features displayed oscillatory or linear zoning to the majority of the metavolcanic zircons analyzed (CMP82 and PPC6046). Rim and center analysis were used when grain size permitted (spot position is indicated in the tables) (Fig. 2). Metasedimentary samples displayed prismatic grains as well, in some cases with acicular features (see Gruber *et al*., 2011 for backscattering images). Some rounded grains were found both in metavolcanic and metasedimentary samples.

U-Pb LA-ICP-MS ANALYSIS (TABLE 1)

Metavolcanic samples results

Nine spots were dated in sample CMP82, displaying concordant ages (>90%) of 660 ± 3, 659 ± 17 and 803 ± 8 Ma, and relict ages varying from 2235 ± 19 to 1659 ± 44 Ma. Seven spots from zircon grains of sample CMP86 gave concordant analysis varying from 660 ± 3 to 2103 ± 10 Ma.

Sample PPC6046 displayed dates of 773 to 825 Ma from nine spots with concordance above 80%, without any significant difference between center and border of grain analysis (see table 1 for location of analysis), with the exception of two grains, with center analysis of 911 ± 10 Ma and 1762 ± 19 Ma.

Metasedimentary samples

Auxiliary metasedimentary samples (CMP85, RIP12, RIP16) were analyzed to amply the range of ages from previously not analyzed sections of the CMP. Analyzed zircons (4) from sample RIP12 gave ages of 620 ± 3 Ma and 1471 ± 5 Ma. Sample RIP16 displayed a varied range of ages within 24 spots, all with Concordance better than 70%. Concordant analysis displayed ages with 3066 ± 45, 1815 ± 33, 1442 ± 25, 1320 ± 37, and 1070 ± 36 Ma, and a conjunct of very concordant ages of 799 ± 6 Ma to 764 ± 5 Ma, same range of a recognized metavolcanic source in the PMC. Sample CMP85 had sixteen spots analyzed, mostly with discordant ages (below 81% concordance), and didn't displayed any variances from Paleoproterozoic (2151 ± 2 Ma) to highly discordant Mesoproterozoic ages, from 1463 ± 18 to 1594 ± 43 Ma.

U-Pb SHRIMP ANALYSIS (TABLE 2)

Metavolcanic samples results

Sample CMP82 had twenty spots analyzed, and displayed concordant (>90%) analysis varying from 660 ± 3 Ma to 659 ± 19 Ma, with concordant analysis of Paleoproterozoic relicts of 2008 ± 4 Ma (93% Concordance). Spot CMP82 8.1 and 8.2 refers to core and rim, which gave ages of 1559 ± 23 and 701 ± 10 Ma, respectively.

Metasedimentary samples results

Sample CMP41 displayed concordant Mesoproterozoic analysis, like 1004 ± 22, 1498 ± 24 (96% Concordance) and 1545 ± 23 Ma and Neoproterozoic 603 ± 14 (86% Concordance) to 658 ± 15 Ma (91% Concordance). A single Paleoproterozoic zircon displayed 1848 ± 17 and 2030 ± 130, although common Pb correction within this analysis was 3.14.

Lu-Hf DATA (TABLE 3)

Lu-Hf METAVOLCANIC SAMPLES RESULTS

Sample CMP82 displayed predominantly negative εHf values, from -26.32 (T_{DM} model age of 2351 and U-Pb age of 700 Ma) to 1.63 (T_{DM} of 1.92 Ga and U-Pb of 1.53 Ga). All T_{DM} model ages obtained for this sample varied from 2.63 to 1.37 Ga. Spot CMP82_8.1 and 8.2 refers to the same center/rim described in the section U-Pb SHRIMP metavolcanic samples results. The T_{DM} obtained are of 1.91 and 1.92, with positive εHf (1.37) to the U-Pb age of 1559 and negative εHf (-16.6) to the U-Pb age of 700 Ma. Sample PPC6046 indicated negative εHf of -21 and -15 to Paleoproterozoic T_{DM} model ages of 2.17 and 2.05 Ga and Neoproterozoic U-Pb zircon ages, and a positive εHf analysis of 2.17, with T_{DM} model age of 2.12 Ga and U-Pb age of 1802 ± 19 Ma.

Lu-Hf METASEDIMENTARY SAMPLES RESULTS

Analysis from sample RIP3, RIP5 and RIP6 (U-Pb analysis from Gruber *et al.*, 2011) indicated T_{DM} model ages varying from 1.56 to 2.95 Ga, with positive εHf with T_{DM} model ages 1.73 Ga (εHf 2.37), 2.0 Ga (εEHf 1.82) and 2.35 Ga (εHf 5.11). Negative values are predominant in Mesoproterozoic T_{DM} model ages. Sample RIP12 displayed one positive εHf (1.06) with T_{DM} value of 1.77 Ga, and negatives for T_{MD} model ages of 2.42, 1.64 and 1.56 Ga. Sample RIP16 indicated mixed positive and negative sources for roughly the same T_{DM} between 2.07 to 1.51 Ga. Sample CMP85 gave almost no variation to T_{DM} model ages of 2.31 to 2.09, with a mix of εHf between 1.83 to -1.19. Sample RIP11 has only Paleoproterozoic T_{DM} (2.74 to 2.22 Ga) with predominantly negative εHf signatures, and 3 positive signatures , varying from 0.08 to 3.81 (T_{DM} of 2.22 Ga). A remarkably negative ratio of -33 was obtained to a zircon with 597 Ma.

DISCUSSION

U-Pb ZIRCON AGES

U-Pb direct dating in zircons of metasedimentary and metavolcanic rocks in the PMC and VCMS provided similar provenance ages for both units in the Paleoproterozoic to upper Neoproterozoic (Fig. 3C, E). A metapelitic schist and a metavolcanic *sensu strictu* (samples

RIP16 and PPC6046, respectively) dated had Concordia diagrams from LA-ICP-MS U-Pb ages of 799.5 ± 4.1 Ma (Fig.3B) 783.4 ± 3.9 Ma (Fig. 3D) in the central Santana da Boa Vista section of PMC. These ca. 800 Ma ages are possibly correlated to Cerro Bori orthogneiss, interpreted as a continental arc (Lenz *et al*., 2012), the Chácara das Pedras Gneisses (Koester *et al.,* in print) and the Pinheiro Machado suit xenoliths of 781 Ma (Silva *et al*., 1999). Another metavolcanic sample (CMP82) from the PMC northern section displayed dates of 663 ± 2.7 Ma (Fig. 3F), the same sample from which a SHRIMP U-Pb 667 ± 24 Ma Concordia age were also obtained. The younger ages obtained in the PMC are ca. 580-620 Ma detrital zircon grains (Basei *et al*., 2008; Pertille *et al*., 2015b), constraining the minimal deposition age for the complex as a whole within Ediacaran, which is the same age that is registered at sequences from the last depositional episodes in Camaquã post-collisional basin (Oliveira *et al*., 2014), thus indicating continuity from the same collisional tectonic system of PMC and VCMS basins to the post collisional Camaquã basin in the DFB (Pertille *et al*., 2015b).

PMC probability density distribution histogram of detrital zircon ages provides an interesting resource in trying to evaluate possible correlations with these metasediments sources at DFB African counterparts, since Damara-Kalahari sequences displays different patterns from Damara-Congo sequences, with main peaks of ca. 1010 Ma and ca. 1750 Ma to both sequences (Foster *et al*., 2015). Damara-Congo displays a younger detrital zircon kernel distribution, and none of these sequences displayed ca. 2.2 or 2.0 Ga, which is the main peaks in both PMC and VCMS.

INSERT FIGURE 3

Lu-Hf ZIRCON DATA

The presence of positive εHf zircons with 2.2 Ga (T_{DM}: 2.3 to 2.8 Ga) indicates that Encantadas Continental Arc (Phillip *et al*., 2008) as a highly evident source of sediments for PMC and VCMS

(Fig. 3A), although there is no current geodynamic reconstruction with this basement in the Mesoproterozoic's Columbia model (Rogers and Santosh, 2002) and afterward. It can be interpreted that this collision occurred with mafic sources, possibly ocean crust, since part of the analysis generated positive εHf zircons from 2.3 to 2.0 Ga. Quartzites from PMC indicates provenance of this Paleoproterozoic arc (Pertille *et al*., 2015a). Nearly all Tonian ages are represented by well rounded, hemiprismatic zircon grains, with T_{DM} varying from 1.5 to 2.0 Ga. Distant sources with this age are commonly found in Brasiliano magmatic arcs, like Brazilian Mara Rosa Volcanic Arc (Pimentel *et al*., 2011) or Damara and Namaqua belts, although εHf suggests that African sources analyzed on Damara Belt (Foster *et al*., 2014) were not the main contributor to the firsts terrain to agglutinate in Western Gondwana. Ectasian and Stenian εHf signatures cannot be linked to the expected sources in Kalahari and Congo either, since highly negative εHf values indicates contribution of crustally contaminated sources, which included local volcanism as indicated by the zircons from metasedimentary rocks with same age of magmatism (780-800 Ma) (Rapela *et al*., 2011; Porcher *et al*., 2010) analyzed in metavolcanic rocks in other works (e.g Porcher *et al*., 1998; Saalmann *et al*., 2010). There is, nonetheless, slightly positive εHf with typical Greenvilian ages (T_{DM} varying from 1.7 to 2.0 Ga), which could be interpreted as Damara-Kalahari distal sediments (possible paleogeology reconstruction displayed in Fig. 3G).

Both PMC and VCMS could also represent sedimentary cover of terrane boundary accretionary prisms, associated with agglutination of continental masses in the Gondwana western margin at ca. 0.7 Ga. This implies that at least a terrain or basement with evolved εHf source-rocks (like those presented in Encantadas and Arroio dos Ratos complexes). This terrain should be present between these accreted terrains in RdLP and Congo-Kalahari cratons at ca. 780 Ma, explaining the absence of Damaran-signature records in the accreted margin of La Plata, thickening the collage terrain domains between the three cratons. There is some possible sources, as the Cunchilla-Dionisio-Pelotas terrain (Frimmel *et al*., 2011), and the Encantadas

Microcontinent (Chemale *et al*.., 2011). Previous studies with characterization of the PMC metapelites (Basei *et al*., 2011; Gruber *et al*., 2011; Pertille *et al*., 2015b) displayed a very linkable signature of sediments with the Encantadas Basement, but there is no further evidence to determine it as a microcontinent or terrain. To avoid tectonic implications, we choose to call it Encantadas Basement. This basement probably started as a tectonic block associated with the Kalahari craton in the Mesoproterozoic (from an arc system of 2.2 Ga to a magmatic continental arc of 2.0 Ga), but was juxtaposed to the RdLP margin at some point after Adamastor ocean opening. The evolution of Encantadas Basement in the Neoproterozoic can be further correlate to the Cerro Bori continental arc on the RdLP margin (Fig. 3G and D) (Lenz *et al*., 2012). The felsic metavolcanic rock with a Concordia Age of 663.8 ± 2.7 Ma with εHf varying from -8 to -14 and Mesoproterozoic T_{DM} (ca. 1.5 - 1.6 Ga) (Fig. 3A) probably represents another evidence for agglutination of a thick crustal basement with crustal-evolved T_{DM} of ca. 1.5 Ga at RdLP craton's margin, possible related to the initial phase of the Dom Feliciano Orogen formation, as indicated by Cordilheira magmatism in the Pelotas Batholith (Frantz *et al*., 2003) and by Cerro Bori high grade metamorphic event with peak age of ca. 670 Ma, and partial melting event at 654 Ma, caused by crustal thickening (Lenz *et al*., 2011).

Testing Kalahari-Congo-La Plata Convergence Models

Using the geodynamic reconstructions proposed by many authors (e.g. Frimmel *et al*., 2011; Rapela *et al*., 2011; Lenz *et al*., 2012; Chemale *et al*., 2012; Lena *et al*., 2014 Pertille *et al*., 2015a and b) and including the presented data, some considerations can be made to evaluate and include new factors to the pre to post-agglutination of West Gondwana from DFB point of view.

PRE-GONDWANA ISLAND ARCS AND RIFTING SYSTEMS

The positive εHf obtained in various analysis corroborates to the interpretation of the Encantadas Complex as an active continental arc of 2.2 Ga (Philipp *et al*., 2008), probably being agglutinated in a craton before Rodínia formation. The proposed agglutination of Encantadas to RdLP craton in the Mesoproterozoic (Pertille *et al*., 2015a) can be contested, since zircons with 2.2 Ga with positive εHf were found in Damara-Kalahari sediments (Foster *et al*., 2015). On the contrary, the lithodemic units of Encantadas Complex are interpreted as a microcontinent, agglutinating on La Plata reworked margin at ca.640 Ma (Chemale *et al*., 2012), having its origin in the Western Kaoko Batolith in the Kaoko Belt. Remarkable similarities between crystallization of sin tectonic granitoids in the DFB (Pelotas Batolith), the Cuchila Dionisio in Uruguay and Florianópolis Batholith in northern DFB could had been generated in an oblique subduction system with Kaoko Batolith, followed by a transpressive continental collision at ca. 600-540 Ma (Chemale *et al*., 2012). While this model appeals the similarities of Kalahari εHf signatures on Paleoproterozoic and includes a continental arc on La Plata margin at ca. 800-680 Ma, it doesn't explain the total disagreement between Kalahari-Congo and DFB εHf signatures or the positive Mesoproterozoic (ca. 1.0 – 1.3 Ga) in the same belt. The island arc system of Encantadas Complex is registered in detrital zircon grains of metapelites of VCMS (Gruber et al., submitted) as well as is the Anorthosite Capivarita, interpreted as a rifting system of ca. 1.4 Ga (Chemale *et al*., 2011). VCMS marbles and metapelites are interpreted as the record of a passive margin or a plataformal sequence (Fragoso-César, 1991; Fernandes *et al*., 1992), and could be included in a passive margin from a basement-like terrain, in this case, Encantadas Complex in the Neoproterozoic. The system of detachment of this basement from the Damara-Kalahari side should be earlier than Ediacaran, so the basement could act as the forefront of the agglutination of RdLP-Kalahari-Congo at 800 Ma.

ONE BIG OCEAN MODEL (ADAMASTOR)

A model with one Adamastor Ocean between RdLP/Kalahari-Congo doesn't explain in simpler terms at least two events that generated continental volcanism in RdLP margin at ca. 800 and ca. 640 Ma or the passive margin in Santana Formation (Pertille *et al*., 2015a), part of CMP and the VCMS being transformed in a continental arc/foreland between the Passinho island arc and Pelotas-Cuchila-Dionisio terrain.

MULTIPLE SMALL SEAS OR OCEANS MODELS (CHARRUA SEA, BRAZILIDES OCEAN)

A multiple small seas or oceans in the way between RdLP/Kalahari-Congo agglutination better explain the multiple accretions on the margins of RdLP, but doesn't explain lack of ca. 800 Ma subduction-slab records (ophiolites) in the DFB. It can be argued that oblique subduction between RdLP-Congo would not generate subduction on the transpressive site, favoring this type of model. However, the exact motion plate between the three cratons would remain speculative. Other possibility is represented by the model of Marmora terrain, generated by ocean plate subduction under Kalahari (Frimmel *et al*., 2011). In this scenery, the plataformal sequences of VCMS should be located at an inner sea or small ocean among RdLP Craton to SW, a continental terrain (Encantadas Basement) in the middle and Marmora terrain to NE (Kalahari side) (see Fig. 3.G).

CONCLUSION

Neoproterozoic negative εHf signatures indicates crustal contaminated sources, thus implying that accretion of basement terrains worked as the main continent builder in the South American Western Gondwana crust. Distal sources to PMC and VCMS metasedimentary samples included both Kalahari and Congo, taking in account detrital age and εHf spectra, although it appears that the main contributor were crustal evolved εHf source-rocks from Congo (Neoproterozoic) and positive εHf of Damara in the Mesoproterozoic (Fig. 3A). It is difficult to constrain the paleogeography at this time because there are no paleomagnetic poles from the Kalahari craton and/or basement of the DFB, nor a consensus about position of arcs and terrains relative to the established cratons magnetic poles. Despite the limitations with paleocontinental reconstruction in South American crust, it's possible to disregard Congo as being source to ca. 1.4 Ga DFB detrital zircons from metasedimentary belts, as well as suggest a close resemblance of PMC and VCMS εHf signatures of ca. 0.9 to 0.7 Ga to those found in Congo, but not those of Kalahari craton. This shift in provenance could also be resulted from shift in polarity subduction between RdLP and Congo/Kalahari cratons. Such event is suggested by many authors (e.g. Fernandes *et al*., 1995a, Chemale *et al*., 2012), and could imply in the timing of agglutination of the different terrains at Kalahari and Congo cratons in Gondwana. The Dom Feliciano Orogeny in this section could have started with the Cerro Bori Continental Arc, and this arc is thus generated by the juxtaposition of possible various terranes at different portions of RdLP Craton. In the case of PMC and VCMS, we included the hypothesis of the Encantadas basement as an initial phase of Cunchilla-Dionisio-Pelotas terrain agglutination. This interpretation is still questionable, since there are still open possibilities in the Mawson and Paranapanema cratons and others terrains/microcontinents participating in the same agglutination of pre-Gondwana, and that could lead to even more complexes evolutions of the Pan-African-Brasilian belt genesis. The peak age of metamorphism recorded in a partial melting event in Cerro Bori gneisses (Lenz *et al*., 2012) are recorded in the PMC as well, indicating continuity of the same building margin of Rio de La Plata Craton from 800 Ma until the assembly of Gondwana in its western portion.

ACKNOWLEDGMENTS

We would like to thank Agência Nacional do Petróleo, Gás Natural e Biocombustíveis (ANP), Financiadora de Estudos e Projetos (FINEP) and Ministério da Ciência e Tecnologia (MCT), (PRH-ANP/MCT), Petrobras PRH-PB215 for studentship (first author) and LGI-UFRGS staff for providing analysis and technical support.

REFERENCES

Almeida, F.F.M., Hasui, Y., Brito Neves, B.B., Fuck, R.A. 1981. Brazilian Structural Provinces: An introduction. *Earth Science Reviews* **17**, 1-29.

Basei, M. A. S., Frimmel, H. E., Nutman, A. P., Preciozzi, F. 2008. West Gonduana amalgamation based on detrital zircon ages from Neoproterozoic Ribeira and Dom Feliciano belts of South America and comparison with coeval sequences from SW Africa. *Geological Society, London, Special Publications 2008*; **294**; 239-256, doi:10.1144/SP294.13.

Basei, M.A.S., Campos Neto, M.C., Castro, N.A., Nutman, A.P., Wemmer, K., Yamamoto, M.T., Hueck, M., Osako, L., Siga, O., Passarelli, C.R. 2011. Tectonic evolution of the Brusque Group, Dom Feliciano belt, Santa Catarina, Southern Brazil. *Journal of South American Earth Sciences*, **32**, 24-350, doi:10.1016/j.precamres.2010.07.015.

Bertotti, A.L. ; Chemale, F. ; Sylvester, P.J. ; Kayser, V.T. ; Gruber, L. 2014. Changing provenance of Late Jurassic to Early Cretaceous rift-related sedimentary rocks of the South Atlantic Margin: LA-MC-ICPMS U-Pb and Lu-Hf isotopic study of detrital zircons from the Camamu Basin, Eastern Brazil. *Chemical Geology*, **363**, p. 250-261, 2014.

Bom, F.M., Philipp, R.P., Zvirtes, G. 2014. Evolução metamórfica e estrutural do Complexo Várzea do Capivarita, Cinturão Dom Feliciano, Encruzilhada do Sul, RS. *Pesquisas em Geociências*, **41** (2), 131-153.

Bouvier, A., Vervoort, J.D., and Patchett, P.J., 2008, The Lu-Hf and Sm-Nd isotopic composition of CHUR: Constraints from unequilibrated chondrites and implications for the bulk composition of terrestrial planets. *Earth and Planetary Science Letters*, **273**, p. 48–57, doi:10.1016/j.epsl.2008.06.010.

Chemale Jr., F., Phillip, R.P., Dussin, I.A., Formoso, M.L.L., Kawashita, K., Bertotti, A.L. 2011. Lu-Hf and U-Pb age determination of Capivarita Anorthosite in the Dom Feliciano Belt, Brazil. *Precambrian Research*, **186**, 117-126, doi:10.1016/j.precamres.2011.01.005.

Chemale Jr., F., Mallmann, G., Bitencourt, M.F., Kawashita, K. 2012. Time constraints on magmatism along the Major Gercino Shear Zone, southern Brazil: Implications for West Gondwana reconstruction. *Gondwana Research* **22**, 184-199, doi:10.1016/j.gr.2011.08.018.

Cordani, U.G., Pimentel, M.M., Araújo, C. E. G., Fuck, R. A. 2013. The significance of the Transbrasiliano-Kandi tectonic corridor for the amalgamation of West Gondwana. *Brazilian Journal of Geology* **43**(3): 583-597, doi:110.5327/Z2317-48892013000300012.

Fernandes, L.A.D., Menegat, R., Costa, A.F.U., Koester, E., Kramer, G., Tommasi, A., Porcher, C.C., Ramgrab, G.E., Camozzato, E. 1995a. Evolução tectônica do Cinturão Dom Feliciano no Escudo Sul-rio-grandense: Parte I - uma contribuição a partir do registro geológico. *Revista Brasileira de Geociências*, **25**: 351-374

Fernandes, L.A.D., Menegat, R., Costa, A.F.U., Porcher, C.C., Tommasi, A., Kraemer, G., Rambgrab, G.E., Camozzato, E. 1995b. Evolução tectônica do Cinturão Dom Feliciano no Escudo Sul-riograndense: uma contribuição a partir das assinaturas geofísicas. *Revista Brasileira de Geociências*, **25**, 375–384.

Fernandes, L.A.D., Tommasi, A., Porcher, C.C., 1990. Esboço estrutural de parte do Batólito de Pelotas - região de Quitéria-Capivarita. *Acta Geol. Leopoldensia*, **13**, 117–138.

Fernandes, L.A.D., Tommasi, A., Porcher, C.C. 1992. Deformation patterns in the southern Brazilian branch of the Dom Feliciano belt: A reappraisal*. Journal of South American Earth Sciences* **5**, 77-96.

Foster, D.A., Goscombe, B.D., Newstead, B., Mapani, B., Mueller, P.A., Gregory, L.C., Muvangua, E. 2015. U–Pb age and Lu–Hf isotopic data of detrital zircons from the Neoproterozoic Damara Sequence: Implications for Congo and Kalahari before Gondwana. *Gondwana Research*, **28** (1), pp. 179-190. doi:10.1016/j.gr.2014.04.011

Fragoso-César, A. R. S. 1991. *Tectônica de Placas no Ciclo Brasiliano: As Orogenias dos Cinturões Dom Feliciano e Ribeira no Rio Grande do Sul*. Tese de Doutorado, USP, São Paulo. 367 p.

Frantz J.C., Botelho N.F., Pimentel M.M., Potrel A., Koester E., Teixeira R.S. 1999. Relações isotópicas Rb-Sr e Sm-Nd e idades do magmatismo granítico brasiliano da região leste do Cinturão Dom Feliciano no Rio Grande do Sul: evidências de retrabalhamento de crosta continental paleoproterozóica. *Revista Brasileira de Geociências*, **29**(2):227-232.

Frantz, J.C., McNaughton, N.J., Marques, J.C., Hartmann, L.A., Botelho, N.F., Caravaca, G., 2003. SHRIMP U-Pb zircon ages of granitoids from southernmost Brazil: constraints on the temporal evolution of the Dorsal do Canguçu transcurrent shear zone and the eastern Dom Feliciano Belt. Short Papers. *In*: IV SSAGI, pp. 174e177.

Frimmel, H.E., Basei, M.S., Gaucher, C. 2011. Neoproterozoic geodynamic evolution of SW Gondwana: a southern African perspective. *Int J Earth Sci (Geol Rundsch)*, **100**:323–354

Goodge, J., and Vervoort, J.D., 2006, Origin of Mesoproterozoic A-type granites in Laurentia: Hf isotope evidence: *Earth and Planetary Science Letters*, **243**, p. 711–731, doi:10.1016/j.epsl.2006.01.040.

Gross, A.O.M.S., Porcher C.C., Fernandes L.A.D., Koester E. 2006. Neoproterozoic low pressure/high-temperature collisional metamorphic evolution in the Varzea do Capivarita Metamorphic Suite, SE Brazil: thermobarometric and Sm/Nd evidence. *Precambrian Research* **147**:41–64.

Gruber, L., Porcher, C. C., Lenz, C., Fernandes, L.A.D. 2011. Proveniência de metassedimentos das sequências Arroio Areião, Cerro Cambará e Quartzo Milonitos no Complexo Metamórfico Porongos, Santana da Boa Vista, RS. *Pesquisas em Geociências*, **38**, n.1: 205-224.

Hartmann, L.A. 1991. Condições de metamorfismo no Complexo Granulitico Santa Maria Chico, RS. *Revista Brasileira de Geociências*, **21**, pp. 107-1 13.

Leite, J. A. D., Hartmann, L. A., McNaughton, N. J., Chemale, F. 1998. SHRIMP U/Pb Zircon Geochronology of Neoproterozoic Juvenile and Crustal- Reworked Terranes in Southernmost Brazil. *International Geology Review* **40**, 688–705.

Lena, L., Pimentel, M.M., Phillip, R.P., Armstrong, R., Sato, K. The evolution of the Neoproterozoic São Gabriel juvenile terrane, southern Brazil based on high spatial resolution U-Pb ages and δ18O data from detrital zircons. *Precambrian Research*, **247**, 126-138.

Lenz, C.C., Porcher, C.C., Fernandes, L.A.D., Masquelin, H., Koester, E., Conceição, R.V. 2012. Geochemistry of the Neoproterozoic (800–767 Ma) Cerro Bori orthogneisses, Dom Feliciano

Belt in Uruguay: tectonic evolution of an ancient continental arc. *Mineralogy and Petrology*, **107**(5):785-806.

Li, Z.X., Bogdanova, S.V., Collins, A.S., Davidson, A., de Waele, B., Ernst, R.E., Fitzsimons, I.C.W., Fuck, R.A., Gladkochub, D.P., Jacobs, J., Karlstrom, K.E., Lu, S., Natapov, L.M., Pease, V., Pisarevsky, S.A., Thrane, K., Vernikovsky, V. 2008. Assembly, configuration, and break-up history of Rodinia: A synthesis, *Precambrian Research*, **160**, 1-2: 179-210.

Lopes, C.G., Pimentel, M.M., Phillip, R.P., Gruber, L., Armstrong, R., Junges, S. 2015. Provenance of the Passo Feio Complex: Implications for the age of supracrustal rocks of the São Gabriel Arc, southern Brazil. *Journal of South American Earth Sciences*, **58**, p. 9-17.

Ludwig, K.R. 2003. Isoplot 3.0 – A geochronological toolkit for Microsoft Excel. Berkley Geochronology Center, *Special Publications* No. **4**.

Meert, J. G. & Torsvik, T.H. 2003. The making and unmaking of a supercontinent: Rodinia revisited. *Tectonophysics* **375**, 261– 288.

Neves, B. B. B., Fuck, R. A., Pimentel, M. M. 2014. The Brasiliano collage in South America: a review. *Brazilian Journal of Geology*, **44**(3): 493-518.

Pertille, J., Hartman, L.A., Phillip, R.P. 2015a. Zircon U-Pb age constraints on the Paleoproterozoic sedimentary basement of the Ediacaran Porongos Group, Sul-Riograndense Shield, southern Brazil. *Journal of South American Earh Sciences,* **63**, pp.334-345. DOI: 10.1016/j.jsames.2015.08.005

Pertille, J., Hartmann, L.A., Phillip, R.P., Petry, T.S., Lana, C.C. 2015b. Origin of the Ediacaran Porongos Group, Dom Feliciano Belt, southern Brazilian Shield, with emphasis on whole rock and detrital zircon geochemistry and U-Pb, Lu-Hf isotopes. *Journal of South American Earth Sciences,* **64**, pp. 69-93. DOI: 10.1016/j.jsames.2015.09.001

Pimentel, M.M., Rodrigues, J. B., Emilia S DellaGiustina, M.E.S., ; Junges, S. L., Matteini, M. 2011. The tectonic evolution of the neoproterozoic Brasília Belt, Central Brazil, based on Shrimp and La-Icpms U-Pb sedimentary provenance data: A Review. *Journal of South American Earth Sciences*, **31**, p. 345-357.

Philipp, R.P., Lusa, M., Nardi, L. 2008. Petrology of dioritic, tonalitic and trondhjemitic gneisses from Encantadas Complex, Santana da Boa Vista, southernmost Brazil: Paleoproterozoic continental-arc magmatism. *Anais da Academia Brasileira de Ciências*, **80**, n.4.

Pisarevsky, S.A., Elming, S.A., Pesonen, L.J., Li, Z.X. 2014. Mesoproterozoic paleogeography: supercontinent and beyond. *Precambrian Research*, **244**, p. 207–225.

Porcher, C. C. ; Fernandes, L. A. D. 1994. Zoneamento metamórfico da Suíte Porongos: uma discussão. *In*: 38o Congresso Brasileiro de Geologia, 1994, Balenário Cambouriú. Boleitm de Resumos Expandidos. São Paulo: Sociedade Brasileira de Geologia, v. 1. p. 275-277.

Porcher, C. C. ; Fernandes, L. A. D. ; Lenz, C. ; Gruber, L. ; Vignol-Lelarge, M.L. ; Jourdan, F. 2010. Metamorphic ages from Porongos Metamorphic Complex: Rb-Sr and Ar-Ar in muscovite and apatite fission track results.. *In*: VII SSAGI, 2010, Brasilia. In: VII SSAGI, 2010, Brasília. Abstracts...VII SSAGI, 2010. v. 1. p. 121., 2010.

Rapela, C.W., Fanning, C.M., Casquet, C., Pankhurst, R.J., Poiré, L.S.D. Baldo, E.G. 2011. The Rio de la Plata craton and the adjoining Pan-African/brasiliano terranes: Their origins and incorporation into south-west Gondwana, *Gondwana Research*, **20**:4, p. 673-690, doi:10.1016/j.gr.2011.05.001

Rogers, J.J.W and Santosh, M. 2002. Configuration of Columbia, a Mesoproterozoic Continent. *Gondwana Research*, **5**, pp5-22.

Saalmann, K., Remus, M. V. D., Hartmann, L.A, Koester, E., Conceição, R.V. 2006. Sm–Nd isotope geochemistry of metamorphic volcano-sedimentary successions in the São Gabriel Block, southernmost Brazil: evidence for the existence of juvenile Neoproterozoic oceanic crust to the east of the Rio de la Plata craton. *Precambrian Research,* **136,** 159–175, doi 10.1016/j.precamres.2004.10.006.

Scherer, E., Münker, C., and Mezger, K., 2001, Calibration of the lutetium-hafnium clock: *Science*, **293**, p. 683–687, doi:10.1126/science.1061372.

Silva, L.C., Hartmann, L.A., McNaughton, N.J., Fletcher, I.R., 1999. SHRIMP U/Pb zircon timing of Neoproterozoic granitic magmatism and deformation in the Pelotas Batholith in southernmost Brazil. *International Geology Review,* **41**, 531e551.

Steiger., R.H., Jäger, E. 1977. Subcommission on geochronology: convention on the use of decay constants in geo- and cosmochronology. *Earth and Planetary Science Letters* **36**, 359–362.

Vermeesch, P., 2012. On the visualisation of detrital age distributions. *Chemical Geology*, **312-313**, 190-194, doi: 10.1016/j.chemgeo.2012.04.021

Williams, I.S. 1998. U-Th-Pb Geochronology by Ion Microprobe. *In* McKibben, M. A., Shanks III, W. C., and Ridley, W. I. (eds.): Applications of microanalytical techniques to understanding mineralizing processes. *Reviews in Economic Geology*, **7**. 1-35.

FIGURE CAPTIONS

Figure 1: (A) Geological sketch of Dom Feliciano Belt. Both PMC and VCMS are indicated. (Modified from Porcher *et al*., 1994; 2010; Lenz *et al*., 2012); (B and C) Location map of PMC (B) and VCMS (C), displaying sample locations (1 – sample CMP41; 2 – Cerro do Facão Antiform, sample CMP 85 and 86; 3 - samples RIP 4, 5 and 6; 4 – sample CMP 82; 5 – sample RIP 7-8 and 11, POR 08 and 12; 6 – sample POR 18, 7 – sample RIP 16; 8 – sample RIP 15; 9 – sample SMVCA) .

Figure 2: Selected cathodoluminescense zircon images with Lu-Hf and U-Pb data.

Figure 3: A - εHf vs. U-Pb ages obtained from both PMC and VCMS rocks, compared to others related provinces through time and possible source-terrains. Data from Congo and Kalahari cratons from Foster *et al*., 2015; data from Capivarita Anorthosite from Chemale *et al*., 2011; B – Concordia age obtained by selecting grains in the sample RIP16. It's the same age obtained in metavolcanics from PMC and Cerro Bori orthogneisses, another evidence for an active continental margin in the RdLP margin at this time.

C – Várzea do Capivarita Metamorphic Suite histogram, displaying the same patterns of U-Pb detrital zircon ages for Paleoproterozoic (ca. 2.2 Ga) and Mesoproterozoic (ca. 1.4 Ga) ages found in E –D – Concórdia Age for PPC6040 (metavolcanic rock), corroborating to the interpretation of a continental arc in RdLP margin at ca. 0.8 Ga; E - Detrital zircon ages histogram from metasedimentary rocks of Santana da Boa Vista Antiform in the PMC. Identical ages of ca. 800 Ma were found in Punta Mogotes fm. (Rapela *et al*., 2011) and in the Cerro Bori orthogneiss arc of 800-770 Ma (Lenz *et al*., 2012); (some data from Basei *et al*., 2011; Gruber *et al*., 2011; Porcher *et al*., 2010); F – Metavolcanic zircon Concordia Age of sample CMP82. In this case, a new register of volcanism in this portion of the DFB; G, H - Reconstruction of Gondwana western margin from ca. 780 (G) to ca. 580 Ma (H), using dynamic reconstruction argued by Frimmel *et al*., 2011; Meert & Torsvik (2003); Rapela *et al*. (2011), Chemale *et al*. (2012), Pisavreksy, 2014); Red dot in G – possible location to Cerro Bori Continental Arc; . 1 – Encantadas Basement/ PMC; 2 – Cerro Bori Continental Arc; SYSZ – Sarandi del Yí Shear Zone; SBSZ - Sierra Balena Shier Zone; MGSZ- Major Gerciliano Shear Zone/Dorsal de Canguçu Shear Zone.

TABLE CAPTIONS

Table 1 – LA-ICP-MS U-Pb zircon analisys from samples CMP41, RIP12, RIP16, PPC6046, CMP82, CMP85 and CMP86 (complementary data).

Table 2 – SHRIMP U-Pb zircon analisys from samples CMP82 (concordia data) and CMP41.

Table 3 – Lu-Hf analisys from samples RIP3, RIP5, RIP6, RIP11, RIP12, PPC6046, CMP82, CMP85 and SMVCA (SMVCA U-Pb zircon ages from Gruber et al., subm.; RIP11, 3, 5 and 6 had zircon ages published in Gruber *et al*., 2011).

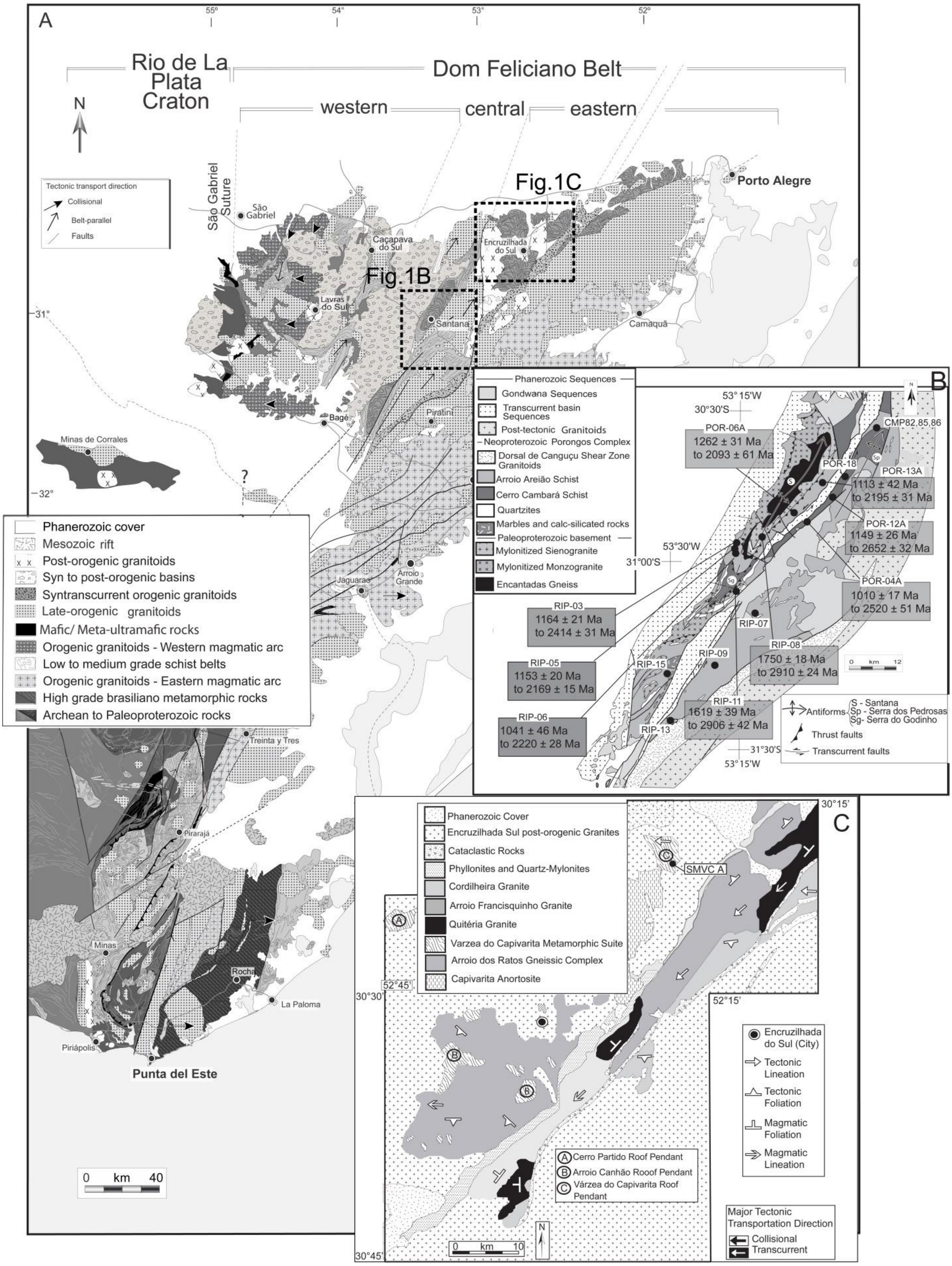
A
Rio de La Plata Craton
Dom Feliciano Belt
western
central
eastern
Fig.1C
Fig.1B
Porto Alegre
São Gabriel Suture
Tectonic transport direction
Collisional
Belt-parallel
Faults
Phanerozoic cover
Mesozoic rift
Post-orogenic granitoids
Syn to post-orogenic basins
Syntranscurrent orogenic granitoids
Late-orogenic granitoids
Mafic/ Meta-ultramafic rocks
Orogenic granitoids - Western magmatic arc
Low to medium grade schist belts
Orogenic granitoids - Eastern magmatic arc
High grade brasiliano metamorphic rocks
Archean to Paleoproterozoic rocks
Punta del Este
B
Phanerozoic Sequences
Gondwana Sequences
Transcurrent basin Sequences
Post-tectonic Granitoids
Neoproterozoic Porongos Complex
Dorsal de Canguçu Shear Zone Granitoids
Arroio Areião Schist
Cerro Cambará Schist
Quartzites
Marbles and calc-silicated rocks
Paleoproterozoic basement
Mylonitized Sienogranite
Mylonitized Monzogranite
Encantadas Gneiss
POR-06A 1262 ± 31 Ma to 2093 ± 61 Ma
POR-13A 1113 ± 42 Ma to 2195 ± 31 Ma
POR-12A 1149 ± 26 Ma to 2652 ± 32 Ma
POR-04A 1010 ± 17 Ma to 2520 ± 51 Ma
RIP-03 1164 ± 21 Ma to 2414 ± 31 Ma
RIP-05 1153 ± 20 Ma to 2169 ± 15 Ma
RIP-06 1041 ± 46 Ma to 2220 ± 28 Ma
RIP-08 1750 ± 18 Ma to 2910 ± 24 Ma
RIP-11 1619 ± 39 Ma to 2906 ± 42 Ma
Antiforms S - Santana Sp - Serra dos Pedrosas Sg- Serra do Godinho
Thrust faults
Transcurrent faults
C
Phanerozoic Cover
Encruzilhada Sul post-orogenic Granites
Cataclastic Rocks
Phyllonites and Quartz-Mylonites
Cordilheira Granite
Arroio Francisquinho Granite
Quitéria Granite
Varzea do Capivarita Metamorphic Suite
Arroio dos Ratos Gneissic Complex
Capivarita Anortosite
Encruzilhada do Sul (City)
Tectonic Lineation
Tectonic Foliation
Magmatic Foliation
Magmatic Lineation
A Cerro Partido Roof Pendant
B Arroio Canhão Rooof Pendant
C Várzea do Capivarita Roof Pendant
Major Tectonic Transportation Direction
Collisional
Transcurrent

Figure 1

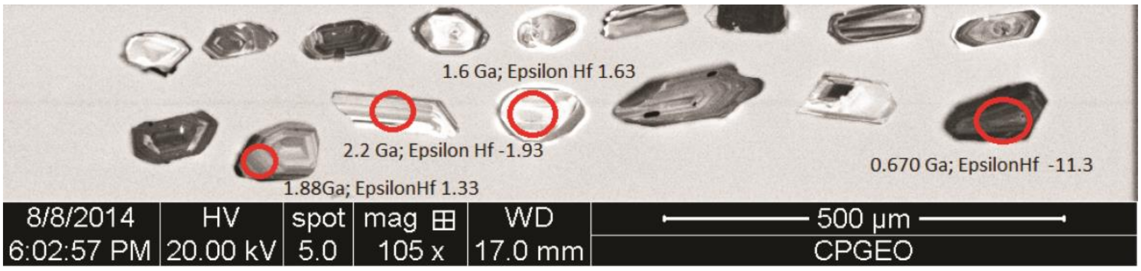
1.6 Ga; Epsilon Hf 1.63
2.2 Ga; Epsilon Hf -1.93
1.88Ga; EpsilonHf 1.33
0.670 Ga; EpsilonHf -11.3
8/8/2014
6:02:57 PM
HV
20.00 kV
spot
5.0
mag
105 x
WD
17.0 mm
500 µm
CPGEO

Figure 2

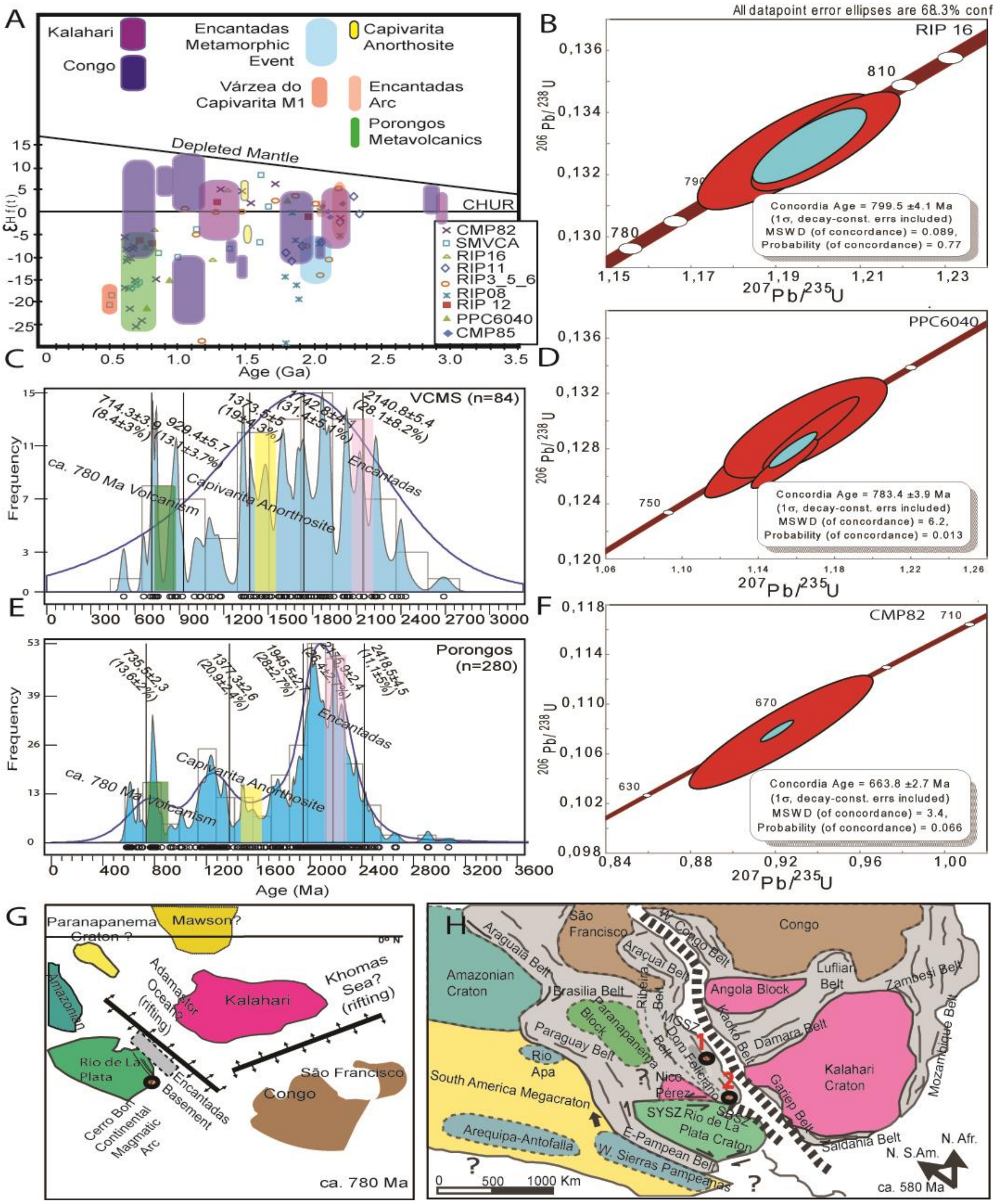

A
Kalahari
Congo
Encantadas Metamorphic Event
Capivarita Anorthosite
Várzea do Capivarita M1
Encantadas Arc
Porongos Metavolcanics
Depleted Mantle
CHUR
CMP82
SMVCA
RIP16
RIP11
RIP3_5_6
RIP08
RIP 12
PPC6040
CMP85
Age (Ga)
B
All datapoint error ellipses are 68.3% conf
RIP 16
Concordia Age = 799.5 ±4.1 Ma
(1σ, decay-const. errs included)
MSWD (of concordance) = 0.089,
Probability (of concordance) = 0.77
C
VCMS (n=84)
Frequency
ca. 780 Ma Volcanism
Capivarita Anorthosite
Encantadas
D
PPC6040
Concordia Age = 783.4 ±3.9 Ma
(1σ, decay-const. errs included)
MSWD (of concordance) = 6.2,
Probability (of concordance) = 0.013
E
Porongos (n=280)
Age (Ma)
F
CMP82
Concordia Age = 663.8 ±2.7 Ma
(1σ, decay-const. errs included)
MSWD (of concordance) = 3.4,
Probability (of concordance) = 0.066
G
Paranapanema Craton ?
Mawson?
Amazonian
Adamastor Ocean (rifting)
Kalahari
Khomas Sea? (rifting)
Rio de La Plata
Encantadas Basement
Cerro Bori Continental Magmatic Arc
São Francisco
Congo
ca. 780 Ma
H
Amazonian Craton
São Francisco
Congo
Angola Block
Kalahari Craton
South America Megacraton
Rio de La Plata Craton
Arequipa-Antofalla
ca. 580 Ma

Figure 3

Table 1

	Sample	f(206)%	Th/U	6/4 ratio	7/6 ratio	1s(%)	7/5 ratio	1s(%)	6/8 ratio	1s(%)	Rho	7/6 age	1s(Ma)	7/5 age	1s(Ma)	6/8 age	1s(Ma)	Conc (%)
RIP12	03_zr38_1	2.22	0.38	181375	0.06741	0.6	0.9383	0.8	0.10095	0.5	0.56	850.4	13.2	672.0	4.1	620.0	3.1	72.90
	04_zr38_2	2.74	0.29	295326	0.06472	1.4	0.9696	3.2	0.10865	2.9	0.89	765.4	30.3	688.3	16.1	664.9	18.2	86.87
	09_zr23	0.13	0.37	4602	0.09219	0.3	3.2847	0.8	0.25840	0.8	0.94	1471.4	5.1	1477.4	6.5	1481.7	10.4	100.70
	10_zr21	0.91	0.06	-112	0.08572	0.5	2.9530	1.5	0.24987	1.4	0.95	1331.8	9.1	1395.6	11.1	1437.8	17.9	107.96
RIP16	03_zr1	0.02	0.38	181375	0.11743	1.7	5.1506	2.8	0.31810	2.1	0.77	1917.5	31.2	1844.5	23.4	1780.5	33.2	92.85
	04_zr2	0.05	0.29	295326	0.06600	0.5	1.2020	1.0	0.13208	0.8	0.81	806.5	11.3	801.5	5.3	799.7	6.0	99.16
	06_zr4	0.07	0.21	256747	0.08520	1.9	2.6269	3.2	0.22362	2.5	0.93	1320.1	37.6	1308.2	23.2	1301.0	29.3	98.55
	10_zr_6	1.34	0.16	15260	0.08072	2.6	1.0001	9.1	0.08985	8.7	0.96	1214.7	50.2	703.8	46.2	554.7	46.4	45.66
	11_zr7	0.99	0.37	2433	0.07052	2.5	1.4040	7.3	0.14440	6.8	0.94	943.5	51.6	890.6	43.2	869.5	55.7	92.15
	12_zr8	0.43	0.21	2213	0.06954	1.1	1.2066	1.4	0.12583	0.9	0.81	914.9	22.8	803.6	7.9	764.1	6.5	83.51
	17_zirc9	0.32	0.12	24977	0.08296	2.1	1.7268	4.8	0.15097	4.3	0.90	1268.2	40.1	1018.5	30.6	906.4	36.3	71.47
	19_zr11	0.21	0.37	2433	0.11096	1.8	5.0192	3.9	0.32807	3.5	0.89	1815.2	33.3	1822.6	33.4	1829.0	55.7	100.76
	24_zirc14	0.91	0.16	15260	0.10460	1.3	1.4353	3.4	0.09951	3.2	0.93	1707.3	23.0	903.7	20.5	611.6	18.6	35.82
	25_zr15	0.03	0.37	2433	0.06530	0.4	1.2727	2.5	0.14136	2.5	0.99	784.0	8.0	833.6	14.4	852.3	20.0	108.71
	29_zr17	0.03	0.12	24977	0.11425	0.4	4.8753	1.9	0.30948	1.8	0.97	1868.1	7.4	1798.0	15.7	1738.2	27.7	93.04
	30_zr18	0.04	0.16	15260	0.08292	4.5	1.9575	8.0	0.17122	6.6	0.83	1267.3	87.2	1101.0	53.8	1018.8	62.7	80.40
	31_zr19	0.10	0.37	2433	0.06737	0.7	1.3217	1.8	0.14228	1.6	0.92	849.3	14.5	855.2	10.2	857.6	13.1	100.98
	36_zr22	0.01	0.27	119737	0.08647	0.5	2.7236	1.6	0.22844	1.6	0.95	1348.7	9.9	1334.9	12.1	1326.3	18.6	98.34
	37_zr23	1.60	0.18	1090	0.09715	1.2	1.7515	2.5	0.13076	2.2	0.87	1570.1	22.9	1027.7	16.1	792.2	16.2	50.46
	43_zr25	0.24	0.25	5452	0.23210	2.8	18.1615	5.4	0.56752	4.6	0.85	3066.6	45.3	2998.3	51.9	2897.6	107.0	94.49

	45_zr27	1.02	0.35	1656	0.08115	0.9	2.1235	1.4	0.18978	1.0	0.75	1225.1	17.2	1156.5	9.4	1120.2	10.8	91.44
	49_zr29	0.32	0.24	4837	0.12125	0.5	5.5886	3.4	0.33428	3.4	0.99	1974.7	9.3	1914.3	29.4	1859.1	54.5	94.14
	50_zr30	0.15	0.26	10988	0.07508	1.8	1.9928	2.5	0.19249	1.7	0.69	1070.7	36.4	1113.1	17.0	1134.9	18.2	105.99
	51_zr31	0.09	0.12	17753	0.09499	2.5	3.4184	11.7	0.26099	11.4	0.98	1527.9	46.7	1508.6	91.7	1494.9	152.2	97.84
	55_zr33	0.07	0.12	24977	0.06566	0.7	1.1926	1.2	0.13174	0.9	0.79	795.5	14.4	797.2	6.4	797.8	7.0	100.29
	56_zr34	0.11	0.16	15260	0.12278	4.9	4.4677	6.8	0.26391	4.6	0.68	1997.0	87.8	1725.0	56.3	1509.8	62.5	75.61
	57_zr35	0.67	0.37	2433	0.12627	2.9	4.4425	15.6	0.25517	15.3	0.98	2046.6	51.3	1720.3	129.0	1465.1	200.5	71.59
	58_zr36	0.74	0.21	2213	0.09080	1.3	3.1231	2.4	0.24946	1.9	0.94	1442.4	25.5	1438.4	18.1	1435.7	25.0	99.54
PPC6046	03_zr7border	0.07	0.38	181375	0.06548	0.4	1.1515	1.3	0.12755	1.2	0.95	789.8	8.4	778.0	6.9	773.8	8.8	97.98
	04_zr7center	0.09	0.29	295326	0.06499	0.9	1.1503	2.2	0.12836	2.0	0.92	774.1	18.1	777.4	11.9	778.5	14.7	100.57
	~~05_zr_21~~	~~0.12~~	~~0.43~~	~~113172~~	~~0.07445~~	~~12.7~~	~~1.6004~~	~~15.0~~	~~0.15589~~	~~7.9~~	~~0.53~~	~~1053.8~~	~~256.5~~	~~970.4~~	~~93.8~~	~~933.9~~	~~69.1~~	~~88.62~~
	11_zr_06	0.08	0.30	22418	0.06524	1.6	1.1652	2.4	0.12952	1.9	0.76	782.2	32.9	784.4	13.3	785.1	13.7	100.37
	15_zr20border	0.02	0.18	73120	0.06560	0.5	1.1680	1.4	0.12913	1.3	0.94	793.6	9.8	785.7	7.8	782.9	9.9	98.65
	15_zr20center	0.02	0.20	100900	0.06596	0.4	1.1541	1.0	0.12691	0.9	0.91	805.0	8.3	779.2	5.5	770.2	6.7	95.69
	19_zr56center	0.01	0.13	192140	0.11017	1.1	3.8389	2.0	0.25271	1.7	0.84	1802.3	19.5	1600.9	16.1	1452.4	22.0	80.59
	~~21_zr74center~~	~~0.13~~	~~0.19~~	~~10884~~	~~0.32520~~	~~503.0~~	~~22.0062~~	~~504.5~~	~~0.49079~~	~~39.2~~	~~0.15~~	~~3594.6~~	~~7722.1~~	~~3184.0~~	~~4900.0~~	~~2574.1~~	~~832.6~~	~~71.61~~
	24_zr11center	0.05	0.21	32051	0.07027	0.8	1.3237	1.7	0.13662	1.5	0.88	936.2	16.3	856.1	9.7	825.5	11.5	88.18
	25_zr18center	0.01	0.44	196964	0.10777	1.1	4.4930	2.8	0.30236	2.6	0.93	1762.1	19.6	1729.7	23.6	1703.0	39.4	96.65
	26_zr18border	0.03	0.10	63919	0.06733	1.4	1.4102	1.9	0.15191	1.2	0.62	847.9	30.0	893.2	11.1	911.7	10.1	107.52
	~~27_zr25border~~	~~0.03~~	~~0.23~~	~~62974~~	~~0.05903~~	~~6.3~~	~~1.0792~~	~~6.5~~	~~0.13259~~	~~1.6~~	~~0.45~~	~~568.2~~	~~137.1~~	~~743.2~~	~~34.3~~	~~802.6~~	~~12.2~~	~~141.25~~
CMP85	03_zirc16.1	0.55	0.43	113172	0.12974	1.9	3.7169	3.9	0.20778	3.4	0.87	2094.5	34.1	1575.0	31.2	1217.0	37.6	58.10
	~~08_zr10.1~~	~~0.52~~	~~0.15~~	~~3414~~	~~0.13497~~	~~0.8~~	~~1.7872~~	~~9.6~~	~~0.09603~~	~~9.6~~	~~1.00~~	~~2163.6~~	~~13.3~~	~~1040.8~~	~~62.4~~	~~591.1~~	~~54.0~~	~~27.32~~
	08_zirc11.1	0.33	0.53	4888	0.13655	0.8	5.2835	3.9	0.28064	3.9	0.98	2183.8	13.8	1866.2	33.6	1594.6	54.4	73.02

	~~08_zirc11.2~~	~~0.41~~	~~0.66~~	~~4098~~	~~0.13760~~	~~2.3~~	~~3.9655~~	~~20.4~~	~~0.20901~~	~~20.3~~	~~0.99~~	~~2197.2~~	~~39.6~~	~~1627.2~~	~~165.8~~	~~1223.6~~	~~226.5~~	~~55.69~~
	14_zirc34.1	0.24	0.13	6859	0.12357	1.4	3.7860	5.5	0.22220	5.3	0.97	2008.5	24.5	1589.8	44.4	1293.5	62.7	64.40
	14_zirc15.1	1.11	0.22	1508	0.13657	1.2	3.8064	5.4	0.20215	5.3	0.98	2184.1	20.8	1594.1	43.4	1186.9	57.1	54.34
	~~15_zirc32.1~~	~~1.35~~	~~0.10~~	~~1244~~	~~0.17287~~	~~18.0~~	~~4.5337~~	~~23.6~~	~~0.19021~~	~~15.3~~	~~0.65~~	~~2585.6~~	~~300.1~~	~~1737.2~~	~~196.6~~	~~1122.5~~	~~158.1~~	~~43.41~~
	15_zirc32.2	1.56	0.09	1126	0.14698	2.4	2.3121	5.5	0.11409	4.9	0.97	2311.0	41.0	1216.0	38.9	696.5	32.6	30.14
	~~19_zirc29.1~~	~~0.08~~	~~0.21~~	~~21758~~	~~0.12617~~	~~0.5~~	~~1.3852~~	~~10.5~~	~~0.07963~~	~~10.5~~	~~1.00~~	~~2045.3~~	~~8.1~~	~~882.7~~	~~62.1~~	~~493.9~~	~~50.0~~	~~24.15~~
	19_zirc29.2	0.21	0.16	7473	0.13402	0.4	5.8054	3.1	0.31416	3.1	0.99	2151.4	6.6	1947.2	27.1	1761.1	47.8	81.86
	~~20_zirc12.1~~	~~0.82~~	~~0.24~~	~~2095~~	~~0.14018~~	~~0.9~~	~~2.9937~~	~~9.8~~	~~0.15489~~	~~9.8~~	~~1.00~~	~~2229.5~~	~~15.6~~	~~1406.0~~	~~74.7~~	~~928.3~~	~~84.5~~	~~41.64~~
	24_zirc28.1	0.36	0.10	4738	0.13609	0.8	3.2003	7.3	0.17055	7.2	0.99	2178.1	14.5	1457.2	56.3	1015.1	68.0	46.61
	25_zirc27.1	1.03	0.18	1625	0.13882	1.5	3.8969	3.0	0.20359	2.6	0.86	2212.6	26.3	1613.0	24.0	1194.6	27.9	53.99
	32_zirc1	0.02	1.35	82949	0.13683	0.7	3.2281	3.6	0.17110	3.6	0.98	2187.5	11.5	1463.9	28.0	1018.2	33.5	46.54
	34_zr08border	1.43	0.16	1214	0.16157	0.8	3.1165	4.0	0.13989	3.9	0.98	2472.2	13.8	1436.8	31.0	844.1	31.2	34.14
	34_zr08center	0.14	0.23	11935	0.13857	2.7	3.6676	8.0	0.19196	7.5	0.98	2209.4	46.0	1564.3	63.6	1132.0	78.0	51.24
CMP82 (LA-ICP-MS Complementary Data)	zr_05border	1.11	0.43	113172	0.14769	1.6	5.9895	4.3	0.29412	4.0	0.93	2319.4	27.7	1974.3	37.5	1662.1	58.4	71.66
	zr_05center	0.82	0.21	256747	0.12771	2.5	7.0260	4.4	0.39902	3.6	0.94	2066.7	43.7	2114.7	39.1	2164.5	66.7	104.73
	zr06border	1.12	0.06	1456	0.10192	2.4	3.3687	2.9	0.23972	1.7	0.56	1659.4	44.5	1497.2	22.9	1385.2	20.8	83.48
	zr6center	1.02	0.09	1430	0.13506	2.8	7.9401	4.4	0.42637	3.4	0.76	2164.8	49.7	2224.2	39.7	2289.3	64.7	105.75
	zr_10center	5.74	0.11	303	0.11833	2.2	2.1707	7.0	0.13305	6.7	0.95	1931.2	40.0	1171.7	48.8	805.2	50.3	41.70
	zr01	0.56	0.38	181375	0.06194	0.2	0.9212	0.6	0.10786	0.5	0.92	672.1	4.2	663.0	2.8	660.3	3.4	98.25
	zr1_center	0.46	0.29	295326	0.06214	1.3	0.9231	3.1	0.10775	2.8	0.90	678.9	28.7	664.0	15.1	659.6	17.5	97.16
	zr_2	1.84	0.43	113172	0.06994	1.2	1.2807	1.7	0.13280	1.2	0.67	926.7	25.4	837.2	9.6	803.8	8.7	86.74
	zr_3	0.24	0.21	256747	0.12357	0.2	5.7337	0.8	0.33654	0.8	0.97	2008.3	4.4	1936.5	7.1	1870.0	12.6	93.11
C M	11_zirc61	0.58	0.38	181375	0.13603	0.6	7.5316	1.3	0.40156	1.1	0.87	2177.2	10.6	2176.8	11.3	2176.2	20.5	99.95

13_zr02	1.71	0.43	113172	0.06511	0.3	1.2983	3.2	0.14462	3.2	0.99	778.0	7.0	845.0	18.6	870.7	26.3	111.92
11_zirc61	1.12	0.43	1576	0.06290	0.8	0.9357	1.2	0.10789	1.0	0.77	704.9	16.0	670.6	6.0	660.5	6.1	93.69
18_zr31	0.37	0.64	4077	0.14065	1.1	6.8448	3.2	0.35295	3.0	0.93	2235.2	19.8	2091.5	28.7	1948.7	50.9	87.18
19_zr28	0.13	0.51	11368	0.13790	0.3	8.7278	3.4	0.45904	3.4	1.00	2200.9	5.3	2310.0	30.7	2435.3	68.1	110.65
25_zr35	0.26	0.27	5505	0.13785	0.3	8.5201	2.9	0.44825	2.9	0.99	2200.4	5.1	2288.1	26.7	2387.5	58.4	108.50
26_zr21	0.12	0.09	12113	0.13041	0.6	6.8599	1.6	0.38151	1.5	0.97	2103.5	10.0	2093.5	13.8	2083.3	25.8	99.04

Table 2

Spot Name	% comm 206	ppm U	ppm Th	232Th /238U	204corr 206Pb/ 238U Ratio	% Err	204corr 207Pb /206Pb Ratio	% Err	204corr 207Pb /206Pb Age	1s err	204corr 206Pb /238U Age	1s err	% Dis-cor-dant
CMP41-1.1	0.59	245	178	0.75	10,19	2,5	~~,0625~~	~~3,9~~	690	83	603.4	14.6	14
CMP41-2.1	0.15	606	258	0.44	4,00	2,4	,0935	1,3	1498	24	1439.1	31.5	4
CMP41-3.1	0.87	304	158	0.54	5,05	2,5	,0797	2,3	1190	47	1163.8	26.4	2
CMP41-4.1	2.16	331	76	0.24	4,23	2,5	,0951	4,1	1531	80	1363.3	31.3	12
CMP41-4.2	0.39	305	87	0.29	3,67	2,5	,0959	1,4	1545	27	1553.1	34.0	-1
~~CMP41-5.1~~	~~4.23~~	~~313~~	~~149~~	~~0.49~~	~~15,09~~	~~2,6~~	~~,0619~~	~~11,4~~	671	246	~~412.9~~	~~10.5~~	~~62~~
CMP41-6.1	0.78	519	425	0.85	5,93	2,5	,0749	2,1	1066	44	1004.5	22.8	6
CMP41-7.1	0.38	478	320	0.69	3,48	2,5	,1069	0,9	1747	17	1626.3	36.1	7
CMP41-8.1	3.14	25	10	0.43	2,85	3,3	,1237	7,1	2010	130	1926.5	55.0	4
~~CMP41-9.1~~	~~1.53~~	~~172~~	~~87~~	~~0.52~~	~~6,77~~	~~3,1~~	~~,0785~~	~~5,1~~	1160	103	~~887.3~~	~~25.9~~	~~31~~
CMP41-10.1	0.68	325	109	0.35	3,56	2,5	,0995	1,6	1615	31	1595.3	35.0	1
~~CMP41-11.1~~	~~1.35~~	~~958~~	~~296~~	~~0.32~~	~~6,09~~	~~2,5~~	~~,0922~~	~~2,1~~	1472	41	~~978.6~~	~~22.4~~	~~50~~
CMP41-12.1	0.41	418	413	1.02	2,94	2,4	,1130	0,9	1848	17	1883.6	40.0	-2
CMP41-13.1	0.60	405	226	0.58	9,29	2,5	,0598	3,7	597	80	658.6	15.7	-9
CMP41-14.1	1.47	207	201	1.00	9,94	2,6	,0611	6,7	643	145	617.3	15.3	4
CMP41-15.1	2.01	446	242	0.56	10,06	2,9	,0621	6,2	676	135	610.5	16.9	11
CMP82-1.1	1,45	154	141	0,94	8,57	1,5	,0659	4,8	,0659	4,8	708,8	10,6	13
CMP82-2.1	0,35	412	170	0,43	4,88	1,4	,0811	1,0	,0811	1,0	1199,9	16,3	2
CMP82-3.1	0,28	144	93	0,67	2,42	1,5	,1379	0,6	,1379	0,6	2234,1	33,3	-1
CMP82-4.1	0,12	273	119	0,45	9,72	1,4	,0611	1,6	,0611	1,6	631,2	8,9	2
CMP82-5.1	2,62	430	323	0,78	9,94	1,4	,0612	5,7	,0612	5,7	617,2	8,8	5
CMP82-6.1	0,71	1128	383	0,35	9,02	1,4	,0619	3,5	,0619	3,5	678,2	9,3	-1

CMP82-7.1	-0,04	390	99	0,26	3,91	1,4	,0857	0,6	,0857	0,6	1480,1	20,3	-9
CMP82-8.1	3,09	1334	264	0,20	8,70	1,5	,0622	6,0	,0622	6,0	701,8	10,6	-3
~~CMP82-9.1~~	~~5,04~~	~~194~~	~~90~~	~~0,48~~	~~10,47~~	~~1,6~~	~~,0634~~	~~11,6~~	~~,0634~~	~~11,6~~	~~585,2~~	~~9,3~~	~~23~~
CMP82-10.1	0,55	859	180	0,22	6,40	1,4	,0778	1,3	,0778	1,3	927,6	12,7	22
~~CMP82-11.1~~	~~3,69~~	~~193~~	~~70~~	~~0,37~~	~~19,70~~	~~1,7~~	~~,0601~~	~~11,1~~	~~,0601~~	~~11,1~~	~~316,2~~	~~5,3~~	~~91~~
CMP82-12.1	0,13	1069	331	0,32	9,22	2,8	,0610	0,8	,0610	0,8	664,4	18,0	-4
CMP82-13.1	2,89	741	528	0,74	10,54	1,4	,0606	6,0	,0606	6,0	583,5	8,3	7
CMP82-14.1	0,52	204	82	0,42	7,73	1,5	,0650	2,2	,0650	2,2	784,7	11,3	-1
CMP82-15.1	0,15	311	183	0,61	7,98	1,5	,0632	1,6	,0632	1,6	762,0	11,0	-6
CMP82-16.1	2,03	239	136	0,59	10,11	1,6	,0599	5,8	,0599	5,8	608,1	9,6	-1
CMP82-17.1	1,11	1277	194	0,16	8,48	1,4	,0623	2,7	,0623	2,7	719,2	9,8	-5
CMP82-18.1	1,39	110	48	0,45	9,46	1,6	,0609	5,9	,0609	5,9	648,0	9,9	-2
CMP82-19.1	1,13	426	156	0,38	7,68	1,4	,0647	2,8	,0647	2,8	789,8	10,9	-3
CMP82-8.2	0,35	913	75	0,08	3,66	1,4	,0956	0,8	,0956	0,8	1559,9	21,3	-1

Table 3

Samples	$^{176}Lu/^{177}Hf$	$^{176}Hf/^{177}Hf$	Erro (1 SD)	Epsilon Hf (0)	Epsilon Hf (t1)	$^{176}Hf/^{177}Hf$ (DM)	Age U/Pb	T_{DM} (Ma)	f (Lu/Hf)	Int. 178Hf (V)
037_RIP3_71	0.000327	0.281347	0.00024	-50.39	-7.23	0.281794	1.956	2615	-0.99	1.17
040_RIP3_106	0.000553	0.281972	0.00075	-28.30	-0.03	0.282282	1.297	1781	-0.98	1.48
040_RIP3_106	0.000561	0.281803	0.00033	-34.25	-6.01	0.282282	1.297	2012	-0.98	1.52
016_RIP6_97	0.000427	0.282128	0.00017	-22.79	0.59	0.282448	1.071	1562	-0.99	1.63
017_RIP6_96	0.000742	0.281864	0.00018	-32.11	0.15	0.282143	1.486	1938	-0.98	1.44
018_RIP6_95	0.000661	0.281771	0.00021	-35.41	2.37	0.281961	1.732	2062	-0.98	1.19
020_RIP5_87	0.001157	0.281589	0.00024	-41.82	1.82	0.281742	2.026	2339	-0.97	1.14
009_RIP6_98	0.000574	0.281104	0.00017	-59.00	-13.80	0.281714	2.063	2959	-0.98	1.34
010_RIP6_92	0.000281	0.281699	0.00020	-37.93	3.31	0.281861	1.866	2138	-0.99	1.44
030_RIP5_81	0.001050	0.282065	0.00018	-24.99	-12.62	0.282805	0.581	1674	-0.97	1.27
031_RIP5_80	0.000474	0.281158	0.00015	-57.08	-10.37	0.281669	2.124	2879	-0.99	1.27
032_RIP5_82	0.000670	0.281925	0.00036	-29.95	-4.96	0.282388	1.153	1851	-0.98	1.09
033_RIP3_68	0.001750	0.281282	0.00029	-52.70	-27.70	0.282357	1.195	2805	-0.95	0.96
020_RIP5_87	0.001151	0.281576	0.00024	-42.30	5.11	0.281615	2.196	2357	-0.97	1.14
68_cmp82_1.1	0.000980	0.281894	0.00027	-31.04	-15.92	0.282713	0.708	1908	-0.97	1.46
70_cmp82_3.1	0.000966	0.281367	0.00021	-49.68	-1.47	0.281596	2.201	2631	-0.97	1.56
71_cmp82_4.1	0.000458	0.282042	0.00021	-25.81	-12.12	0.282769	0.631	1680	-0.99	1.63
74_cmp82_5.1	0.001758	0.282174	0.00047	-21.15	-8.29	0.282779	0.617	1552	-0.95	0.48
75_cmp82_6.1	0.000911	0.282044	0.00016	-25.75	-11.30	0.282737	0.675	1698	-0.97	1.48
76_cmp82_7.1	0.001122	0.282103	0.00041	-23.66	4.87	0.282257	1.331	1625	-0.97	0.75
77_cmp82_8.1	0.001073	0.281894	0.00016	-31.07	-16.59	0.282733	0.700	1914	-0.97	1.84
80_cmp82_8.2	0.000714	0.281872	0.00016	-31.83	1.63	0.282104	1.559	1926	-0.98	1.62
82_cmp82_10.1_B	0.002018	0.281619	0.00049	-40.77	-26.32	0.282719	0.700	2351	-0.94	0.56
83_cmp82_11.1	0.001324	0.282289	0.00022	-17.08	-4.24	0.282786	0.608	1372	-0.96	1.17
86_cmp82_12.1	0.001230	0.281826	0.00051	-33.44	-19.91	0.282763	0.639	2015	-0.96	1.14
87_cmp82_13.1	0.002723	0.281939	0.00028	-29.45	-16.84	0.282773	0.625	1935	-0.92	1.11
88_cmp82_14.1	0.001583	0.281627	0.00017	-40.51	-24.27	0.282664	0.775	2314	-0.95	1.73

89_cmp82_15.1	0.000371	0.282133	0.00027	-22.61	-7.05	0.282709	0.714	1553	-0.99	1.01
92_cmp82_16.1	0.000631	0.282119	0.00048	-23.10	-7.97	0.282719	0.700	1582	-0.98	1.51
93_cmp82_17.1	0.001089	0.281941	0.00039	-29.39	-14.81	0.282730	0.685	1849	-0.97	0.92
94_cmp82_18.1	0.000371	0.282060	0.00194	-25.17	-11.31	0.282765	0.637	1652	-0.99	1.51
11_RIP12_21	0.001300	0.282000	0.00082	-27.29	1.06	0.282257	1.331	1777	-0.96	0.90
12_RIP12_36	0.000996	0.281520	0.00031	-44.28	-0.67	0.281750	2.015	2424	-0.97	1.10
13_RIP12_38A	0.000520	0.282067	0.00018	-24.95	-6.49	0.282610	0.850	1649	-0.98	1.50
14_RIP12_38B	0.000500	0.282130	0.00027	-22.69	-6.08	0.282672	0.765	1561	-0.98	1.12
002_RIP16_01	0.002007	0.282086	0.00026	-24.28	-7.58	0.282642	0.806	1689	-0.94	1.60
003_RIP16_02	0.001726	0.282199	0.00033	-20.27	-3.42	0.282642	0.806	1515	-0.95	0.95
004_RIP16_03	0.001227	0.282114	0.00026	-23.29	4.91	0.282265	1.320	1615	-0.96	1.43
005_RIP16_06	0.000535	0.281753	0.00035	-36.02	-9.59	0.282343	1.214	2078	-0.98	1.68
111_CMP82_05	0.000863	0.281938	0.00019	-29.48	6.55	0.282013	1.662	1841	-0.97	1.63
112_CMP82_06	0.000517	0.282061	0.00015	-25.13	5.13	0.282217	1.385	1656	-0.98	1.99
106_CMP82_01	0.000720	0.281922	0.00022	-30.05	-14.98	0.282719	0.700	1857	-0.98	1.21
004_CMP85_16	0.000609	0.281463	0.00028	-46.30	-0.40	0.281691	2.094	2478	-0.98	1.02
005_CMP85_16B	0.000432	0.281484	0.00027	-45.54	0.62	0.281691	2.094	2437	-0.99	1.42
016_CMP85_29	0.000677	0.281436	0.00023	-47.24	-0.16	0.281649	2.151	2518	-0.98	1.22
017_CMP85_28	0.001282	0.281415	0.00030	-47.98	-1.19	0.281628	2.178	2587	-0.96	0.93
020_CMP85_32	0.000724	0.281393	0.00025	-48.76	1.83	0.281529	2.311	2580	-0.98	1.16
076_PPC6046_7	0.000688	0.281693	0.00027	-38.16	-21.51	0.282666	0.773	2170	-0.98	0.82
096_PPC6046_56	0.000626	0.281720	0.00018	-37.21	2.17	0.281909	1.802	2129	-0.98	1.74
066_PPC6046_09	0.000440	0.282080	0.00014	-24.49	-7.68	0.282666	0.773	1628	-0.99	1.54
071_PPC6046_11	0.000183	0.281760	0.00033	-35.77	-15.24	0.282547	0.936	2050	-0.99	0.91
033_RP11_01	0.000154	0.281386	0.00014	-49.00	-8.69	0.281895	1.820	2551	-1.00	1.94
034_RP11_02	0.000237	0.281306	0.00018	-51.85	0.08	0.281509	2.337	2664	-0.99	1.68
035_RP11_03	0.000608	0.281453	0.00022	-46.66	3.81	0.281539	2.297	2491	-0.98	1.38
036_RP11_04	0.000116	0.281353	0.00021	-50.17	-6.98	0.281802	1.945	2593	-1.00	1.21
038_RP11_05	0.000441	0.281464	0.00022	-46.24	-33.32	0.282794	0.597	2465	-0.99	1.15
039_RP11_06	0.000474	0.281298	0.00018	-52.11	-6.54	0.281708	2.072	2690	-0.99	1.28
040_RP11_07	0.000148	0.281337	0.00018	-50.74	-1.79	0.281612	2.200	2616	-1.00	1.48

041_RP11_08	0.000425	0.281326	0.00024	-51.13	-10.56	0.281875	1.847	2650	-0.99	0.87
044_RP11_10	0.000377	0.281412	0.00017	-48.11	-7.39	0.281873	1.850	2532	-0.99	1.11
045_RP11_11	0.000233	0.281384	0.00019	-49.07	-4.24	0.281743	2.024	2559	-0.99	1.43
046_RP11_12	0.001286	0.281679	0.00033	-38.66	3.50	0.281787	1.966	2223	-0.96	0.75
048_RP11_13	0.001988	0.281348	0.00029	-50.36	-8.81	0.281774	1.983	2730	-0.94	0.84
049_RP11_14	0.000566	0.281264	0.00045	-53.31	-8.78	0.281738	2.032	2743	-0.98	0.46
051_RP11_15	0.000366	0.281257	0.00020	-53.59	-2.50	0.281530	2.309	2739	-0.99	1.09
04_ SMVCA _01	0.000257	0.281880	0.00019	-31.56	-15.57	0.281876	0.732	1893	-0.99	1.45
06_ SMVCA _03	0.000122	0.281877	0.00017	-31.63	-16.77	0.282735	0.678	1889	-1.00	1.49
07_ SMVCA _04	0.000315	0.281896	0.00019	-30.99	-15.82	0.282722	0.696	1874	-0.99	1.44
12_ SMVCA _06	0.000262	0.281923	0.00017	-30.01	-18.42	0.282841	0.532	1834	-0.99	1.70
14_ SMVCA _09	0.000649	0.281684	0.00020	-38.47	-8.04	0.282206	1.400	2179	-0.98	1.54
23_ SMVCA _14	0.000573	0.281763	0.00029	-35.68	1.27	0.281992	1.690	2067	-0.98	1.23
24_ SMVCA _15	0.000080	0.281994	0.00012	-27.51	8.50	0.282042	1.622	1729	-1.00	1.84
25_ SMVCA _16	0.000566	0.281581	0.00017	-42.11	-6.71	0.282043	1.621	2314	-0.98	1.66
29_ SMVCA _20	0.000614	0.281871	0.00019	-31.85	-9.74	0.282485	1.020	1922	-0.98	1.51
30_ SMVCA _23	0.000136	0.281945	0.00019	-29.25	-3.73	0.282384	1.158	1798	-1.00	1.50
31_ SMVCA _24	0.000439	0.281975	0.00018	-28.17	-9.09	0.282590	0.877	1771	-0.99	1.48
18_ SMVCA _11A	0.000431	0.281880	0.00019	-31.55	-20.39	0.282853	0.515	1901	-0.99	1.57
19_ SMVCA _11B	0.000347	0.281884	0.00019	-31.41	-20.22	0.282853	0.515	1891	-0.99	1.37